

# UCLA

## UCLA Previously Published Works

### Title

The Chlamydomonas Genome Project, version 6: Reference assemblies for mating-type plus and minus strains reveal extensive structural mutation in the laboratory

### Permalink

<https://escholarship.org/uc/item/2pg9x5cp>

### Journal

The Plant Cell, 35(2)

### ISSN

1040-4651

### Authors

Craig, Rory J  
Gallaher, Sean D  
Shu, Shengqiang  
[et al.](#)

### Publication Date

2023-02-20

### DOI

10.1093/plcell/koac347

Peer reviewed

1 **The Chlamydomonas Genome Project, version 6:**  
2 **reference assemblies for mating type *plus* and *minus***  
3 **strains reveal extensive structural mutation in the**  
4 **laboratory**

5  
6 Rory J. Craig<sup>1,2</sup>, Sean D. Gallaher<sup>1</sup>, Shengqiang Shu<sup>3</sup>, Patrice Salomé<sup>4,5</sup>, Jerry W. Jenkins<sup>6</sup>,  
7 Crysten E. Blaby-Haas<sup>7</sup>, Samuel O. Purvine<sup>8</sup>, Samuel O'Donnell<sup>9</sup>, Kerrie Barry<sup>3</sup>, Jane  
8 Grimwood<sup>6</sup>, Daniela Strenkert<sup>1</sup>, Janette Kropat<sup>4</sup>, Chris Daum<sup>3</sup>, Yuko Yoshinaga<sup>3</sup>, David M.  
9 Goodstein<sup>3</sup>, Olivier Vallon<sup>10</sup>, Jeremy Schmutz<sup>3,6</sup>, Sabeeha S. Merchant<sup>1,11,12,13</sup>

10  
11 <sup>1</sup> California Institute for Quantitative Biosciences, University of California, Berkeley, CA 94720,  
12 USA

13 <sup>2</sup> Institute of Ecology and Evolution, School of Biological Sciences, University of Edinburgh,  
14 Edinburgh, UK

15 <sup>3</sup> United States Department of Energy, Joint Genome Institute, Berkeley, CA 94720, USA

16 <sup>4</sup> Department of Chemistry and Biochemistry, University of California, Los Angeles, CA 90095,  
17 USA

18 <sup>5</sup> Institute for Genomics and Proteomics, University of California, Los Angeles, CA 90095, USA

19 <sup>6</sup> HudsonAlpha Institute for Biotechnology, Huntsville, AL 35806, USA

20 <sup>7</sup> The Molecular Foundry, Lawrence Berkeley National Laboratory, Berkeley, CA 94720, USA

21 <sup>8</sup> Environmental Molecular Sciences Laboratory, Pacific Northwest National Laboratory,  
22 Richland, WA 99354, USA

23 <sup>9</sup> Laboratory of Computational and Quantitative Biology, UMR 7238, CNRS, Institut de  
24 Biologie Paris-Seine, Sorbonne Université, Paris, France

25 <sup>10</sup> Unité Mixte de Recherche 7141, CNRS, Institut de Biologie Physico-Chimique, Sorbonne  
26 Université, Paris, France

27 <sup>11</sup> Department of Molecular and Cell Biology, University of California, Berkeley, CA 94720,  
28 USA

29 <sup>12</sup> Department of Plant and Microbial Biology, University of California, Berkeley, CA 94720,  
30 USA

31 <sup>13</sup> Division of Environmental Genomics and Systems Biology, Lawrence Berkeley National  
32 Laboratory, Berkeley, CA 94720 USA

33  
34 Correspondence: jschmutz@hudsonalpha.org; sabeeha@berkeley.edu

35  
36 **Short title:** The Chlamydomonas Genome Project, version 6

37  
38 The author responsible for distribution of materials integral to the findings presented in this article in  
39 accordance with the policy described in the Instructions for Authors  
40 (<https://academic.oup.com/plcell/pages/General-Instructions>) is: Sabeeha S. Merchant  
41 (sabeeha@berkeley.edu).  
42

43 **ABSTRACT**

44 Five versions of the *Chlamydomonas reinhardtii* reference genome have been produced over the  
45 last two decades. Here we present version 6, bringing significant advances in assembly quality  
46 and structural annotations. PacBio-based chromosome-level assemblies for two laboratory  
47 strains, CC-503 and CC-4532, provide resources for the *plus* and *minus* mating type alleles. We  
48 corrected major misassemblies in previous versions and validated our assemblies via linkage  
49 analyses. Contiguity increased over ten-fold and >80% of filled gaps are within genes. We used  
50 Iso-Seq and deep RNA-seq datasets to improve structural annotations, and updated gene symbols  
51 and textual annotation of functionally characterized genes via extensive manual curation. We  
52 discovered that the cell wall-less classical reference strain CC-503 exhibits genomic instability  
53 potentially caused by deletion of the helicase *RECQ3*, with major structural mutations identified  
54 that affect >100 genes. We therefore present the CC-4532 assembly as the primary reference,  
55 although this strain also carries unique structural mutations and is experiencing rapid  
56 proliferation of a *Gypsy* retrotransposon. We expect all laboratory strains to harbor gene-  
57 disrupting mutations, which should be considered when interpreting and comparing experimental  
58 results. Collectively, the resources presented here herald a new era of *Chlamydomonas* genomics  
59 and will provide the foundation for continued research in this important reference.

60  
61  
62  
63  
64  
65  
66  
67  
68  
69  
70  
71  
72  
73  
74  
75  
76  
77  
78  
79

## 80 INTRODUCTION

81 The unicellular green alga *Chlamydomonas* (*Chlamydomonas reinhardtii*) is one of the primary  
82 model organisms in plant and cell biology. *Chlamydomonas* has been instrumental to discoveries  
83 in photosynthesis, chloroplast biology, and cilia structure and function, facilitated by its  
84 experimental tractability and amenability to classical genetics (Salomé and Merchant 2019).  
85 More recently, the species has been used as a powerful model for investigating the eukaryotic  
86 cell cycle (Cross and Umen 2015) and conserved mechanisms of sexual reproduction (Ning et al.  
87 2013; Fédry et al. 2017), for discovery of optogenetic tools (Deisseroth and Hegemann 2017),  
88 and for *in situ* structural analyses by cryo-electron microscopy (Engel et al. 2015; Freeman  
89 Rosenzweig et al. 2017). Genome-wide mutant libraries form part of a growing suite of tools for  
90 exploiting high-throughput functional genomics approaches (Li et al. 2019; Fauser et al. 2022).  
91 As the most thoroughly studied green alga, *Chlamydomonas* also serves as an integral reference  
92 for the rapidly expanding fields of algal biology and biotechnology (Crozet et al. 2018; Blaby-  
93 Haas and Merchant 2019). The *Chlamydomonas* Genome Project was initiated two decades ago  
94 (Grossman et al. 2003; Merchant et al. 2007), and its continued development has kept the species  
95 at the forefront of plant and algal genomics (Blaby et al. 2014). Maintained at Phytozome  
96 (Goodstein et al. 2012), the genome assembly and structural annotations are a fundamental  
97 resource for contemporary *Chlamydomonas* research.

98  
99 The *Chlamydomonas* genome is ~111 Mb in length, GC-rich (~64% genome-wide) and consists  
100 of 17 chromosomes. Preceded by two preliminary versions (Grossman et al. 2003), the initial  
101 draft genome (v3) was assembled from ~13x coverage of Sanger-sequenced reads (Merchant et  
102 al. 2007). Utilizing targeted sequencing of assembly gaps and molecular mapping data (Kathir et  
103 al. 2003; Rymarquis et al. 2005), the first chromosome-level assembly (v4) quickly followed in  
104 2008 (Table 1). With the onset of next-generation sequencing, the v5 assembly was released in  
105 2012 and applied both 454 and further Sanger sequencing to target all remaining gaps,  
106 successfully filling approximately half of those in v4 (Blaby et al. 2014). At 111.1 Mb, with  
107 1,441 gaps (~3.7% of the genome) and 37 unplaced scaffolds (~2.0% of the genome), v5 has  
108 been the most long-standing release to date.

109

110 Although the assembly metrics of v5 represented a considerable achievement, there remained  
111 substantial room for improvement relative to the highest quality Sanger-sequenced  
112 contemporaries. A decade earlier, near complete assemblies featuring just tens of gaps in the  
113 most repetitive regions had been produced for Arabidopsis (*Arabidopsis thaliana*) (Arabidopsis  
114 Genome Initiative 2000) and rice (*Oryza sativa*) (Goff et al. 2002). Recently, long-read  
115 sequencing technologies have provided a platform to achieve similar contiguity, and even  
116 complete telomere-to-telomere assemblies, for far more complex genomes such as maize (*Zea  
117 mays*) (Jiao et al. 2017; Liu et al. 2020). Pacific Biosciences (PacBio) sequencing has been  
118 applied to close relatives of Chlamydomonas, yielding assemblies more contiguous than v5 for  
119 multiple unicellular and multicellular volvocine algae (Hamaji et al. 2018; Craig et al. 2021a;  
120 Yamamoto et al. 2021). Most recently, O'Donnell et al. (2020) used ultra-long Nanopore  
121 sequencing (Liu et al. 2019) to produce an unannotated assembly of Chlamydomonas strain CC-  
122 1690 (classically named 21gr) featuring only four gaps. It is worth noting that many of the gaps  
123 in the v5 assembly are expected to be in genic regions (Tulin and Cross 2016), and  
124 improvements to contiguity should therefore advance biological discovery via improved  
125 structural and functional annotation.

126

127 Perhaps of greater significance than contiguity, recent studies have highlighted inconsistencies  
128 between genetic mapping and the v5 assembly, potentially indicating misassemblies. Salomé and  
129 Merchant (2019) reported that the phytoene synthase gene (*PSY1*) is presently located on  
130 chromosome 2, although its corresponding white mutant *lts1* was mapped to chromosome 11  
131 (McCarthy et al. 2004). Likewise, Ozawa et al. (2020) characterized *MTH11*, which encodes an  
132 octotricopeptide repeat protein and is mutated in the non-photosynthetic strain *ac46*, observing  
133 that the gene is located on chromosome 17 despite having been mapped to chromosome 15  
134 (Dutcher et al. 1991). Notably, both inconsistencies were introduced during the transition from  
135 v4 to v5, raising the possibility that past assembly improvements may have come at the expense  
136 of new errors.

137

138 There is also a potential issue with the classical reference strain, the cell wall-less CC-503  
139 (*cw92*), which was chosen to meet the high DNA yield requirements of the early genome project.  
140 The *cw* phenotype was induced by mutagenesis of the mating type *plus* (*mt+*) “wild-type” strain

141 137c+ (later deposited as CC-125) with the methylating agent *N*-methyl-*N'*-nitro-*N*-  
142 nitrosoguanidine (MNNG) (Hyams and Davies 1972). MNNG primarily induces G:C to A:T  
143 transitions, although it can also induce double-strand breaks (DSBs) and chromosomal  
144 aberrations in high doses (Kaina 2004; Wyatt and Pittman 2006). For CC-503, the *cw* phenotype  
145 shows aberrant segregation in crosses, suggesting that there may be more than one causal  
146 mutation (Davies 1972; Hyams and Davies 1972). However, no causal mutations have been  
147 identified, and the potential genome-wide effects of mutagenesis in CC-503 have not been  
148 analyzed. More broadly, little is known about the extent of structural mutations, such as  
149 transposable element (TE) insertions and large duplications and deletions, during routine  
150 laboratory culture, which have the potential to introduce substantial genomic heterogeneity  
151 among strains.

152

153 Finally, a single strain does not represent the genomic diversity present among *Chlamydomonas*  
154 laboratory strains, which are interrelated but not isogenic. This fact is most obvious for the  
155 mating type locus (*MT*) located on the left arm of chromosome 6. The *plus* (*MT+*) and *minus*  
156 (*MT-*) alleles, which respectively control the sexual differentiation of *plus* or *minus* gametes,  
157 feature a small number of mating type-specific genes and several rearrangements that suppress  
158 crossover recombination (Ferris et al. 2010; De Hoff et al. 2013). While the CC-503 reference  
159 harbors the *MT+* sequence, an *MT-* assembly is only available for the divergent field isolate CC-  
160 2290 (S1D2) (Ferris et al. 2010). Furthermore, all previous assembly versions have only included  
161 sequence and structural annotations for the nuclear genome, despite the relevance of organelle  
162 biology in the *Chlamydomonas* literature and the long availability of resources for the organelle  
163 genomes (Vahrenholz et al. 1993; Maul et al. 2002; Smith and Lee 2009; Gallaher et al. 2018).

164

165 Beyond the assembly itself, the structural annotations, which define the genomic coordinates of  
166 genes and the proteins they encode, are the foundation of omics analyses, most notably high-  
167 throughput transcriptomics and proteomics. The *Chlamydomonas* structural annotations have  
168 also been subject to several rounds of improvement (see Blaby et al. (2014) and Blaby and  
169 Blaby-Haas (2017)). Previous versions incorporated evidence from expressed sequence tags  
170 (ESTs) and assembled cDNAs, with protein homology support from *Volvox carteri* genes  
171 (Prochnik et al. 2010). The annotations performed for v5 incorporated over one billion RNA-seq

172 reads, resulting in several major changes to gene models (Blaby and Blaby-Haas 2017). The  
173 most recent v5 annotation (v5.6) features 17,741 protein-coding genes with 1,785 alternative  
174 transcripts. Recent advances in sequencing again provide substantial opportunities to update  
175 structural annotations. For example, Gallaher et al. (2021) used PacBio Iso-Seq (long-read  
176 sequencing of cDNA) to discover more than 100 polycistronic loci in *Chlamydomonas* (i.e.  
177 genes producing a single transcript that encodes more than one protein), although these data have  
178 not yet been used to systematically improve structural annotations.

179

180 Here we present the first major update to the *Chlamydomonas* Genome Project in nearly a  
181 decade. We present PacBio-based assemblies for the classical *mt+* reference strain CC-503 and  
182 for the *mt-* laboratory strain CC-4532, bringing extensive improvements to both assembly and  
183 annotation quality. Using comparative analyses, we specifically test whether the mutagenesis of  
184 CC-503 has resulted in genomic aberrations and explore the wider influence of TE insertions in  
185 the genomes of *Chlamydomonas* laboratory strains. We find that the CC-503 genome carries  
186 many large structural mutations predicted to affect ~100 genes, while the genomes of all  
187 laboratory strains are likely to harbor a non-negligible and potentially highly variable number of  
188 TE insertions. We therefore present the CC-4532 assembly as the primary v6 reference genome  
189 and discuss the implications of mutation in the laboratory. These updates mark the start of an  
190 exciting new era for *Chlamydomonas* genomics, with developing opportunities to produce high-  
191 quality assemblies and annotations for several strains and divergent isolates of the species.

192

## 193 **RESULTS and DISCUSSION**

### 194 **CC-4532 version 6: a long-read *Chlamydomonas* reference assembly**

195 As the first step in updating the reference genome, we produced *de novo* contig-level assemblies  
196 from high coverage (>120x) PacBio Sequel datasets for the *mt+* CC-503 and *mt-* CC-4532. In  
197 line with the reported inconsistencies with mapping data, we detected multiple contradictions  
198 between the prior v5 assembly and the newly assembled contigs of both CC-503 and CC-4532.  
199 We thus reassembled all well-supported contigs to chromosomes without reference to previous  
200 versions, which we primarily achieved by mapping the contigs to the near complete Nanopore-  
201 based CC-1690 assembly (O'Donnell et al. 2020). This approach not only allowed contigs to be  
202 placed on chromosomes in a manner consistent across all three assemblies, but also enabled the

203 estimation of gap lengths between remaining contig breaks in the PacBio assemblies relative to  
204 CC-1690. We refer to these assemblies as CC-503 v6 and CC-4532 v6, respectively, to highlight  
205 that they are both the product of version 6 of the genome project. We validated all structural  
206 changes by reanalyzing previously published linkage data (Kathir et al. 2003; Liu et al. 2018). In  
207 addition, recent knowledge of centromeric (Lin et al. 2018; Craig et al. 2021a) and subtelomeric  
208 (Chaux-Jukic et al. 2021) repeats provided extrinsic validation. While the CC-4532 v6 and CC-  
209 1690 assemblies are entirely consistent relative to each other and all supporting evidence, we  
210 identified remaining inconsistencies in the CC-503 v6 assembly, indicative of genomic  
211 rearrangements unique to this strain. We describe these structural mutations further below, while  
212 the following text focuses on CC-4542 v6 as the primary reference assembly.

213  
214 CC-4532 v6 is considerably more contiguous than previous versions (Table 1). The number of  
215 contigs decreased by an order of magnitude relative to v5, from 1,495 to 120, with a  
216 corresponding increase in the contig-level N50 from 0.22 Mb to 2.65 Mb (i.e. contigs  $\geq 2.65$  Mb  
217 represent  $>50\%$  of the assembly length). Although unplaced sequence only fell from 2.20 Mb to  
218 1.65 Mb, the 40 highly repetitive unplaced contigs in CC-4532 v6 mostly represent newly  
219 assembled sequences that are unrelated to the 37 unplaced scaffolds in v5, all but three of which  
220 are now at least partially placed on chromosomes. With a genome size of 114.0 Mb, CC-4532 v6  
221 is  $\sim 3$  Mb larger than v5 and the CC-1690 assembly. This discrepancy can be explained in part by  
222 redundancy between the unplaced contigs and the gaps to which they presumably correspond,  
223 since gap lengths (represented by unknown bases i.e. Ns) were estimated relative to CC-1690.  
224 However, we attribute most of the biological increase in genome size to TE activity in the  
225 laboratory. In the following sections we present a thorough assessment of the assembly and  
226 annotation improvements.

227

### 228 **A note on CC-4532 and laboratory strain haplotypes**

229 CC-4532 has been widely used in transcriptomics analyses and was initially selected for genome  
230 sequencing to obtain an assembly of the *MT-* allele. While its promotion to the new reference  
231 over other widely used strains may raise concerns, we note that there is no optimum or  
232 authoritative reference strain for *Chlamydomonas*. Laboratory strains are thought to be derived  
233 from the haploid progeny of a diploid zygospore isolated by G. M. Smith in 1945. Their



234 genomes are thus comprised of two haplotypes, although their frequencies are unbalanced; one  
235 haplotype covers only a maximum of 25% of the genome, but generally much less (Gallaher et  
236 al. 2015). The two haplotypes differ at ~2% of sites and many between-haplotype variants are  
237 expected to be functionally important. Gallaher et al. (2015) arbitrarily defined haplotype 1 as  
238 being that of the classical reference CC-503, with haplotype 2 referring to any region featuring  
239 the alternative haplotype in other strains. Laboratories use a variety of strains, including the  
240 oldest “wild types” (e.g. 137c+/CC-125 and 21gr/CC-1690) and those derived from subsequent  
241 crosses. Therefore, most strains in use differ genetically from the reference genome in multiple  
242 genomic regions, introducing variants in hundreds of genes.

243

244 CC-4532 is a putative subclone of CC-621 (NO-) and is partly descended from 137c+ (the  
245 progenitor of CC-503), although the exact crosses that produced the strain are unknown. It  
246 carries haplotype 1 at more than 95% of the genome and will thus provide a similar user  
247 experience as a reference strain. We later discuss remaining issues with a CC-4532 reference and  
248 solutions to producing a fully representative reference assembly for *Chlamydomonas* laboratory  
249 strains.

250

## 251 **The version 6 assembly corrects misassemblies of version 5**

252 The CC-4532 v6 assembly has major structural differences relative to v5, affecting the ordering  
253 and orientation of sequence both within and between chromosomes. Only six chromosomes (1, 4,  
254 6, 7, 13 and 14) remained consistent with respect to the ordering of scaffolds in v5. The extent of  
255 the changes to the remaining 11 chromosomes ranged from minor intra-chromosomal reordering  
256 of short contigs to major inter-chromosomal rearrangements affecting megabases of sequence.  
257 An overview of the between-chromosome changes is presented in Figure 1A.

258

259 Many of the changes occurred in proximity to the most repetitive genomic regions, particularly  
260 the putative centromeres and the subtelomeres, as well as regions corresponding to unplaced  
261 scaffolds in v5. Although approximate centromeric locations were predicted from molecular  
262 mapping (Preuss and Mets 2002), genomic coordinates and sequence characteristics have only  
263 recently been reported. Lin et al. (2018) identified 200-800 kb regions tightly linked to the  
264 centromeres that featured multiple open reading frames (ORFs) encoding proteins with reverse

265 transcriptase domains. Craig et al. (2021a) linked these ORFs to an *LI* LINE retrotransposon  
266 homologous to *Zepp*, the centromeric component of the trebouxiophyte alga *Coccomyxa*  
267 *subellipsoidea* (Blanc et al. 2012). Termed *Zepp*-like (*ZeppL*) elements in *Chlamydomonas*, this  
268 TE forms highly localized clusters at the putative centromeres, although in v5 chromosomes 2, 3,  
269 5 and 8 featured two clusters, and chromosomes 11 and 15 lacked clusters (Lin et al. 2018; Craig  
270 et al. 2021a). *Chlamydomonas* subtelomeres were recently shown to feature large satellite arrays  
271 termed *Sultans*, with other complex repeats present at specific chromosome termini (Chaux-Jukic  
272 et al. 2021). Subtelomeres are capped by the telomeric repeat (TTTTAGGG)<sub>n</sub> (Petracek et al.  
273 1990). Due to their complexity, subtelomeres were previously poorly assembled, and only half of  
274 chromosome termini featured a scaffold terminating in telomeric repeats in v5.

275  
276  
277 Comparisons of chromosomes 5 (Figure 2A) and 11 (Figure 2B) between v5 and v6 illustrate the  
278 types of misassemblies that affected these regions. In v5, the left arm of chromosome 5  
279 terminated in a 47-kb contig featuring a *ZeppL* cluster (purple, Figure 2A), which in v6 is  
280 assembled within the putative centromere of chromosome 10 (Supplemental Figure S1D). The  
281 remaining regions of chromosome 5, consisting of three blocks of ~0.7, 1.2 and 1.7 Mb (light  
282 blue, yellow and orange, respectively), are now rearranged and reorientated. The misassembly of  
283 the light blue and yellow regions featured a large gap corresponding to part of scaffold 24  
284 (containing *MUT6*), while the misassembly of the yellow and orange regions featured  
285 subtelomeric repeats that are now correctly placed at the left arm terminus in v6. Thus, the  
286 reassembled chromosome 5 features a single internal centromere, subtelomeric repeats at both  
287 termini, and is congruent with the molecular map (Kathir et al. 2003). On chromosome 11, the  
288 movement of an ~750-kb region (orange) from chromosome 2 simultaneously resolved the  
289 absence of a putative centromere on chromosome 11 and the presence of two *ZeppL* clusters on  
290 chromosome 2 (Figure 2B). This region includes *PSYI*, which was mapped genetically to  
291 chromosome 11 (McCarthy et al. 2004; Salomé and Merchant 2019). Independently, an ~860-kb  
292 region (light blue) was inverted, consistent with the tight linkage of *PETC1* and *DLE2* (Kathir et  
293 al. 2003). Misassemblies affecting other chromosomes are shown in Supplemental Figure S1.

294  
295 By far the most substantial changes affected chromosome 15, which approximately tripled in  
296 length from 1.92 Mb in v5 (the shortest chromosome) to 5.87 Mb in CC-4532 v6, acquiring

297 sequence previously assigned to chromosomes 2, 3, 8 and 17, as well as 15 unplaced scaffolds  
298 (Figure 1B). The sequence reassembled from chromosomes 2 (~1.2 Mb) and 17 (~0.3 Mb) each  
299 featured a marker gene previously mapped to chromosome 15: *DHC9* (Porter et al. 1996; Kathir  
300 et al. 2003) and the aforementioned *MTH11* (Dutcher et al. 1991; Ozawa et al. 2020),  
301 respectively. Some of the sequence reassembled from chromosome 8 (~0.4 Mb) and unplaced  
302 scaffolds (~1.1 Mb total) featured *ZeppL* elements, explaining the absence of centromeric repeats  
303 on chromosome 15 in v5. We attribute the degree of past misassembly to the unique sequence  
304 characteristics of chromosome 15. Its repeat content (47.2%) is substantially higher, and its gene  
305 density lower (36.7%), than the remaining 16 chromosomes (mean 17.7% and 79.0%,  
306 respectively) (Supplemental Dataset S1). Furthermore, this pattern is not uniform: the gene  
307 density of the chromosome arms (67.1%, ~2.1 Mb left and ~0.6 Mb right) approaches that of  
308 other chromosomes, while the internal region is massively repetitive (66.7%) and gene-poor  
309 (10.9%). As a result, chromosome 15 remains the most fragmented in CC-4532 v6, featuring 10  
310 gaps spanning 9.2% of the chromosome length, relative to a mean of three gaps and 0.4% for the  
311 remaining chromosomes. We expect that many of the unplaced contigs belong to chromosome  
312 15, although their extreme repeat content (69.8%) hinders efforts to place them without longer  
313 reads.

314  
315 The unusual features of chromosome 15 raise questions about its evolutionary origins, gene  
316 content and chromosomal environment. Except for *MTH11*, all marker genes (*ZYS3*, *CYT1* and  
317 *DHC9*) are located within the relatively gene-rich left arm of the chromosome. This region is  
318 also notable for containing almost all the *NCL* (*NUCLEAR CONTROL OF CHLOROPLAST*  
319 *GENE EXPRESSION-LIKE*) genes, encoding a family of RNA-binding proteins that is  
320 experiencing ongoing diversification (Boulouis et al. 2015). All but one of the 49 *NCL* genes are  
321 on chromosome 15, with 43 present in a cluster spanning ~460 kb, and three forming a shorter  
322 upstream cluster that was assembled on scaffold 19 in v5 (Figure 1B). The mutation responsible  
323 for the *yellow-in-the-dark* mutant *y1* was also mapped to the left arm of chromosome 15 and is  
324 linked to *DHC9* (Porter et al. 1996). The unknown *YI* gene might thus have been assigned to  
325 either chromosome 2 or an unplaced scaffold in v5. The remainder of chromosome 15 contains  
326 only 145 genes, 80 of which are in the highly repetitive internal region. Although most of these  
327 genes are not functionally annotated, we expect at least some to be essential (e.g. the plastid 50S

328 ribosomal protein gene *PRPL3*). It would be interesting to determine if much of chromosome 15  
329 is heterochromatic, and if so, whether genes are expressed from heterochromatic environments  
330 (e.g. as is the case for many genes on the repeat-rich dot chromosome in *Drosophila*  
331 *melanogaster* (Riddle and Elgin 2018)). Similarly, it would be interesting to explore whether the  
332 high repeat content results in an atypical recombination landscape on chromosome 15, and  
333 whether similarly high repeat contents are found on homologous chromosomal regions in closely  
334 related species.

335

336

337

338

339

340

341

342

343

344

345

346

347

348

349

350

351

352

353

354

355

356

357

358

359

360

361

362

363

364

365

366

367

368

369

370

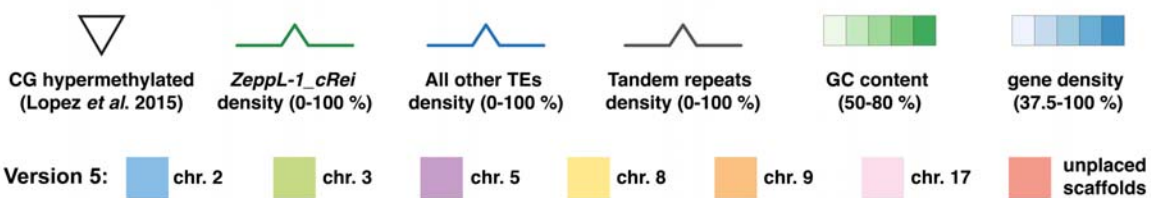
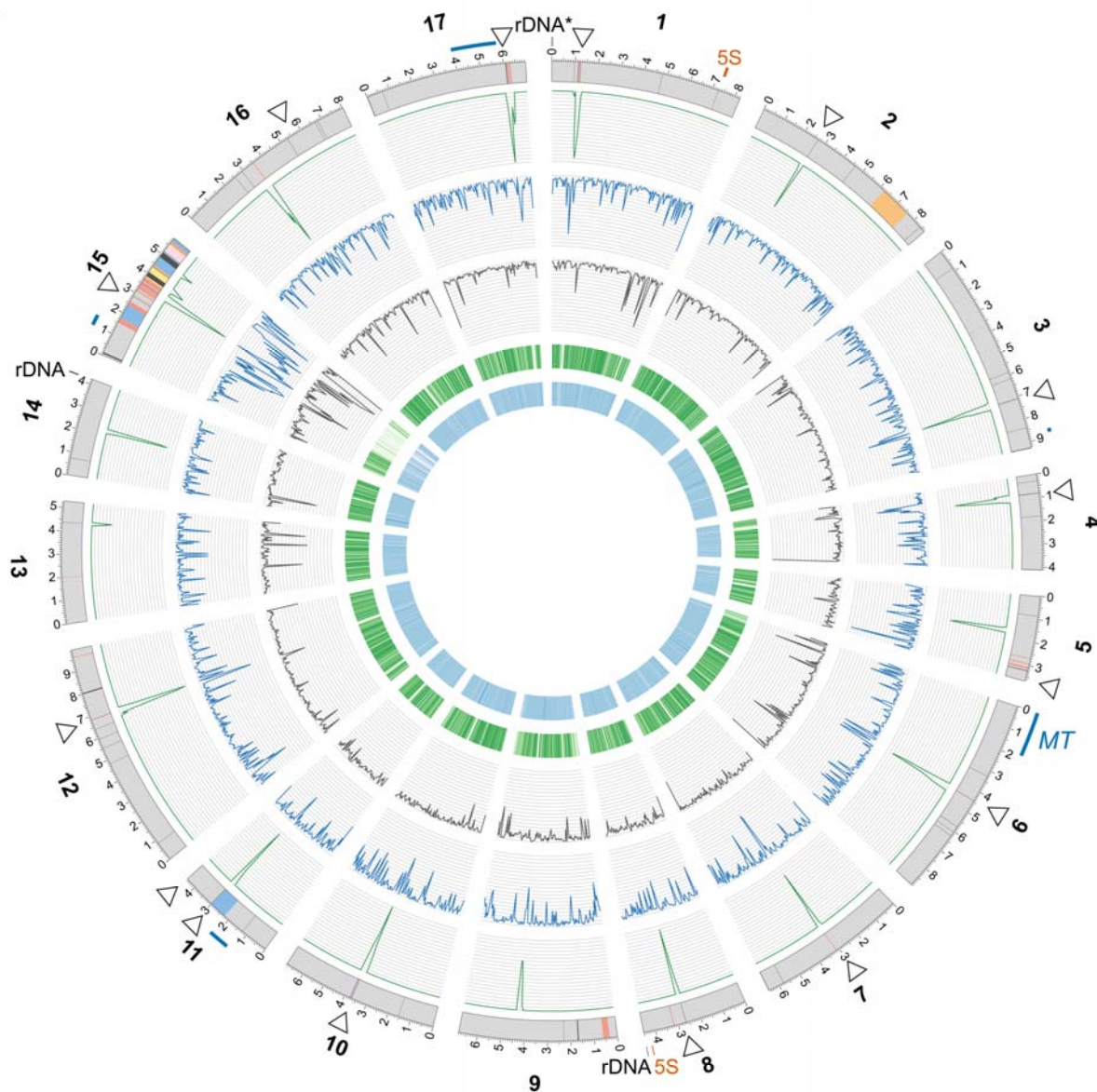
371

372

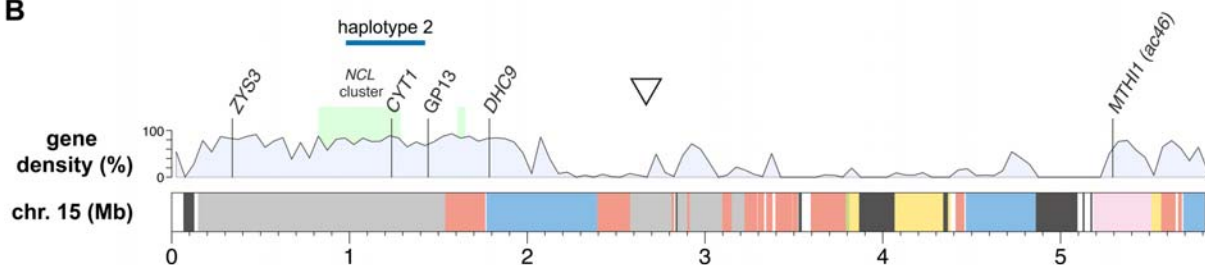
373



A

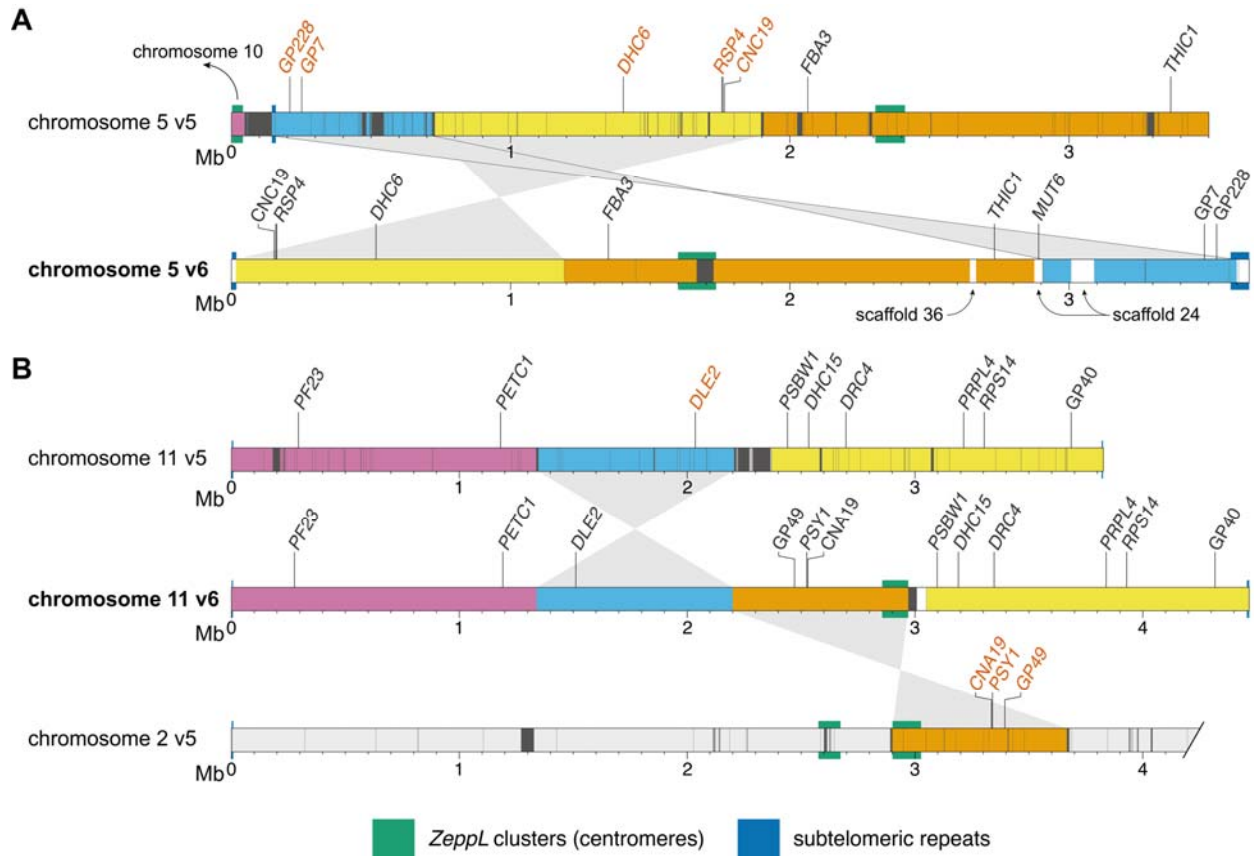


B



376 **Figure 1. The CC-4532 version 6 assembly.**  
377 **(A)** Circos plot (Krzywinski et al. 2009) representation of the CC-4532 v6 genome. Gray outer bands  
378 represent chromosomes, with colors highlighting genomic regions that were assembled on other  
379 chromosomes or unplaced scaffolds in v5. Dark gray regions represent gaps between contigs, with any  
380 gaps <10 kb increased to 10 kb to aid visualization. Outer lines in dark blue represent haplotype 2  
381 regions, including the mating type locus (*MT*) and flanking regions on chromosome 6. All metrics were  
382 calculated for 50-kb windows. Tandem repeats combine microsatellite and satellite annotations. CG  
383 hypermethylated regions were taken from Lopez et al. (2015) and mapped from v5 to v6 coordinates, with  
384 some neighboring regions merged to a single marker in the plot (see Supplemental Figure S2 for all  
385 regions).  
386 **(B)** Linear representation of chromosome 15. Colors are as in **(A)**, with dark gray representing assembly  
387 gaps. Light gray regions were present on chromosome 15 in v5, while white regions are newly assembled  
388 in v6. See Supplemental Dataset S2 for coordinates linking v5 and v6 assembly regions. Marker genes are  
389 from Kathir et al. (2003) and the light green boxes represent the *NCL* gene clusters described by Boulouis  
390 et al. (2015). *CYT1* was previously recorded as *CYTCl*.

391  
392  
393  
394  
395  
396  
397  
398  
399  
400  
401



402  
 403  
 404  
 405  
 406  
 407  
 408  
 409  
 410  
 411  
 412  
 413  
 414  
 415  
 416  
 417  
 418  
 419  
 420  
 421  
 422  
 423

**Figure 2. Version 5 misassemblies and their resolution in version 6.**

Chromosome segments are colored to show the reordering and reorientation of specific regions, and dark gray regions represent assembly gaps. Markers inconsistent with the molecular map of Kathir et al. (2003) are shown in vermillion text. Gene symbols (in italics) were updated where applicable. Note that the plot was made using CC-503 v6 to simplify mapping between versions. CC-503 v6 and CC-4532 v6 are entirely syntenic for chromosomes 5 and 11.

(A) Reassembly of chromosome 5. The purple region was reassigned to chromosome 10. White regions on the v6 chromosome correspond to sequence not assembled on the v5 chromosome (e.g. the region containing *MUT6* corresponds to part of scaffold 24 in v5). In the original map *RSP4* corresponded to the *pf1* marker (and the neighboring *RSP6* to *pf26*, not shown) (Dutcher 2014). Updated gene symbols: *FBA3* was *ALD*, *THIC1* was *THI8*.

(B) Reassembly of chromosome 11; only the first 4.2 Mb of chromosome 2 is shown. Genes that originally corresponded to genetic markers are: *PSY1*, *lts1*; *PF23*, *pf23* (Yamamoto et al. 2017); *DRC4*, *pf2* (Dutcher 2014); *PRPL4*, *ery1*; *RPS14*, *cry1*. Updated gene symbols: *PETC1* was *PETC*, *DLE2* was *VFL2*, *DHC15* was *ODA2*, *PSBW1* was *PSBW*.



424 **Assembly improvements reveal novel genic sequence and hypermethylated**  
425 **centromeres**

426 To assess the functional effect of assembly improvements in CC-4532 v6, we next analyzed the  
427 filled and remaining assembly gaps relative to the gene and repeat landscape of the  
428 *Chlamydomonas* genome. We annotated almost 1,000 filled v5 gaps based on their sequence  
429 context in CC-4532 v6, either as “TE” (~8% of the gaps), “microsatellite” (16%) or “satellite”  
430 (12%) if the novel sequence featured >50% of the corresponding repeat class, “repetitive” (15%  
431 gaps) if the sequence otherwise had >25% repeat content, and “other” (26%) for less repetitive  
432 sequences (Figure 3A). We further classified gaps relative to genic features annotated *de novo* in  
433 CC-4532 v6 (described below), as either entirely intergenic (~19% of the gaps), entirely intronic  
434 (34%) or at least partially exonic (47%) (i.e. the filled sequence featured some novel exonic  
435 sequence). Tandem repeats were associated with nearly four times as many gaps as TEs, despite  
436 covering almost half as much of the genome (Table 1). Furthermore, while 81% of TE-associated  
437 gaps were intergenic, 84% of gaps associated with tandem repeats were within genes (Figure  
438 3A). These results are consistent with the underrepresentation of TEs (Philippsen et al. 2016) and  
439 overrepresentation of tandem repeats (Zhao et al. 2014) in introns, and are consistent with our  
440 own annotation of repeats by site class (Supplemental Dataset S3). The high proportion of genic  
441 gaps supports the study of Tulin and Cross (2016), which identified more than 100 “hidden”  
442 exons by comparing a *de novo*-assembled transcriptome to the v5 assembly. Overall, our results  
443 suggest that prior targeted gap filling was largely successful in assembling intergenic TEs, while  
444 the higher density of intronic tandem repeats precluded the more complete assembly of genic  
445 regions by Sanger and short-read technologies. Finally, 23% of gaps were not filled in v6 but  
446 instead lost redundant sequence from one or both flanks (class “redundant”, Figure 3A).  
447 Approximately half of these cases resulted in the removal of redundant exonic sequence,  
448 providing further potential to improve structural annotation.

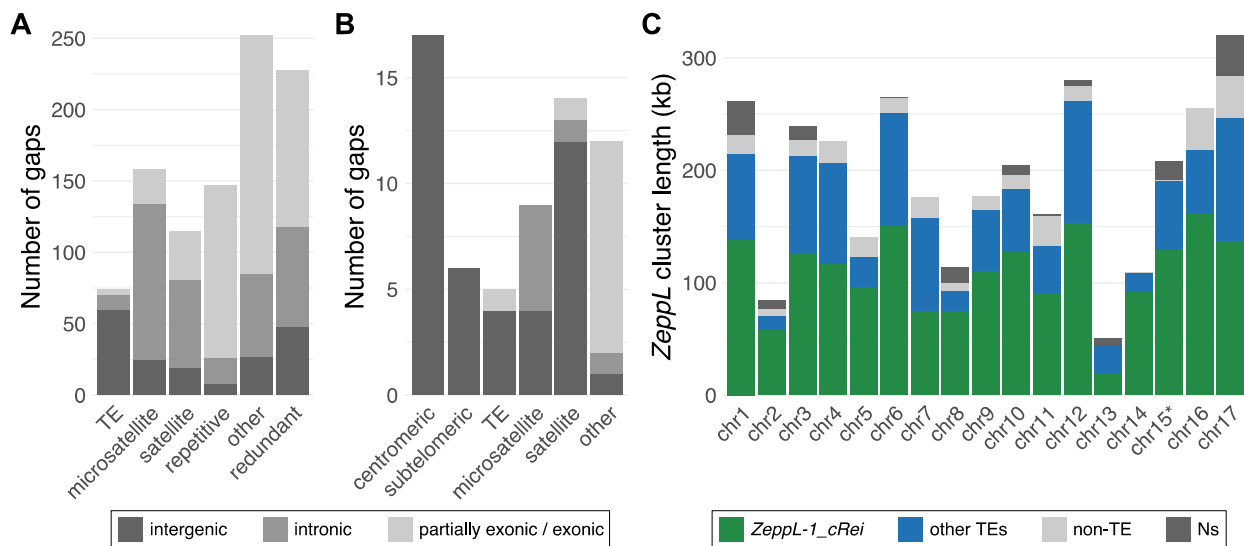
449  
450 The CC-4532 v6 chromosomes still contain 63 gaps that generally coincide with the most  
451 repetitive genomic regions. Approximately one third fall within the putative centromeres and  
452 subtelomeres, with another third accounted for by tandem repeats, especially large satellites  
453 (Figure 3B). Despite the complexity of the repeats present at subtelomeres, 26 of the 34  
454 chromosome termini are capped with telomeric repeats. Among the incomplete termini are the

455 two ribosomal DNA (rDNA) arrays on the right arms of chromosome 8 and 14 (Figure 1A; note  
456 that the chromosome 1 rDNA array is truncated and likely non-functional in laboratory strains,  
457 but potentially not so in field isolates (Chaux-Jukic et al. 2021)). One gap corresponds to the 5S  
458 rDNA array on chromosome 1, while the second 5S rDNA array on chromosome 8 is putatively  
459 complete (Figure 1A). Although approximately half of the microsatellite-associated gaps are  
460 intronic, almost all the remaining repeat-associated gaps are intergenic. Unfortunately, 12 gaps  
461 contain exonic sequence, potentially affecting 18 genes based on comparison to *de novo*  
462 annotation of CC-503 v6 (Supplemental Dataset S4). Most of these gaps are not obviously  
463 repetitive (“other” class, Figure 3B) and will be prime targets for future manual finishing.

464  
465 Following the misassembly corrections, each v6 chromosome features a single localized cluster  
466 of *ZeppL* elements (Figure 1A), except for chromosome 15, where we identified two minor  
467 clusters (~30 kb and 9 kb) downstream of the major cluster. Although most putative centromeres  
468 feature at least one gap, they are not particularly long; by comparison to the CC-1690 assembly,  
469 we estimate that more than 95% of putatively centromeric sequence is assembled in CC-4532 v6  
470 (Figure 3C, Supplemental Dataset S5). Based on the span of *ZeppL* elements, the putative  
471 centromeres range from 51 to 320 kb, with a mean of 192 kb. Approximately 60% of the  
472 sequence is composed of the *ZeppL* element itself, with most of the remaining sequence  
473 contributed by other TEs (Figure 1A and 3C, see also Supplemental Figure S2 for CC-1690),  
474 especially *Dualen* LINEs (Craig et al. 2021a). Satellite DNA does not appear to be a major  
475 component of the clusters (except chromosome 16, Supplemental Dataset S5), although we  
476 observed satellites immediately flanking the clusters on some chromosomes (e.g. 4 and 5,  
477 Supplemental Figure S2). The structure of these regions warrants further study, as does the  
478 localization of centromeric histone H3, which may be encoded by two paralogous genes in  
479 *Chlamydomonas* (Cui et al. 2015).

480  
481 Finally, we revisited the genomic landscape of CG methylation ( $C^5$ -methylcytosine, 5mC) in  
482 *Chlamydomonas*. Lopez et al. (2015) identified 23 hypermethylated loci relative to a genomic  
483 background of very low methylation (<1%). We determined that 19 of the hypermethylated  
484 regions coincide with the putative centromeres on 11 chromosomes, with a further two localizing  
485 to subtelomeres (Figure 1A, Supplemental Figure S2). Chaux-Jukic et al. (2021) called CG

486 methylation directly from Nanopore reads, which facilitates mapping to highly repetitive regions,  
 487 revealing ubiquitous hypermethylation of subtelomeres. Using the same Nanopore dataset (Liu et  
 488 al. 2019), we extended this analysis to the entire CC-1690 assembly and established that all  
 489 putative centromeres are hypermethylated (Supplemental Figure S2). Alongside subtelomeres, a  
 490 few other highly repetitive regions were hypermethylated (e.g. a ~200-kb region on the left arm  
 491 of chromosome 12), while we observed many more localized methylation peaks of smaller  
 492 magnitude. Presumably, these regions were previously overlooked due to the limitations of  
 493 mapping short-read bisulfite sequencing data to repeats and the incompleteness of the most  
 494 repetitive regions in v5. Strenkert et al. (2022) reported an atypical chromatin architecture for the  
 495 previously identified hypermethylated regions, suggesting that the hypermethylated centromeres,  
 496 subtelomeres, and potentially some other repeat-rich islands, may constitute heterochromatin in  
 497 *Chlamydomonas*.



498  
 499 **Figure 3. Filled gaps and the remaining assembly challenges in CC-4532 version 6.**  
 500 (A) Repeat classification of v5 gaps filled in CC-4532 v6. Bars are split into entirely intergenic gaps,  
 501 entirely intronic gaps and gaps with at least partial exonic overlap. See main text for details of gap  
 502 definitions by repeat class.  
 503 (B) Classification of the remaining gaps in CC-4532 v6, shading follows (A). “Other” gaps were  
 504 associated with other repeat types (e.g. large duplications) or were not clearly associated with repeats.  
 505 (C) Summary of the length of putative centromeric *ZeppL* clusters. Colors represent the number of bases  
 506 annotated as *ZeppL-1\_cRei* (the only *ZeppL* family in *Chlamydomonas*), any other TE, non-TE sequence,  
 507 and assembly gaps (Ns). Note that chromosome 15 contains two short *ZeppL* clusters downstream of the  
 508 main cluster (Supplemental Dataset S5), which are not shown.

509  
 510  
 511

512

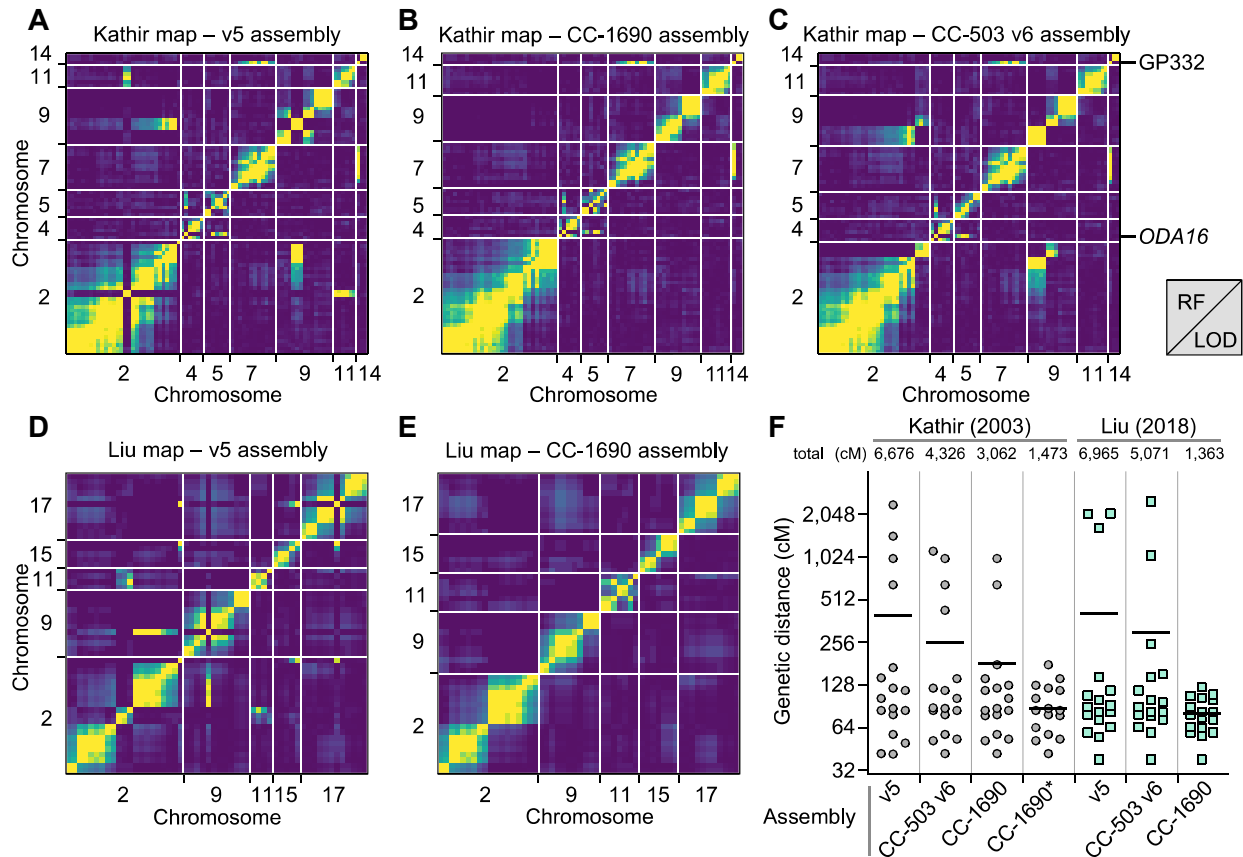
### 513 **Linkage data validates the CC-1690 and version 6 assemblies**

514 To systematically validate the improvements between v5 and v6, we turned to two independent  
515 genetic recombination datasets. We primarily compared v5 to the CC-1690 assembly, since CC-  
516 1690 was used as a reference to scaffold the v6 assemblies, and the CC-1690 and CC-4532 v6  
517 assemblies are entirely syntenic. We repeated these analyses using CC-503 v6 following the  
518 discovery of outstanding inconsistencies in this assembly. We first identified the v5  
519 chromosomal coordinates of 239 molecular markers described by Kathir et al. (2003)  
520 (Supplemental Dataset S6). We then ordered the genotype data used to generate the genetic map  
521 based on the v5 coordinates before estimating a new genetic map with the R/QTL package  
522 (Broman et al. 2003). To assess the concordance between assigned and true genomic positions,  
523 we visualized recombination frequencies between marker pairs: two unlinked markers should  
524 exhibit random segregation and appear as dark blue squares (low log of the odds [LOD] score),  
525 whereas linked markers should appear in yellow. While most markers agreed with their v5  
526 chromosomal locations, we identified 10 misplaced markers, eight of which mapped to  
527 chromosomes 2 or 9 (Figure 4A, Supplemental Figure S3). Markers CNA19 and GP49 were  
528 located on chromosome 2 in v5, but showed strong linkage with chromosome 11. Satisfyingly,  
529 both markers relocated to chromosome 11 in CC-1690 (Figure 4B) and subsequently in both v6  
530 assemblies (Figure 2B). We also resolved the genomic location of most other mismatched  
531 markers when using CC-1690 coordinates. Conversely, inconsistencies remained between  
532 chromosomes 2 and 9 when using the CC-503 v6 coordinates (Figure 4C), which as detailed  
533 below stems from a putative chromosomal rearrangement unique to CC-503. The two further  
534 misplaced markers remained apparently wrongly assigned when using CC-1690 or CC-503 v6  
535 coordinates: GP332 and *ODA16*, which were assigned to the top of chromosome 14 and 4,  
536 respectively, in both assemblies. The genetic mapping data indicated strong linkage between  
537 GP332 and chromosome 7 markers (*CNC43*, *CHL27A* and *GLTR1*), and between *ODA16* and  
538 chromosome 5 markers (*DHC6*, *CNC19* and *RSP6* – see Figure 2A). In both cases, the chance of  
539 the regions corresponding to these sequences being misassembled in the exact same location on  
540 independent contigs in CC-1690, CC-4532 v6 and CC-503 v6 is negligible, and their previous  
541 mapping locations or associated sequences are presumably incorrect.

542

543  
544  
545  
546  
547  
548  
549  
550  
551  
552  
553  
554  
555  
556  
557  
558  
559  
560  
561  
562  
563  
564  
565  
566  
567  
568  
569  
570  
571  
572  
573

We followed the same steps to generate a genetic map from whole-genome resequencing data of tetrads derived from crosses between two Quebec field isolates (Liu et al. 2018). We reduced the data to keep only single nucleotide polymorphisms (SNPs) that were informative of haplotype transitions (164 SNPs). Again, the deduced recombination map largely agreed with v5 chromosomal positions, except for 14 SNPs, eight of which had been wrongly assigned to chromosome 2 (Figure 3D). The CC-1690 genomic coordinates corrected all mismapping (Figure 4E) and greatly reduced the overall length of the genetic map, from over 6,000 cM using v5 coordinates to ~1,400 with CC-1690 coordinates (Figure 4F). As with the molecular markers, any discordance between CC-1690 and CC-503 v6 mapped to the putative rearrangement affecting chromosomes 2 and 9. We therefore conclude that CC-1690, and thus the v6 assemblies, receives strong recombination support from two independent mapping datasets, which were derived from a laboratory strain (CC-1690) and diverse field isolates (CC-1952 in one case, CC-2935 and CC-2936 in the other). It is now expected that the order and orientation of chromosomal sequence in the CC-1690, CC-4532 v6 and CC-503 v6 assemblies represents the biological reality for these strains.



575

#### 576 **Figure 4. Validation of the *Chlamydomonas* genome reassemblies by recombination maps.**

577 **(A)** Partial plot of recombination frequencies between molecular markers from Kathir et al. (2003).  
 578 Strong linkage is indicated by a yellow color; absence of linkage is shown as dark blue.

579 **(B, C)** Partial recombination frequency plots between the same molecular markers with updated genomic  
 580 coordinates according to the CC-1690 **(B)** or CC-503 v6 **(C)** assembly. Note that the markers GP332 and  
 581 *ODA16* are consistently mismapped.

582 **(D, E)** Partial recombination frequency plots between informative SNPs extracted from Liu et al. (2018),  
 583 when using the genomic coordinates from the v5 **(D)** or CC-1690 **(E)** assemblies. RF, recombination  
 584 fraction; LOD, logarithm of the odds.

585 **(F)** Gradual improvement of the estimation of genetic map length, from v5, to CC-503 v6, to CC-1690.  
 586 Chromosome lengths are plotted in cM for each increment of the genetic maps. CC-1690\* denotes the use  
 587 of CC-1690 genomic coordinates with the removal of the GP332 and *ODA16* molecular markers from the  
 588 analysis. Total map length, in cM, is listed above each dot plot. Horizontal bar, mean.

589

590

591

592

593

594

595

596 **The CC-503 genome is unstable and harbors major structural mutations**

597 Following the discovery of remaining inconsistencies between CC-503 v6 and the CC-4532 v6  
598 and CC-1690 assemblies, we set out to characterize structural mutations in the CC-503 genome.  
599 This endeavor was possible since the three assemblies feature the same ancestral haplotype over  
600 most of their genomes, meaning that any variant segregating uniquely in CC-503 could be  
601 attributed to mutation arising in the laboratory, potentially as a result of historic mutagenesis.

602

603 The most conspicuous mutation affected chromosomes 2 and 9. Indeed, these chromosomes were  
604 misassembled in all past versions, and changes that occurred between v4 and v5 were noted  
605 previously (Lin et al. 2013). In v5, the aberration was misassembled as a complex translocation  
606 that would have involved at least five DSBs (Figure 5A). This mistake presumably occurred due  
607 to conflicting evidence between contig assembly, based on mutant-state CC-503 sequencing  
608 reads, and longer range scaffolding based on wild-type linkage data from other laboratory strains  
609 and field isolates. Via manual inspection of the CC-503 v6 contigs, we inferred that  
610 chromosomes 2 and 9 have instead experienced a putative reciprocal translocation, with an  
611 inversion affecting part of the fragment translocated from chromosome 2 to 9 (Figure 5B). This  
612 model posits three DSBs, one on chromosome 9 (DSB2 between purple and vermilion, Figure  
613 5B) and two on chromosome 2 (DSB1 between blue and green, and DSB3 green and orange).  
614 The 0.9-Mb inversion shares DSB1 with the translocation event, suggesting that all three DSBs  
615 occurred, and were subsequently misrepaired, simultaneously. Notably, all DSBs and their repair  
616 events were associated with insertions and deletions (InDels), ranging from a few bp to 1,950 bp,  
617 and all were predicted to disrupt coding sequence relative to the CC-4532 *de novo* structural  
618 annotations (Supplemental Figure S4). For example, the deletion at DSB2 entirely removed the  
619 second exon of a gene (Cre09.g390100) encoding a 318-amino acid (aa) protein with an *S*-  
620 adenosylmethioine-dependent methyltransferase domain, with the remaining (and presumably  
621 pseudogenized) exons now split between the derived chromosomes 2 and 9 in CC-503 v6  
622 (Supplemental Figure S5). Illumina resequencing data from CC-125 (the progenitor of CC-503)  
623 mapped across the deletions at each DSB (Supplemental Figure S6), confirming that the  
624 mutation is unique to CC-503.

625

626

627 Remarkably, we identified 71 additional structural mutations (i.e. >50 bp) present in CC-503 v6  
628 and absent in CC-4532 v6 and CC-1690, putatively affecting 103 genes (Supplemental Dataset  
629 S7). This number excludes TEs, which are presented separately below. In full, we called 63  
630 deletions (cumulatively 302.1 kb and including events >10 kb), six duplications, one insertion  
631 and one inversion. Many of the mutations were complex, for example the duplications were often  
632 associated with InDels and inversions. One of the most striking mutations was a ~508-kb  
633 inversion between 0.81 and 1.32 Mb on chromosome 16 (Figure 5C). Inspection of the two  
634 DSBs and their subsequent repair revealed that this event is an unusual dupINVdup (duplication-  
635 inversion-duplication) mutation (Brand et al. 2015), in which both flanks (3.7 kb to the left and  
636 2.3 kb to the right) of the unique inverted sequence are duplicated and themselves inverted.  
637 Genic sequence was disrupted and partially duplicated at both flanks (Figure 5C). Surprisingly,  
638 the inverted region itself harbored a 47-kb deletion that partially or fully deleted 10 genes  
639 (Supplemental Dataset S7).

640

641 Although it is tempting to directly attribute the exceptional number of structural mutations in  
642 CC-503 to its past mutagenesis with MNNG (Hyams and Davies 1972), we unexpectedly  
643 observed that 46 of the 72 structural mutations were not present in past assembly versions  
644 (Supplemental Dataset S7), including the chromosome 16 dupINVdup/deletion. Previous  
645 assemblies were primarily based on Sanger sequencing from the initial genome project, while the  
646 v6 PacBio sequencing was performed on a CC-503 culture obtained from the Chlamydomonas  
647 Resource Center by Gallaher et al. (2015). Given that many of the mutations are shared between  
648 past versions and CC-503 v6, some of which are very distinctive (e.g. the reciprocal  
649 translocation described above), the more recently acquired culture undoubtedly shares a clonal  
650 common ancestor with that used in the original genome project. It therefore appears that  
651 approximately two thirds of the structural mutations have occurred over the past two decades,  
652 and that the CC-503 genome may be unstable. Two main lines of evidence support this  
653 hypothesis. First, in a reciprocal analysis we discovered only 10 structural mutations unique to  
654 CC-4532 v6 (Supplemental Dataset S8, see below) and no large rearrangements in CC-1690,  
655 suggesting an elevated rate of chromosomal aberrations in CC-503. Second, many of the  
656 mutations were complex and featured large InDels or duplications at their repair points,



657 potentially indicating a deficiency in DSB repair. High rates of deletions, duplications and  
658 rearrangements have recently been documented in the *Chlamydomonas* field isolate CC-2931,  
659 however this was partly attributed to TE activity and similar patterns of mutational complexity at  
660 repair points were not observed (López-Cortegano et al. 2022).

661  
662 We attempted to find candidate loci for genomic instability by examining each gene affected by  
663 a mutation that was common to CC-503 v6 and all past assembly versions, under the assumption  
664 that these mutations could have originated during mutagenesis, or at least prior to the initial  
665 genome project. We identified a *RecQ* helicase gene (Cre16.g801898) as a possible candidate,  
666 which was fully deleted in CC-503 as part of a 48-kb deletion on chromosome 16 that partially  
667 or fully deleted at least six genes (note that this is unrelated to the chromosome 16 deletion  
668 described above, see Supplemental Dataset S7). *RecQ* helicases have been referred to as  
669 “guardians of the genome” and play key roles in genome maintenance and all DSB repair  
670 pathways in humans (Croteau et al. 2014; Lu and Davis 2021). Many eukaryotes possess  
671 multiple *RecQ* helicase genes that belong to ancient gene families, with five genes in human and  
672 seven in *Arabidopsis* (Dorn and Puchta 2019). We performed a phylogenetic analysis including  
673 the protein encoded by the deleted gene Cre16.g801898 and homologous proteins in algae and  
674 plants, which demonstrated that Cre16.g801898 encodes a putative ortholog of the plant *RecQ3*  
675 subfamily (Figure 5D), which is homologous to human RECQ-LIKE HELICASE 5 (RECQL5)  
676 (Wiedemann et al. 2018). Furthermore, the *RecQ3* subfamily is present across Archaeplastida  
677 (the green lineage plus red algae and glaucophytes). Interestingly, our analysis also revealed a  
678 green algal-specific subfamily, *RecQ3-like*, which formed a clade with the canonical *RecQ3*  
679 subfamily (Figure 5D). All analyzed species from the Chlorophyceae and Trebouxiophyceae had  
680 both *RecQ3* and *RecQ3-like* subfamily genes, indicating strong conservation. However, the  
681 *RecQ3* subfamily appeared to be absent in prasinophytes (e.g. *Micromonas* spp.) and ulvophytes  
682 (*Caulerpa lentillifera* and *Ulva mutabilis*). Such a deep evolutionary division between the *RecQ3*  
683 and *RecQ3-like* subfamilies is roughly analogous to the plant-specific *RecQsim* subfamily,  
684 which forms a clade with the eukaryotic *RecQ6/WRN* group (Wiedemann et al. 2018).

685  
686 The specific functions of *RecQ* helicases have not been studied in green algae and it is difficult  
687 to draw parallels with other species, since the evolution of *RecQ* helicases is dynamic in many

688 lineages. Certain plants have lost specific subfamilies and duplicated others e.g. the moss  
689 *Physcomitrium patens* has no *RecQ1* or *RecQ3* genes but two *RecQsim* paralogs, and  
690 *Arabidopsis* lacks a *RecQ6* gene but has two *RecQ4* paralogs. All subfamilies appear to be  
691 represented in *Chlamydomonas*, although only a mutant of the *RecQ5* subfamily gene  
692 (Cre15.g634701; homologous to human *RECQL4*), which is unable to undergo cell division, has  
693 been described (Tulin and Cross 2014). These findings suggest that neo- and  
694 subfunctionalization may occur in RecQ helicase evolution and that orthologous proteins may  
695 not have identical functions in different species. In humans, *RECQL5* downregulation results in  
696 genomic instability and chromosomal rearrangements, and *recql5* mutants are associated with  
697 tumorigenesis (Lu and Davis 2021). However, *Arabidopsis recq3* mutants were viable and had  
698 no growth abnormalities, although this observation does not rule out longer term genomic  
699 instability (Röhrig et al. 2018). It remains to be seen if the deletion of *RECQ3* in  
700 *Chlamydomonas* can explain the genomic instability of CC-503, and it will likely never be  
701 known if this specific deletion was caused by mutagenesis or arose later in culture.

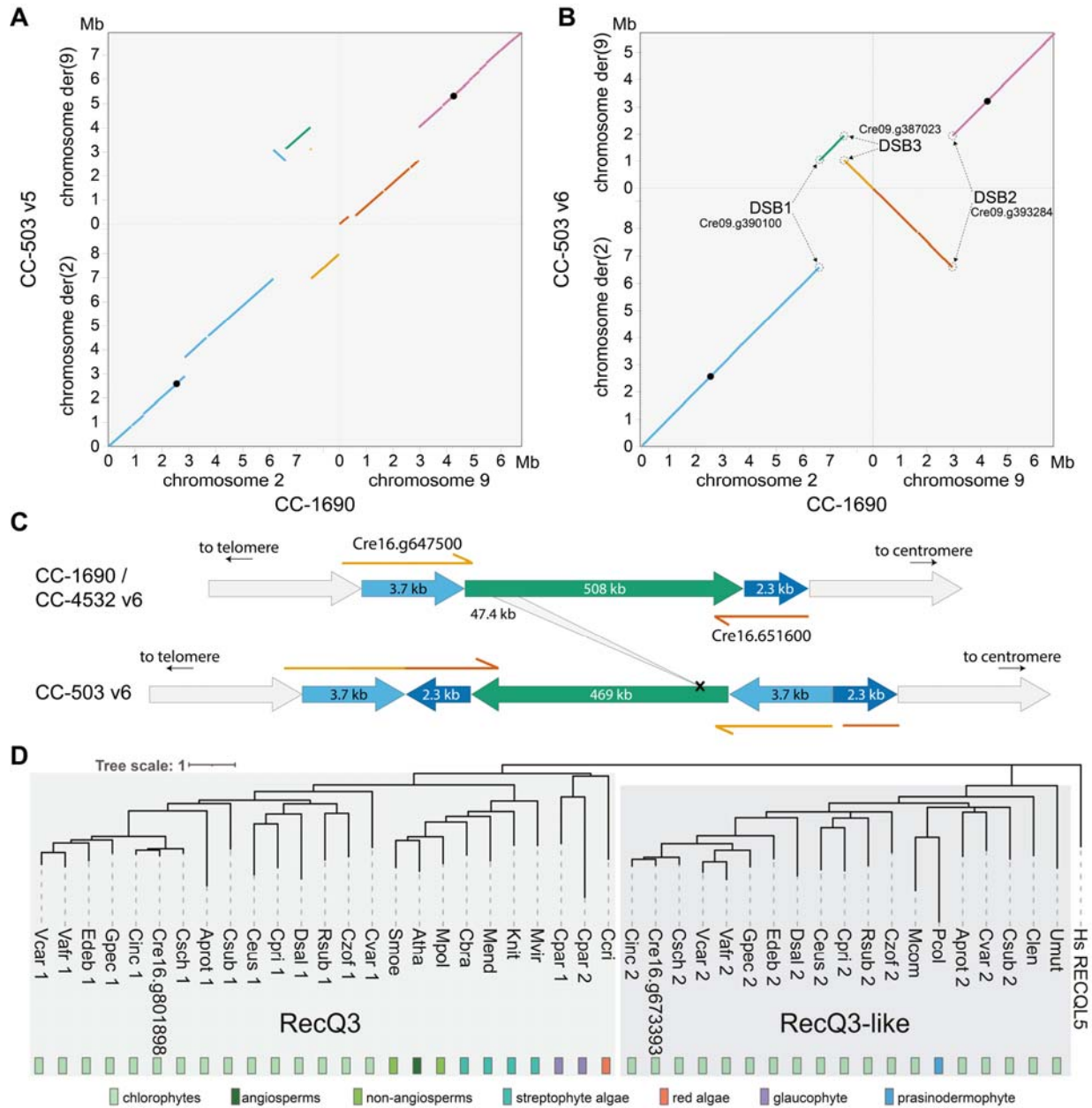
702

703 Finally, we also identified a candidate for the cell wall-less phenotype. A 6.0-kb deletion on  
704 chromosome 1 almost entirely removed a putative prolyl 4-hydroxylase (*P4H*) gene  
705 (Cre01.g800047; Supplemental Figure S7). P4Hs catalyze the formation of 4-hydroxyproline  
706 (Gorres and Raines 2010), a major post-translational modification of the hydroxyproline-rich  
707 glycoproteins (HRGPs) that comprise the *Chlamydomonas* cell wall (Woessner and Goodenough  
708 1994; Sumper and Hallmann 1998). The *Chlamydomonas* genome encodes more than 20  
709 putative P4Hs, and although their specific roles are generally unknown, *P4Hs* have different  
710 patterns of expression and are unlikely to be redundant. Keskiaho et al. (2007) showed that the  
711 knockdown of *P4H-1* (now annotated as *PFH12*; Cre03.g160200), was sufficient to induce  
712 abnormal cell wall assembly. Notably, the deleted gene in CC-503 has one paralog, *PFH5*  
713 (Cre01.g014650; encoding a protein sharing 76% aa identity with Cre01.g800047), immediately  
714 downstream that appears to be intact, although its regulation may be affected by the deletion. It is  
715 therefore unclear whether the loss of Cre01.g800047 can be responsible for the *cw* phenotype  
716 alone. Indeed, as introduced, more than one mutation may underlie the loss of the cell wall  
717 (Davies 1972; Hyams and Davies 1972).

718

719

720  
721  
722  
723  
724  
725



726  
727  
728  
729  
730  
731  
732

**Figure 5. Structural mutations in the CC-503 version 6 genome.**

(A, B) Dotplot representation of chromosomes 2 and 9 between v5 and CC-1690 (A), and CC-503 v6 and CC-1690 (B). Colors link fragments between panels (A) and (B). Black circles represent putative centromeres. CC-503 chromosomes are named as derivatives (der) based on their centromeres. Genes disrupted by DSBs are labeled.

733 (C) Schematic diagram of the dupINVdup and deletion double mutation. The duplicated flanks (light and  
734 dark blue) are shown 50x the scale of the main inverted fragment (green). Disrupted and partly duplicated  
735 genes are labeled. The left flank is predicted to have formed a gene fusion in CC-503 v6.1, although this  
736 is entirely based on ab initio prediction. The 47.4-kb internal deletion is represented by the gray ribbon.  
737 (D) Protein-based phylogeny of the RecQ3 and RecQ3-like subfamilies of RecQ helicases in  
738 Archaeplastida. Branches with bootstrap values <50% were removed. Full species names and protein IDs  
739 can be found in Supplemental Dataset S9.

740

### 741 **Major duplications and insertions in the CC-4532 genome**

742 We also identified 10 non-TE structural mutations unique to CC-4532 v6 and absent in CC-503  
743 v6 and CC-1690, predicted to disrupt eight genes (Supplemental Dataset S8, Supplemental  
744 Figure S8). The largest mutations were both duplications, of 24.5 kb on chromosome 3 and 89.1  
745 kb on chromosome 12, which together caused the duplication of 17 complete genes. Using a  
746 coverage-based approach, Flowers et al. (2015) inferred the presence of several large  
747 duplications among various laboratory strains, hinting that duplications may be an important  
748 source of laboratory mutation. Interestingly, three gene-disrupting insertions in CC-4532 v6  
749 consisted entirely of a satellite, *MSAT-11\_cRei*, ranging from ~8 kb to >19 kb (two caused  
750 assembly gaps and their full length is unknown). For example, one insertion interrupted the first  
751 exon of a gene possibly encoding nicotinate phosphoribosyltransferase (Cre03.g188800),  
752 catalyzing the first step of the nicotinamide adenine dinucleotide (NAD) salvage pathway.  
753 *MSAT-11\_cRei* arrays consist of a 1.9-kb tandemly repeated monomer and are present on  
754 chromosomes 7 and 12 in all three available genomes, with two additional unique insertions in  
755 CC-1690 (not shown). Similarly, *MSAT-11\_cRei de novo* insertions have been observed in  
756 experimental lines of the field isolate CC-2931 (López-Cortegano et al. 2022). There are very  
757 few observations of *de novo* satellite dissemination and its mechanisms are generally unclear  
758 (Ruiz-Ruano et al. 2016), although rolling circle replication and reinsertion via  
759 extrachromosomal circular DNA intermediates has been proposed (Navrátilová et al. 2008).  
760 Collectively, these results suggest that all laboratory strains may harbor at least a small number  
761 of gene-disrupting structural mutations relative to the ancestral wild type.

762

### 763 **Transposable element proliferation in the laboratory and the strain history of 137c**

764 We next aimed to characterize the extent of TE activity in the CC-503 v6 and CC-4532 v6  
765 genomes. We identified 26 TE insertions unique to CC-503 v6 (nine of which were absent in v5,  
766 suggesting recent activity; Supplemental Dataset S10) and 109 insertions unique to CC-4532 v6  
767 (Supplemental Dataset S11, Supplemental Figure S8), which collectively involved 14 different

768 TE families. Remarkably, 86 of the 109 CC-4532 v6 insertions were of the same 15.4-kb *Gypsy*  
769 long terminal repeat (LTR) retrotransposon (*Gypsy-7a\_cRei*, Figure 6A), adding ~1.3 Mb of  
770 unique sequence (all TE insertions ~1.4 Mb). Together with the large duplications and insertions  
771 described above, these TE insertions were responsible for the expanded length of the CC-4532  
772 v6 assembly, which is more than 1% longer than CC-1690 (Table 1). *Gypsy-7a\_cRei* has not  
773 previously been reported as active, and we identified no insertions in CC-503 v6, where the  
774 element is present as only one partial and two full-length ancestral copies. Only 10 of the 86  
775 insertions were predicted to disrupt coding sequence (in some cases breaking the annotated gene  
776 model, Supplemental Dataset S11), and we observed intergenic insertions 2.6 times more  
777 frequently than expected by chance. *Gypsy-7a\_cRei* may have a mechanism of targeted insertion,  
778 or genic insertions may have been selected against in the laboratory. The *Gypsy-7a\_cRei* Gag-  
779 Pol polyprotein contains a plant homeodomain (PHD) finger, an accessory domain found in  
780 several *Chlamydomonas* TEs (Perez-Alegre et al. 2005; Craig 2021) that may be involved in  
781 chromatin remodeling to minimize deleterious insertions (Kapitonov and Jurka 2003).  
782 Nonetheless, intergenic insertions may still affect gene expression, and we observed 10  
783 insertions into introns and 25 into untranslated regions (UTRs), including the 3' UTR of *TUB2*,  
784 the gene encoding beta-tubulin.

785  
786 We next used whole-genome resequencing data (Gallaher et al. 2015) to test whether *Gypsy-*  
787 *7a\_cRei* is active in any other laboratory strains. We analyzed 14 laboratory strains, including the  
788 oldest extant strains (CC-124, CC-125, CC-1009, CC-1010, CC-1690, and CC-1691) that are  
789 parental to all laboratory strains. Insertions were identified by extracting read pairs where one  
790 read mapped uniquely to a non-repetitive genomic region and the other mapped to *Gypsy-*  
791 *7a\_cRei* (see Supplemental Dataset S12 for insertion coordinates). This approach retrieved 68 of  
792 the 86 *Gypsy-7a\_cRei* insertions in CC-4532 v6, the difference being attributable to insertions  
793 occurring in the ~8 years between the Illumina and PacBio sequencing, or the inability to call  
794 insertions in repetitive regions (e.g. centromeres, see Supplemental Figure S8). All strains carry  
795 two to four ancestral *Gypsy-7a\_cRei* copies, depending on their proportions of haplotype 1 and 2  
796 (collectively three copies in haplotype 1 and one in haplotype 2). Six of the fourteen strains (CC-  
797 124, CC-503, CC-620, CC-1690, CC-1009, CC-1010) had only these ancestral loci, despite  
798 being propagated for over seven decades, suggesting that *Gypsy-7a\_cRei* is largely quiescent.

799 However, in a few strains, particularly those descended from 137c+, we observed massive  
800 expansions of *Gypsy-7a\_cRei*, like that in CC-4532. Indeed, CC-125, the linear descendant of  
801 137c+, had the most novel insertions of any strain (83, Figure 6B). This result was unexpected,  
802 since there are no new insertions in CC-503, which was derived from 137c+ by mutagenesis, and  
803 no insertions in CC-620, another direct descendent of 137c+. CC-4532 shared 19 of its 68  
804 laboratory insertions with CC-621 (Figure 6B), which corroborates our understanding that CC-  
805 4532 and CC-621 are both subclones of NO– from Ursula Goodenough that have been separated  
806 by at least three decades. Strains CC-4286 and CC-4287 also had some shared and unique  
807 insertions relative to CC-4532 and CC-621, indicating shared ancestry.

808  
809 We attempted to reconcile the distribution of the *Gypsy-7a\_cRei* insertions with described strain  
810 histories (Pröschold et al. 2005; Gallaher et al. 2015), which is presented as the proposed strain  
811 history in Figure 6C. Since all insertions were unique to CC-125, we hypothesize that *Gypsy-*  
812 *7a\_cRei* became active in the 137c+ culture that became CC-125 after being separated from the  
813 cultures that became CC-503 and CC-620, which occurred several decades ago. *Gypsy-7a\_cRei*  
814 became active independently in a strain from the laboratory of Ursula Goodenough (NO–/CC-  
815 621) that was produced by crossing 137c+ and unknown strains, and it remains active and  
816 continues to expand in strains derived from NO–, e.g. CC-4286 and CC-4287 from Paul  
817 Lefebvre and CC-4532 from Sabeeha Merchant. A third reactivation of *Gypsy-7a\_cRei* likely  
818 occurred in Ruth Sager's 6145 strain, which eventually became CC-1691. This event contributed  
819 novel insertions to strain D66+ (CC-4425), which in turn contributed a single laboratory  
820 insertion to Martin Jonikas' strain, CC-4533. This last strain, the parental strain of the  
821 Chlamydomonas Library Project (CLiP), may represent a fourth reactivation of *Gypsy-7a\_cRei*  
822 (or an increase in transposition frequency), since it carries 21 private insertions despite being  
823 separate from CC-4425 by approximately a decade.

824  
825 Aside from *Gypsy-7a\_cRei*, the most active TE family was *MRC1*, with 17 insertions in CC-503  
826 v6 and 16 insertions in CC-4532 v6 (Supplemental Datasets S10 and S11). *MRC1* was originally  
827 described as a non-autonomous LTR element (Kim et al. 2006), however we recently reclassified  
828 it as a non-autonomous *Chlamys Penelope*-like element (Craig et al. 2021b). Gallaher et al.  
829 (2015) and Neupert et al. (2020) reported activity of *MRC1*, and it may generally be one of the  
830 most active TEs in the laboratory. We identified four active DNA transposons that have been

831 described previously, namely one insertion each of *Gulliver* (Ferris 1989), *Tcr1* (Schnell and  
832 Lefebvre 1993) and *Tcr3* (Wang et al. 1998) (*hAT*, *Kyakuja* and *EnSpm* superfamilies,  
833 respectively), and three insertions of the non-autonomous *hAT* family *Bill* (Kim et al. 2006). The  
834 eight remaining TEs have only been described in Repbase (Bao et al. 2015) or the more recent  
835 Chlamydomonas TE library (Craig 2021).

836

837 Taken collectively, these results suggest that TE activity between laboratory strains can be highly  
838 heterogenous, with the potential for rapid TE proliferation to cause significant increases in  
839 genome size and to disrupt genic sequence. Indeed, serendipitous or screened-for TE insertions  
840 have caused several informative Chlamydomonas mutants (e.g. Moseley et al. (2002); Helliwell  
841 et al. (2015)) and led to the discovery of many of the TEs active in laboratory strains. It is  
842 presently unclear why suppression of *Gypsy-7a\_cRei* is unstable in certain strains, and why this  
843 family exhibits a far higher transposition frequency than other active TEs upon activation.  
844 Similar copy number variation among laboratory strains has been reported for the  
845 nonautonomous DIRS retrotransposon *TOCI* (Day et al. 1988), although curiously we did not  
846 find any *de novo* insertions of this element in CC-503 v6 nor CC-4532 v6. Given the wealth of  
847 transcriptomics data available, it would be interesting to explore expression patterns of *Gypsy-*  
848 *7a\_cRei* and other TE genes under various stress and culture conditions. It is possible that certain  
849 avoidable conditions induce transposition, as has been documented elsewhere e.g. temperature-  
850 sensitive TEs in *V. carteri* (Ueki and Nishii 2008) and Arabidopsis (Ito et al. 2011).

851

852

853

854

855

856

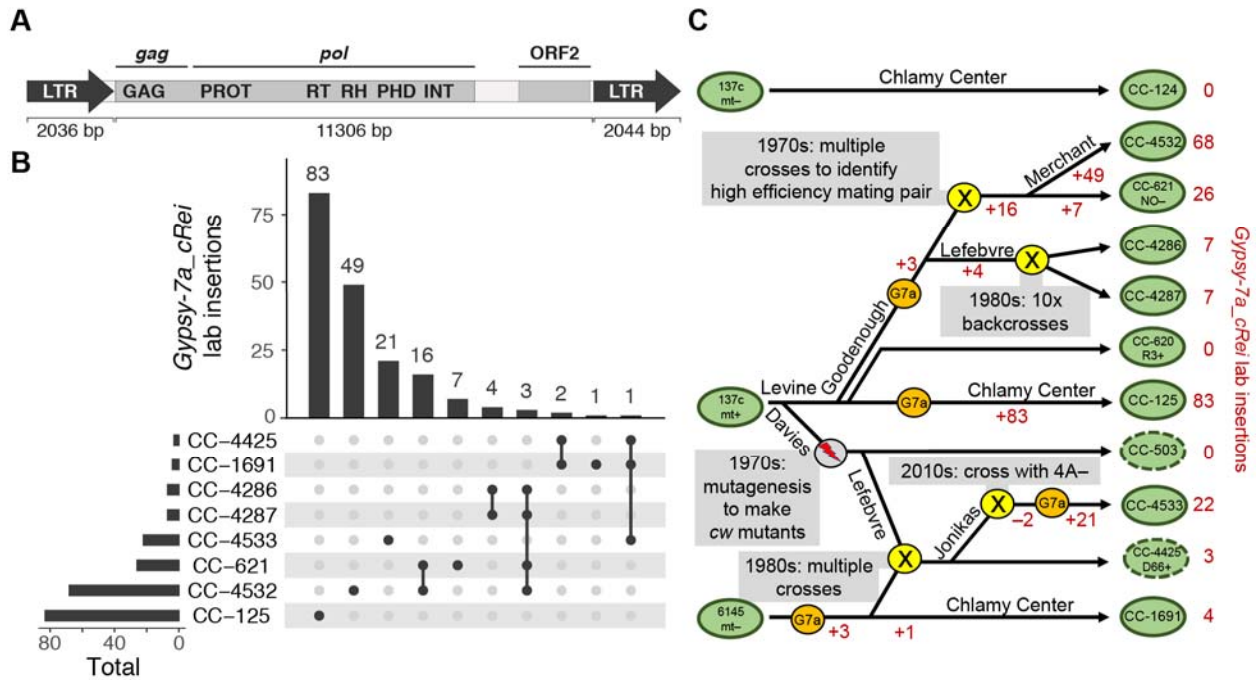
857

858

859

860

861



863

864 **Figure 6. *Gypsy-7a\_cRei* insertions and the strain history of 137c+.**

865 (A) Structure of the 15.4-kb *Gypsy* LTR retrotransposon. LTR subparts are shown as block arrows, note  
 866 that the left LTR is missing the final 8-bp of the right LTR. The two ORFs are highlighted within the  
 867 11.3-kb internal section and the *gag* and *pol* sections of the polyprotein are highlighted. Protein domains:  
 868 GAG, group-specific antigen; PROT, pepsin-like aspartate protease; RT, reverse transcriptase; RH,  
 869 RNase H; PHD, plant homeodomain finger; INT, integrase.

870 (B) Upset plot (Lex et al. 2014) showing the number of shared and strain-specific laboratory insertions of  
 871 *Gypsy-7a\_cRei* in select laboratory strains. Ancestral copies of *Gypsy-7a\_cRei* are excluded.

872 (C) Schematic diagram representing a putative strain history of several inter-related laboratory strains.  
 873 Presented is the most parsimonious interpretation of the shared and independent insertions (B) coupled  
 874 with known strain histories. Green ovals represent strains as indicated, with a dashed line indicating cell  
 875 wall defective strains. A gray circle indicates the MNNG mutagenesis that produced *cw* mutants. Yellow  
 876 circles indicate crosses as labeled. Orange circles indicate likely activation of *Gypsy-7a\_cRei* (“G7a”).  
 877 Changes in the net number of *Gypsy-7a\_cRei* loci due to addition by retrotransposition (+) or loss during  
 878 crossings (–) are indicated in red. The names of several key Chlamydomonas researchers (R.P. Levine,  
 879 D.R. Davies, U.W. Goodenough, P.A. Lefebvre, S.S. Merchant) are indicated where relevant.

880

881

882

883

884

885

886

887



## 888 **Version 6 structural annotations**

889 We annotated both the CC-4532 v6 and CC-503 v6 assemblies *de novo*, incorporating Iso-Seq  
890 data, more than 500 Gb of RNA-seq data, and protein homology from the growing number of  
891 green algal structural annotations. Notably, more than 1.6 billion strand-specific 150-bp RNA-  
892 seq read pairs were introduced from the JGI Gene Atlas ([https://phytozome-  
893 next.jgi.doe.gov/geneatlas/](https://phytozome-next.jgi.doe.gov/geneatlas/)), which assessed gene expression under 25 conditions. We predicted  
894 gene models using several annotation tools, with the model receiving the best support from  
895 transcriptomic and protein homology evidence retained in cases of redundancy. Focusing on CC-  
896 4532 v6, we then made several further improvements (see below) to the *de novo* gene models to  
897 arrive at the final CC-4532 v6 annotation, named CC-4532 v6.1, featuring 16,801 protein-coding  
898 genes (Table 2). The number of predicted alternative transcripts also increased more than eight-  
899 fold relative to v5.6. Dedicated analyses will be required to validate these new isoforms (see  
900 Labadorf et al. (2010); Raj-Kumar et al. (2017)). One highlight of the annotations was that the  
901 longest transcripts overlap for 29% of adjacent genes, 64% of which are on opposite strands (see  
902 examples in Figure 7). While the longest transcripts may not always be the most abundant, this  
903 result nevertheless speaks to the compactness of the genome. Overlapping models were  
904 essentially absent from v5.6 (1% of neighboring genes) and were made possible by Iso-Seq  
905 support, and the present count may be an underestimate since these data do not cover all genes.  
906 Although poorly characterized, overlapping genes are a feature of many eukaryotes (Wright et al.  
907 2022) and can be widespread in the most compact genomes (Williams et al. 2005). This result  
908 may have important implications for understanding gene regulation in *Chlamydomonas*.

909

910 Since so many of the v5 assembly gaps were within genes, the assembly improvements provided  
911 considerable potential to improve gene models. Highlighted by Tulin and Cross (2016) as a gene  
912 featuring “hidden exons”, *PARALYZED FLAGELLA 20 (PF20)* encodes a 606-aa protein  
913 important for cilia function (Smith and Lefebvre 1997). The filling of a v5 assembly gap in *PF20*  
914 resulted in the correction of the gene model in CC-4532 v6.1, adding three new exons (exons 9,  
915 10 and 11 in CC-4532 v6.1) and shifting the 3’ splice site of exon 8 (Figure 7A). A second  
916 example is the putative metal ion transporter *NATURAL RESISTANCE-ASSOCIATED*  
917 *MACROPHAGE PROTEIN 2 (NRAMP2)*, which featured two gaps in v5 that were both  
918 classified as “redundant” in our prior analysis. While one “gap” duplicated only 26 bp of intronic

919 sequence, the second duplicated exons 10 and 11 fortuitously maintained the reading frame and  
920 resulted in the erroneous repetition of 63 aa in the v5 protein (Figure 7B). Finally, while *PF20*  
921 and *NRAMP2* were annotated as single genes in v5, some genes were incorrectly split into  
922 separate models by gaps (Supplemental Figure S9). We chose these examples from hundreds of  
923 affected genes, demonstrating the scale of improvement made possible by assembly  
924 improvements.

925

926 We further focused on specific issues that have been previously highlighted. Cross (2015)  
927 showed that more than 4,000 v5 gene models have in-frame upstream ORFs, many of which  
928 likely correspond to genuine N-terminal protein extensions based on comparison to *V. carteri*  
929 orthologs. To address this issue, we generally annotated the first in-frame start codon for each  
930 predicted mRNA as the start codon in the v6 annotations. *NRAMP2* also exemplifies this change,  
931 with the CC-4532 v6.1 protein extended by 126 aa at its N terminus (Figure 7B). Second, two  
932 studies (Blaby and Blaby-Haas 2017; Craig et al. 2021a) reported more than 100 strongly  
933 supported gene models that are absent from the v5 annotations. Many of these genes were  
934 present in the v4 annotations (e.g. *PSBWI*), and 25 are part of polycistronic transcripts (Gallaher  
935 et al. 2021). We attempted to transfer any strongly supported gene model from the v4.3, v5.6 or  
936 preliminary CC-503 v6 annotations to CC-4532 v6.1 if they were absent in the preliminary *de*  
937 *novo* annotation. Third, we manually curated a modest number of genes of interest, including 12  
938 encoding selenoproteins (Novoselov et al. 2002) that were all previously misannotated due to  
939 their use of the canonical stop codon “TGA” to encode selenocysteine. Finally, as detailed  
940 below, the CC-4532 v6.1 annotation was supplemented with *MT+* specific genes and genes  
941 found on the organelle genomes.

942

943 Two further changes caused the nuclear gene count to fall by 940 between v5.6 and CC-4532  
944 v6.1. First, we previously found that several hundred v5.6 genes have low coding potential and  
945 are unlikely to represent protein-coding genes (Craig et al. 2021a). This designation was reached  
946 by combining evidence from functional annotation, comparative genomics, population genetics,  
947 and intrinsic features of *Chlamydomonas* genes and coding sequence (codon usage bias and the  
948 strength of translation initiation sites i.e. Kozak-like sequences). We repeated these analyses on  
949 the preliminary v6 annotations, conservatively calling 1,417 “low coding potential” gene models

950 in CC-4532 v6.1 (Table 2, Supplemental Figures S10 and S11). Validating these analyses, we  
951 found no peptide support for these models in our proteomics analysis (see below). We did not  
952 include these models in the main annotations, but they are available as Supplemental Datasets  
953 S13 and S14. Many of these loci may be long noncoding RNA (lncRNA) genes that contain  
954 spurious short ORFs, or short ORFs located within the UTRs of other genes.

955

956 Second, we previously identified ~1,000 genes in v5.6 that are likely part of TEs (Craig et al.  
957 2021a). There are ~220 TE families in the *Chlamydomonas* genome, and although only a  
958 fraction is active in laboratory strains, many TEs are likely active in the wider species (Craig  
959 2021). Since most TE copies are not degraded, their genes can be readily identified by gene  
960 prediction algorithms. Unknowingly including TE genes within annotations can confound  
961 analyses, such as analyses of methylation, chromatin states or small RNA targeting, where  
962 substantial differences may be expected between non-TE and TE genes. Genome projects  
963 therefore generally aim to exclude TE genes, while highly curated annotations of model  
964 organisms may include TEs as defined entities.

965

966 When comparing v5.6 genes and TE coordinates, the distribution of their intersect is highly  
967 bimodal; 1,023 genes have a >30% overlap between their coding sequence (CDS) and TEs, and  
968 908 genes have >80% overlap (Figure 8A). We obtained similar distributions in the preliminary  
969 v6 annotations, indicating that most genes can be cleanly divided into TE and non-TE subsets.  
970 To designate high-confidence TE genes, we required a gene with a high CDS-TE overlap to have  
971 either sequence similarity to a known TE-encoded protein or a functional domain. This analysis  
972 resulted in the inclusion of 810 TE genes in CC-4532 v6.1 (Figure 8B, Table 2) and 647 in CC-  
973 503 v6.1 (Supplemental Figure S12), which are integrated in the associated GFF3 files under the  
974 field “transposable\_element\_gene”. Users should be aware that these TE gene sets are not  
975 exhaustive, and projects requiring TE coordinates in general should use annotations derived from  
976 the dedicated repeat library (Supplemental Dataset S15).

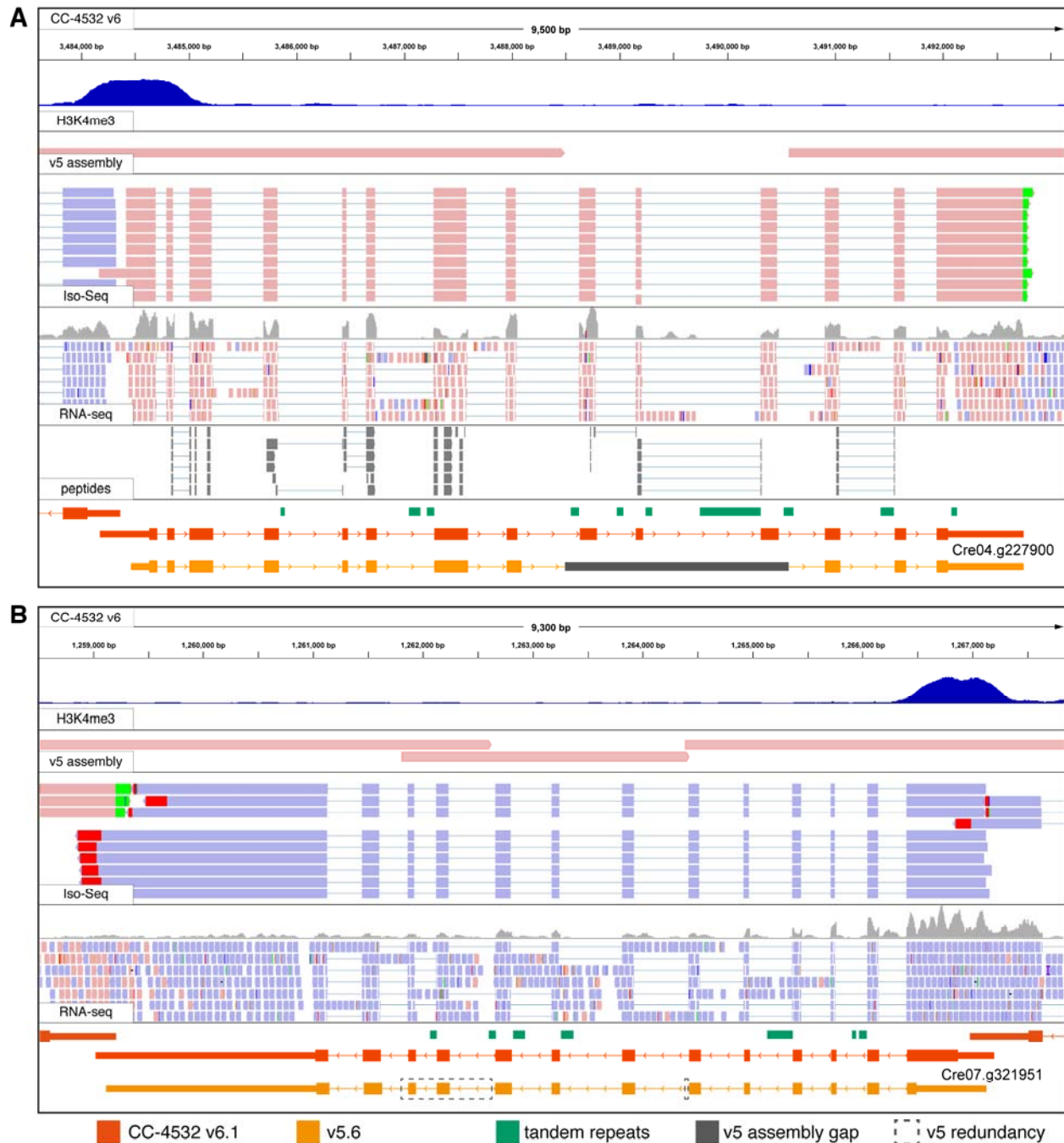
977

978

979

980

981



982  
 983  
 984  
 985  
 986  
 987  
 988  
 989  
 990  
 991

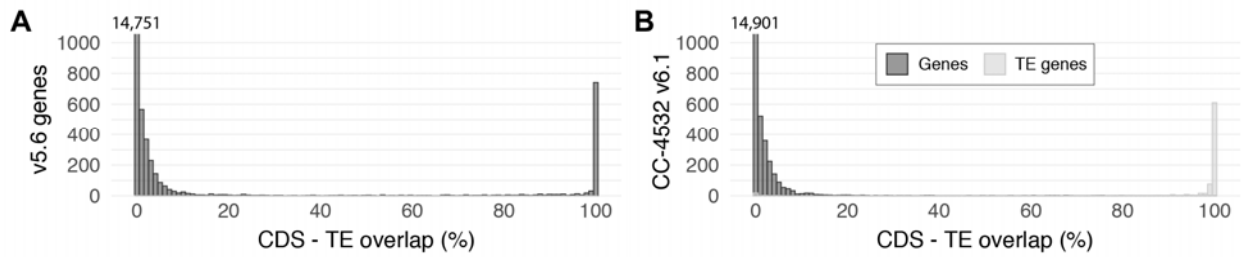
**Figure 7. Browser views of example gene models improved between v5.6 and CC-4532 v6.1.**

(A) *PF20*, CC-4532 v6 coordinates: chromosome 4, 3,483,590 - 3,493,250.

(B) *NRAMP2*, CC-4532 v6 coordinates: chromosome 7, 1,258,513 – 1,267,855. Note that the redundant sequences (boxed) are not included in the gene model converted from v5.6, since these duplicated sequences do not exist in CC-4532 v6. No peptides were identified.

H3K4me3 ChIP-seq (dark blue peaks) marks promoters. The v5 assembly track shows an alignment of v5 contigs to CC-4532 v6, with assembly gaps appearing as unmapped regions and redundant sequence as overlapping regions. Peptides are from mass spectrometry analysis of the proteome. Coordinates for v5.6 gene models (orange) were converted to CC-4532 v6. Thick blocks represent coding sequence, thin

992 blocks UTRs, and joining lines introns. Forward strand mappings are shown in pink and reverse in blue.  
993 Red and green mismatches at the end of Iso-Seq reads correspond to poly(A) tails.  
994



995  
996 **Figure 8. Transposable element genes in v5.6 and CC-4532 v6.1.**  
997 (A) Overlap between gene coding sequence (CDS) and TEs in v5.6. The number of genes with 0%  
998 overlap is written above the first bar.  
999 (B) Overlap between gene coding sequence (CDS) and TEs in CC-4532 v6.1. Genes were split into non-  
1000 TE and TE genes.

1001  
1002  
1003  
1004  
1005  
1006  
1007  
1008  
1009  
1010  
1011  
1012  
1013  
1014  
1015  
1016  
1017  
1018  
1019  
1020  
1021

## The mating type locus and haplotype 2

1022 The mating type locus (*MT*) on the left arm of chromosome 6 is naturally within a region where  
1023 strains carry different haplotypes, *mt+* strains haplotype 1, and *mt-* strains haplotype 2. Except  
1024 for genes unique to either allele, *MT* genes have homologs present on both alleles (i.e.  
1025 gametologs), although those within the rearranged (R) domain are generally not syntenic  
1026 between *MT+* and *MT-* (Ferris and Goodenough 1994; Ferris et al. 2002). Since CC-503 is *mt+*,  
1027 past assembly versions have lacked the two *MT-* specific genes, *MINUS DOMINANCE 1*  
1028 (*MIDI*) and *MATING TYPE REGION D-1 (MTD1)*. With the reference now based on the *mt-*  
1029 CC-4532, the situation is reversed, however this is a greater issue since there are at least 16 *MT+*  
1030 specific genes in five *MT+* specific regions, three of which originated from autosomal insertion  
1031 (*MTP0428*, the MTA region and the SRL region) (De Hoff et al. 2013). To address this issue, we  
1032 appended a 375-kb *MT+* R domain contig extracted from CC-503 v6 to the reference CC-4532  
1033 v6 assembly. To avoid potential mismapping of omics data, we hardmasked (i.e. replaced with  
1034 Ns) any gametologous regions on the appended contig, so that only sequences corresponding to  
1035 *MT+* specific regions and genes were included. Finally, we manually curated all R domain gene  
1036 models and appended *MT+* specific genes to the CC-4532 v6.1 annotation. CC-4532 v6 should  
1037 thus be suitable for analyses of data from both *mt+* and *mt-* strains, and we expect that the  
1038 availability of highly contiguous and well-annotated assemblies of both alleles will be a major  
1039 resource for the *Chlamydomonas* community.

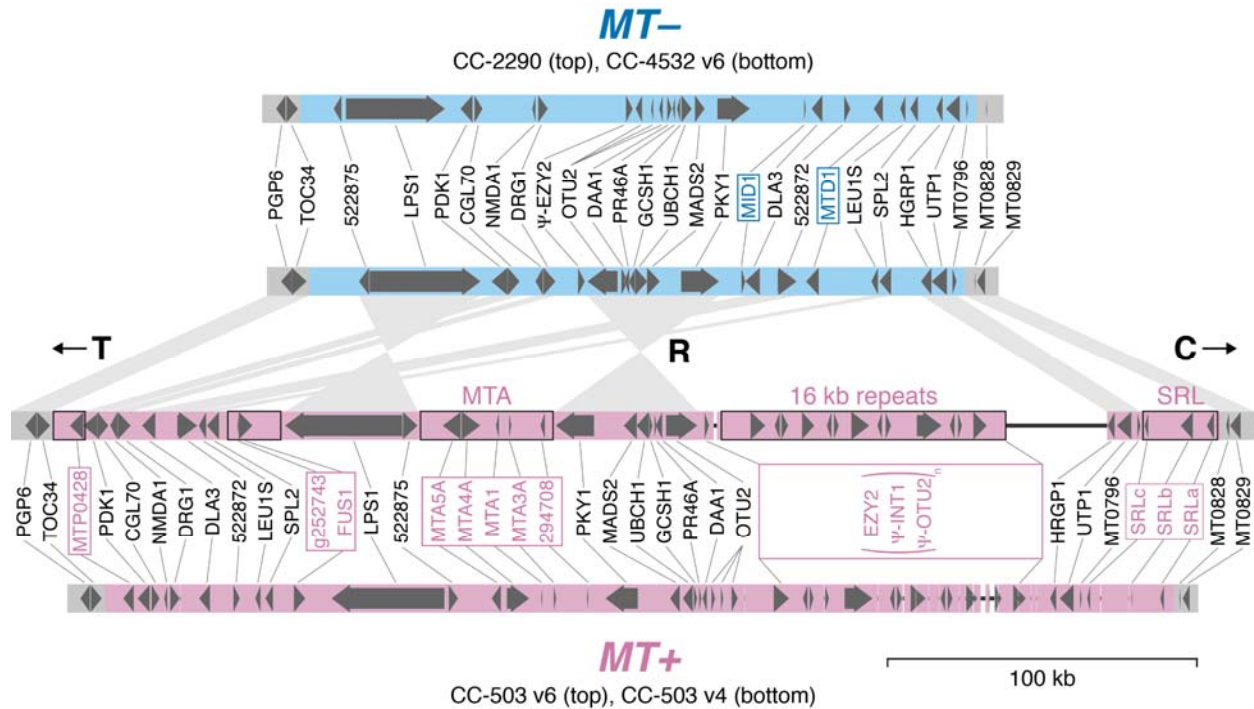
1040  
1041 We compared our resources for CC-503 v6 and CC-4532 v6 to the existing curated *MT+* (CC-  
1042 503 v4) and *MT-* (CC-2290) annotations of De Hoff et al. (2013) (Figure 9). The gapless CC-  
1043 4532 *MT-* R domain (~211 kb) was entirely syntenic with that of CC-2290 (~218 kb), although  
1044 intergenic regions were often unalignable due to polymorphic repeats. The only major change in  
1045 both *MT-* and *MT+* affected *OTUBAIN PROTEIN 2 (OTU2)*, which was extended to incorporate  
1046 the genes *155027* and *MT0618* into a single gene model (i.e. the correct *OTU2* was split across  
1047 three gene models in CC-2290 and CC-503 v4). The *MT+* allele of *OTU2* was recently shown to  
1048 function in the uniparental inheritance of the plastome (Joo et al. 2022). In *MT+*, *OTU2* is  
1049 located immediately upstream of an *MT+* specific region termed the “16-kb repeats” (Ferris et al.  
1050 2002), consisting of a 17.2-kb tandemly repeated region containing multiple copies of *EARLY*  
1051 *ZYGOTE 2 (EZY2)*, *INTEGRASE 1 (INT1)* and what was previously annotated as *OTU2* (i.e. the  
1052 repeats contain duplicates of only a 3' fragment of the full *OTU2* gene, which may be

1053 pseudogenized). *INT1* shares strong sequence similarity to the proteins of DIRS retrotransposons  
1054 from *Chlamydomonas* (e.g. *TOC3* (Goodwin and Poulter 2004)) and is likely derived from a TE  
1055 family that is no longer present elsewhere in the genome. Although the reverse transcriptase  
1056 domain is missing, *INT1* does contain sequence encoding the RNase H and methyltransferase  
1057 domains of a DIRS element in addition to the “integrase” (actually a tyrosine recombinase).  
1058 Assuming *INT1* has not been co-opted, the multiple copies of *EZY2*, which produce zygote-  
1059 specific transcripts (Ferris et al. 2002), may be the only functional genes in the repeat. The *MT+*  
1060 specific regions are collectively responsible for the larger size of the *MT+* allele. However, the  
1061 assembly of the 16-kb repeats remains incomplete in CC-503 v6, with two gaps relative to CC-  
1062 1690 (which is also *mt+*). We detected no structural variants indicative of mutations between  
1063 CC-503 v6 and CC-1690 in the R domain, suggesting that CC-503 v6 provides a typical  
1064 representation of all *mt+* laboratory strains across this region. Notably, there were two full-  
1065 length copies of *OTU2* annotated in v5 (Joo et al. 2022), however we found no evidence for this  
1066 state in either CC-503 v6 or CC-1690, and this was likely a misassembly of the regions flanking  
1067 the 16-kb repeats.

1068  
1069 More broadly, CC-4532 contains five haplotype 2 regions spanning 4.6% of the genome (Figure  
1070 1A, Supplemental Figure S8) and featuring 818 genes (Supplemental Dataset S17). Unlike our  
1071 analysis of structural mutations above, we did not perform a systematic analysis of structural  
1072 variation present between the two haplotypes; the CC-503 – CC-4532 comparison captures less  
1073 than one fifth of the total haplotype variation among laboratory strains (which can affect up to  
1074 ~25% of the genome), and this question would be best addressed by assembling and comparing  
1075 genomes of additional strains. Furthermore, without additional genomes it is currently  
1076 impossible to distinguish ancestral structural variants from derived laboratory mutations in these  
1077 regions. We did however revise the coordinates of the haplotype 2 blocks reported by Gallaher et  
1078 al. (2015) relative to CC-4532 v6 (Supplemental Dataset S18), since some were affected by  
1079 assembly corrections. The distribution of haplotype blocks among many of the most widely used  
1080 laboratory strains is shown in Supplemental Figure S13.

1081  
1082  
1083

1084



1085

1086 **Figure 9. Assembly and annotation comparisons of the plus (*MT+*) and minus (*MT-*) alleles of the**  
1087 **mating type locus rearranged (R) domain.**

1088 Block arrows represent protein-coding genes. Mating type-specific gene symbols are boxed. CC-503 v6  
1089 *MT+* specific regions that were not hardmasked in the *MT+* contig appended to CC-4532 v6 are outlined  
1090 in black. Synteny between CC-4532 v6 *MT-* and CC-503 v6 *MT+* genes is represented by wedges. T and  
1091 C refer to the telomere-proximal and centromere-proximal domains, respectively. Only copies of *EZY2*  
1092 within the 16-kb repeats are included in the *MT+* gene annotation. Copies of *OTU2* within the 16-kb  
1093 repeats are truncated and are marked as putative pseudogenes (as are *INT1* copies, see main text). Thin  
1094 black lines represent assembly gaps. The CC-2290 and CC-503 v4 annotations are from De Hoff et al.  
1095 (2013). Gene symbols are from De Hoff et al. (2013), except for symbols updated herein (Supplemental  
1096 Dataset S16).

1097

1098

1099

1100

1101

1102

1103

1104

1105

1106



1107

## 1108 **Organelle genomes and structural annotations**

1109 The genomes of the plastid and mitochondria, the plastome and mitogenome, respectively,  
1110 encode abundant cellular proteins and contribute disproportionately to the transcriptome: 46% of  
1111 all mRNA in the cell is transcribed from the plastome, and just eight mitochondrial genes  
1112 contribute 1.4% to the total mRNA pool (Gallaher et al. 2018). We recently produced high-  
1113 quality assemblies and annotations of the plastome and mitogenome (Gallaher et al. 2018),  
1114 which are now included in the v6 releases (Table 2). Importantly, there are no genetic variants to  
1115 distinguish the organelle genomes of CC-4532 and CC-503, since the laboratory strains are  
1116 putatively descended from one zygote and the multicopy organelle genomes are inherited  
1117 uniparentally.

1118

1119 The circular 205.6-kb plastome carries 72 protein-coding genes, with two (*psbA* and *I-CreI*)  
1120 duplicated in the inverted repeat regions. Many of the genes are expressed from polycistronic  
1121 transcripts. Cavaiuolo et al. (2017) used small RNA profiling to accurately map the plastid  
1122 genes, and we incorporated their improvements to the v6.1 annotations. The *psaA* gene, which  
1123 encodes photosystem I chlorophyll *a* binding apoprotein A1, is expressed as three separate  
1124 transcripts that are trans-spliced to generate the mature mRNA molecule (Kück et al. 1987). The  
1125 three separate genes that contribute to the mature transcript are out of order and in different  
1126 orientations, and we therefore assigned three separate, but sequential, gene IDs (CreCp.g802280,  
1127 CreCp.g802281, and CreCp.g802282) to the three *psaA* exons.

1128

1129 The linear 15.8-kb mitogenome carries eight protein-coding genes, which are expressed from a  
1130 single bidirectional promoter. Seven of these genes encode components of the respiratory  
1131 complex, while the eighth, *reverse transcriptase-like (rtl)*, is likely required for mitogenome  
1132 replication (Smith and Craig 2021). We incorporated the more accurate annotations of Salinas-  
1133 Giegé et al. (2017), who demonstrated that the 5' end of each mature mitochondrial transcript  
1134 begins immediately at the start codon (i.e. there are no 5' UTRs).

1135

1136

1137

## 1138 **Gene model validation**

1139 To validate the CC-4532 v6.1 annotation, we first queried all predicted proteins against the  
1140 BUSCO (Benchmarking Universal Single Copy Orthologs) chlorophyte dataset (Manni et al.  
1141 2021), with the number of fragmented and missing genes dropping from five and eleven,  
1142 respectively, in v5.6, to only one and two in CC-4532 v6.1 (Table 2). Notably, CC-503 v6.1 had  
1143 no missing genes, and upon inspection, the two missing genes in CC-4532 v6 were found within  
1144 the small number of remaining genic gaps (see above). Nevertheless, we consider the CC-4532  
1145 v6.1 annotation to be superior to that of CC-503: many more genes are affected by major loss-of-  
1146 function mutations in CC-503, although none are genes in the BUSCO dataset (many of which  
1147 may be essential).

1148  
1149 We next turned to chromatin-immunoprecipitation followed by deep-sequencing (ChIP-seq) data  
1150 of trimethylated histone H3 lysine 4 (i.e. H3K4me3), which reliably mark promoter regions  
1151 (Ngan et al. 2015; Strenkert et al. 2022) (see Figure 7). We queried 1,224 H3K4me3 peaks that  
1152 had been called as intergenic relative to the v5 genome and v5.6 annotation, assigning 244 peaks  
1153 to gene transcription start sites (TSSs) in CC-4532 v6.1. Approximately 30% of the genes newly  
1154 associated with H3K4me3 peaks did not have gene IDs mapped forward from v5.6, suggesting  
1155 that the improvements can be attributed to both the inclusion of new genes and changes to the  
1156 TSSs of existing genes. It is not surprising that almost 1,000 H3K4me3 peaks remain  
1157 unannotated, since they are expected to be associated with features other than protein-coding  
1158 genes, such as lncRNAs (Strenkert et al. 2022). Furthermore, ~40% of the remaining peaks  
1159 coincided with TEs, which may be an underappreciated source of active promoters in  
1160 *Chlamydomonas*.

1161  
1162 Finally, we queried the v5.6 and CC-4532 v6.1 predicted proteins against a pool of proteomics  
1163 data. We identified at least one unambiguously assigned peptide for 14,339 v5.6 proteins and  
1164 14,841 v6.1 proteins, an increase of 3.5% (Supplemental Dataset S19). The v6.1 total included  
1165 14,770 proteins encoded by the nuclear genome (including TE proteins), 65 from the plastome,  
1166 and six from the mitogenome. We noted a 7.2% increase in the total number of unique peptides  
1167 assigned to CC-4532 v6.1 relative to v5.6, and a 7.0% increase in the total number of peptides.  
1168 These increases can be attributed to several improvements in v6.1, including the incorporation of

1169 entirely new nuclear genes, the inclusion of new exons within previous assembly gaps, and the  
1170 N-terminal ORF extensions. For example, we identified three unique peptides assigned to the  
1171 previously “hidden” exons of *PF20* (Figure 7A). The addition of the organelle annotations also  
1172 contributed substantially. This was especially true for the total number of peptides, since the 65  
1173 plastome-encoded proteins with identified peptides accounted for 5.0% of all peptides assigned  
1174 to CC-4532 v6.1, and the six mitogenome-encoded proteins accounted for 0.018%. Notably,  
1175 these estimates are far lower than the total mRNA contribution from the organelles to the cell  
1176 mentioned above.

1177

### 1178 **Gene IDs**

1179 Starting with the v4 annotations and becoming standard for all genes in v5.5, *Chlamydomonas*  
1180 locus IDs have taken the form CreYY.gNNNNNN, where YY is the chromosome number and  
1181 NNNNNN is a unique number that nominally increases along the chromosome (Blaby et al.  
1182 2014). We successfully mapped existing “Cre” IDs from v5.6 to 15,224 nuclear genes in the CC-  
1183 4532 v6.1 annotation (90.6%, Supplemental Dataset S20). The remaining gene models were  
1184 either novel or had changed considerably relative to their v5.6 counterparts (e.g. due to gene  
1185 model mergers or splits). For these 2,277 CC-4532 v6.1 genes with no v5 equivalent (including  
1186 most TE and all organelle genes), new NNNNNN numbers were introduced, ranging from  
1187 800000 to 802251 and increasing with genomic coordinates. Plastome and mitogenome genes  
1188 were assigned locus identifiers from CreCp.g802263 to CreCp.g802335, and from  
1189 CreMt.g802337 to CreMt.g802344. Since we also annotated the CC-503 v6 assembly (and many  
1190 more genomes may follow), it was necessary to distinguish between orthologous gene models  
1191 annotated in each assembly. We therefore included a four-digit strain-specific suffix to the IDs:  
1192 CreYY.gNNNNNN\_4532 for CC-4532 v6.1 and CreYY.gNNNNNN\_0503 for CC-503 v6.1.  
1193 With CC-4532 becoming the reference, gene models in other assemblies (including CC-503 v6)  
1194 will be attributed IDs based on their mapping to this annotation.

1195

1196 It is also imperative to note that the misassembly corrections and the CC-503 structural  
1197 rearrangements resulted in many genes having CC-4532 v6.1 gene IDs that refer to the wrong  
1198 chromosome (i.e. YY number). Similarly, the NNNNNN numbers may not be contiguous. In  
1199 fact, this was already an issue for some IDs in v5 due to assembly changes relative to v4.

1200 Unfortunately, both the YY and NNNNNN numbers are now meaningless (and potentially  
1201 misleading), and users are cautioned that no spatial information should be extracted from the IDs  
1202 alone. To counter any confusion, we devised a spatially correct and strain-specific “associated  
1203 locus ID” for each gene. They follow the format XXXX\_YY\_NNNNN, where XXXX is the  
1204 strain identifier from the Chlamydomonas Resource Center, YY is the chromosome number, and  
1205 NNNNN is a unique gene number that increases along the chromosome, with odd numbers for  
1206 forward strand genes and even numbers for reverse strand genes. Successive IDs feature  
1207 NNNNN numbers separated by 3 or 4 unused numbers depending on relative strandedness  
1208 (rising to 53 or 54 for genes on either side of an assembly gap), serving as placeholders for  
1209 possible new gene models. As an example, in CC-4532 v6.1 *PSYI* has the primary ID  
1210 Cre02.g095092\_4532 and the associated locus ID 4532\_11\_52343, with the latter providing the  
1211 correct chromosomal location (Figure 2B). These IDs also carry additional information as  
1212 optional suffixes e.g. all TE genes feature the suffix “\_TE”, making them instantly recognizable.  
1213 The associated locus IDs have a one-to-one relationship with the existing “Cre” IDs  
1214 (Supplemental Dataset S19) and we envision that they will be used in parallel (e.g. to  
1215 simultaneously assess spatial information).

1216

### 1217 **Expert annotation and gene symbols**

1218 Over decades of research, Chlamydomonas genes have been assigned a gene symbol, designed to  
1219 uniquely identify and succinctly characterize a given locus. In v5.6, 5,130 genes (28.9%) were  
1220 annotated with a gene symbol (Supplemental Dataset S21). These symbols have been derived  
1221 from several sources, including protein function, mutant phenotypes, and orthology  
1222 (Supplementary Note S1). The gene symbols are a powerful tool for interpreting, analyzing, and  
1223 communicating research in Chlamydomonas, especially for large-scale and systems biology  
1224 research. Unfortunately, automated annotation has driven the proliferation of uninformative gene  
1225 symbols. For example, the root "ANK" was used to assign gene symbols to 20 genes in v5.6 due  
1226 solely to the presence of a predicted ankyrin repeat domain. Similarly, there are 51 *HEL* genes  
1227 (encoding proteins with a DEAD/DEAH box helicase domain) and 35 *DNJ* genes (encoding  
1228 proteins with a DnaJ domain) in v5.6. The presence of a gene symbol may imply that the gene  
1229 has been at least partially characterized and perhaps has a validated function corresponding to the  
1230 name, while these examples provide no information beyond their automated domain annotations.

1231 Furthermore, some symbols rely on erroneous predictions e.g. *NIKI* (Cre14.g629650) was  
1232 named from homology to a nickel (Ni) transporter, however, *Chlamydomonas* has no known Ni-  
1233 requiring genes and no nutritional requirement for Ni (Blaby-Haas et al. 2016).

1234  
1235 The *Chlamydomonas* annotations are frequently used to guide the annotation of newly sequenced  
1236 Chlorophyte genomes (Roth et al. 2017), which propagates the low information or  
1237 misinformation throughout the Chlorophyte lineage. Therefore, we sought to improve and update  
1238 the gene symbols, which consisted of three phases: 1) the addition of new gene symbols  
1239 wherever those annotations were based on expert analysis or empirical data, 2) transfer of a  
1240 primary gene symbol to “previous identifiers” for uninformative and misleading gene symbols,  
1241 and 3) reformatting or changing existing gene symbols to conform to a uniform style.

1242  
1243 We added 610 new gene symbols to the CC-4532 v6.1 annotation. The majority of these were  
1244 assigned in collaboration with the authors of individual chapters in the forthcoming 3rd edition  
1245 of the *Chlamydomonas* Sourcebook. Still others were based on recent publications. We  
1246 reclassified 1,332 v5.6 gene symbols as “previous identifiers”, preserving connections to  
1247 historical research that may have used those symbols (Supplemental Dataset S22). As a result,  
1248 there are now 4,408 out of 16,801 (26.2%) genes with a gene symbol in v6.1 (excluding TE  
1249 genes). An additional 549 genes had their gene symbol replaced, altered, or reformatted to  
1250 improve clarity, highlight orthologies, and unify formatting. This effort was guided by several  
1251 rules, updated and expanded from our previous work (Blaby et al. 2014), which are documented  
1252 in Supplemental Note S1. We recommend that they be applied for the naming of all  
1253 *Chlamydomonas* genes going forward.

1254  
1255 Beyond symbols, many genes have a defline and associated comments. These may include a  
1256 description of the gene function, relevant expression data, paralogy and orthology information,  
1257 and links to related peer-reviewed literature. This last feature, in the form of PMID accession  
1258 numbers, has also been expanded and updated from 1,852 genes supported by one or more  
1259 PMIDs (2,626 total PMIDs) in v5.6, to 3,042 genes (4,697 total PMIDs) in CC-4532 v6.1  
1260 (Supplemental Dataset S21).

1261

1262 Finally, the rate at which genes are expertly annotated in the literature outpaces that of updates to  
1263 the Chlamydomonas genome and structural annotations. We have therefore created a dedicated  
1264 email account, chlamy.updates@gmail.com, to receive and store user updates. We encourage  
1265 users to send curated annotation updates. This may include gene symbol suggestions, textual  
1266 annotation, PMIDs, expression data, functional validation, among other information. We also  
1267 welcome manually curated gene models (preferably in GFF3 format), either for entirely new  
1268 genes or for evidence-based corrections of existing models. We are committed to collating this  
1269 information so that future updates are both efficient and representative of recent advances in  
1270 Chlamydomonas research.

1271

### 1272 **The present and future of the Chlamydomonas Genome Project**

1273 For almost two decades, the Chlamydomonas Genome Project has been based on the *mt+* strain  
1274 CC-503. In version 6, we have presented near-complete assemblies for both CC-503 and the *mt-*  
1275 strain CC-4532. Following the discovery of numerous structural mutations affecting CC-503,  
1276 CC-4532 v6 was chosen to serve as the reference genome. Despite its replacement, CC-503 v6  
1277 remains a valuable resource, especially for the *MT+* allele and the existing organelle genomes  
1278 that were appended to CC-4532 v6.

1279

1280 It is now clear that laboratory strains can differ extensively from each other, both genetically and  
1281 phenotypically. Most of this variation stems from the mosaic of two haplotypes that comprise the  
1282 genome of each strain (Gallaher et al. 2015). These developments have led to the “know thy  
1283 strain” maxim: researchers are encouraged to consider the genetic differences that exist between  
1284 the reference genome and the strains used in experimental work (Salomé and Merchant 2019).  
1285 Our results suggest that these differences should not only be considered with respect to ancestral  
1286 variation between the haplotypes, but also to derived variation arising by laboratory mutation.  
1287 Although CC-503 may be an extreme case, the CC-4532 genome harbors 10 structural mutations  
1288 and more than 100 TE insertions. Indeed, analyses by Gallaher et al. (2015) and Flowers et al.  
1289 (2015) previously inferred the presence of many derived structural variants among strains,  
1290 including several large duplications. It has also been estimated that ~5-10% of all *de novo*  
1291 mutations in Chlamydomonas experimental lines are structural (i.e. >50 bp) (López-Cortegano et  
1292 al. 2022), supporting a prominent role for structural evolution in the laboratory. While many of

1293 the most characteristic laboratory phenotypes were caused by mutations (e.g. *nit1* and *nit2*), it is  
1294 likely that all strains have experienced unique structural mutations (including TE proliferation at  
1295 various rates), many of which disrupt genes. It is also possible that independently maintained  
1296 cultures of the same strain differ due to independent mutations. Laboratory strains have been  
1297 maintained clonally for as many as 75 years and mutations are an unavoidable consequence,  
1298 especially if strains are evolving under relaxed selection. The implications of “laboratory  
1299 domestication” have been considered in other model systems such as *Caenorhabditis elegans*  
1300 (Sterken et al. 2015), and laboratory mutations should be carefully considered when evaluating  
1301 experimental results. This may be particularly relevant in strains that have been selected for, and  
1302 often actively mutagenized to achieve, specific traits e.g. cell wall-less strains with increased  
1303 transformation efficiency, which has been a major bottleneck in *Chlamydomonas* molecular  
1304 genetics.

1305

1306 With the continuous developments in long-read sequencing, we are entering an exciting era of  
1307 *Chlamydomonas* genomics. Complete “telomere-to-telomere” *Chlamydomonas* genomes are  
1308 within reach, and a pan-genome project has been initiated, targeting genome assemblies for  
1309 multiple laboratory strains and field isolates. As demonstrated herein, many insights can only be  
1310 gleaned by comparing the genomes of different strains, and we can expect substantial benefits  
1311 from sequencing additional strains and isolates moving forward. With respect to the two  
1312 laboratory haplotypes, a “laboratory pan-genome” could be produced where all haplotype 1 and  
1313 2 regions are represented, capturing all ancestral variation present among laboratory strains. This  
1314 dataset could potentially take the form of consensus assemblies for each haplotype, with  
1315 genomes from several strains used to infer the ancestral state at the time of isolation. Such an  
1316 ancestral reconstruction would arguably be the most representative and strain-agnostic  
1317 *Chlamydomonas* reference genome possible, since differences between any laboratory strain and  
1318 the reference would easily be recognized as a mutation. Furthermore, similar to resources  
1319 developed for several important plants (Bayer et al. 2020), the species-level pan-genome aims to  
1320 incorporate the far greater diversity present among *Chlamydomonas* field isolates (Flowers et al.  
1321 2015; Craig et al. 2019). There also remains substantial scope to further enhance structural  
1322 annotations, especially with the continued growth in the availability of omics data for  
1323 *Chlamydomonas* and related species. Such prospects are expected to reveal novel aspects of

1324 Chlamydomonas biology, continuing the development of the species as an integral model in  
1325 plant and algal biology.

1326

1327

## 1328 **METHODS**

### 1329 **Strains and DNA sequencing**

1330 CC-503 was obtained from the Chlamydomonas Resource Center in 2012. CC-4532 has been  
1331 propagated in Sabeeha Merchant's group since the late 1990s (see Gallaher et al. (2015)), when it  
1332 was received from Ursula Goodenough. Cultures were grown as described previously (Gallaher  
1333 et al. 2015).

1334

1335 Genomic DNA was extracted from frozen cell pellets and used for library preparation and  
1336 sequencing at the Joint Genome Institute. Libraries were constructed using a SMRTbell  
1337 Template Prep Kit 1.0 and size-selected to 10-50 kb on a SAGE Blue Pippin instrument.  
1338 Sequencing was performed on a PacBio Sequel platform in CLR (continuous long reads) mode  
1339 using a 10-hour movie time, generating ~127x and 176x coverage for CC-503 and CC-4532,  
1340 respectively (CC-503 mean read length 3.58 kb; CC-4532 mean read length 9.88 kb). Additional  
1341 Illumina sequencing was performed on a HiSeq2000 platform (150-bp paired-end reads, ~400-bp  
1342 insert) to ~50x (CC-503) and 55x (CC-4532) coverage, as reported in Gallaher et al. (2015).

1343

### 1344 **Assembly of CC-4532 v6 and CC-503 v6 genomes**

1345 Preliminary contig-level assemblies were produced from the PacBio datasets. CC-503 was  
1346 assembled using MECAT v1.1 (genomeSize=130000000 ErrorRate=0.02  
1347 Overlapper=mecat2asmpw) (Xiao et al. 2017) and CC-4532 using Canu v1.8  
1348 (genomeSize=120000000) (Koren et al. 2017). Reads were mapped to the raw assembly using  
1349 BLASR, and error correction was performed using a single pass of Arrow correction from the  
1350 GenomicConsensus toolkit. Remaining consensus errors were corrected using the strain-  
1351 appropriate Illumina data. Illumina reads were aligned using bwa mem (Li 2013) and SNPs and  
1352 InDels to be corrected were identified using GATK UnifiedGenotyper (McKenna et al. 2010).  
1353 The corrections were verified by mapping the Illumina reads to the corrected consensus  
1354 sequence.

1355

1356 The CC-1690 assembly (O'Donnell et al. 2020) was used to scaffold the preliminary contigs of  
1357 each assembly to chromosomes. Contigs were mapped to the CC-1690 assembly using minimap2  
1358 v2.17 (-ax asm5) (Li 2018) to produce PAF (Pairwise mApping Format) files. These mapping  
1359 data were used to manually order and orientate uniquely mapping contigs (i.e. the majority of the  
1360 contig received a mapping quality of 60) relative to each CC-1690 chromosome. Any  
1361 inconsistencies between the contigs and CC-1690 chromosomes were inspected against the raw



1362 PacBio reads from the relevant strain (CC-503 or CC-4532) using IGV v2.7.2 (Robinson et al.  
1363 2011). In a small number of cases a misassembled contig was split, while for CC-503 some  
1364 genuine inconsistencies caused by structural mutations were supported by the raw reads and  
1365 maintained. Several short contigs that mostly featured satellite DNA were manually removed  
1366 since they appeared to duplicate a region already assembled on a larger contig. Other short  
1367 contigs entirely consisting of subtelomeric repeats, which generally did not map uniquely, were  
1368 assigned to chromosome termini by specific alignment and phylogenetic analysis (see Chaux-  
1369 Jukic et al. (2021)).

1370  
1371 Gap lengths between contigs were estimated relative to CC-1690 and the appropriate number of  
1372 Ns were inserted between contigs. Occasionally the estimated “gap” length was negative,  
1373 suggesting redundant sequence at the termini of neighboring contigs. These contig termini were  
1374 compared, trimmed to remove redundant sequence, and subsequently merged where possible.  
1375 Arbitrary gaps of 100 Ns were inserted between contigs that could not be successfully merged.

### 1376 1377 **Repeat annotation**

1378 TE sequence was identified in each assembly by providing the latest Chlamydomonas repeat  
1379 library to RepeatMasker v4.0.9 (Smit et al. 2013-2015). This library features updated consensus  
1380 models for all Chlamydomonas repeats available in Repbase (<https://www.girinst.org/replib/>)  
1381 together with >100 newly curated repeats (Craig 2021). Any putative TE copy divergent by  
1382 >20% from its consensus sequence was removed. *ZeppL* clusters were identified as the span  
1383 from the first two consecutive *ZeppL-1\_cRei* copies to the final two consecutive *ZeppL-1\_cRei*  
1384 copies on each chromosome (except for chromosome 15 where three distinct clusters were  
1385 observed, see Results).

1386  
1387 Microsatellites and satellite DNA were primarily identified using Tandem Repeats Finder  
1388 (Benson 1999) with parameters “2 7 7 80 10 50 1000” (i.e. a minimum alignment score of 50 and  
1389 a maximum monomer size of 1000 bp). Tandem repeats consisting of  $\geq 2$  monomers were split  
1390 into microsatellites (monomers <10 bp) and satellite DNA (monomers  $\geq 10$  bp), and if a region  
1391 was called as both, priority was given to satellite DNA since shorter monomers are frequently  
1392 nested within larger ones. Satellite DNA annotations were supplemented with curated satellites  
1393 identified by RepeatMasker from the repeat library, several of which have monomers longer than  
1394 the detection limit of Tandem Repeats Finder.

1395  
1396 Genome-wide CG methylation was quantified for the CC-1690 assembly following Chaux-Jukic  
1397 et al. (2021). Briefly, the raw signal of the CC-1690 Nanopore reads (i.e. fast5 files) generated  
1398 by Liu et al. (2019) were mapped to the CC-1690 assembly using Tombo  
1399 (<https://nanoporetech.github.io/tombo/>) and CG methylation was called using DeepSignal (Ni et  
1400 al. 2019).

1401

## 1402 **Validation of assembly improvements**

1403 Misassemblies in the v5 assembly were identified by mapping the v5 contigs to the chromosomal  
1404 CC-503 v6 and CC-4532 v6 assemblies using minimap2 as described above. Genomic  
1405 coordinates of intra- and inter-chromosomal inconsistencies were assessed manually from the  
1406 PAF files and converted to input files for Circos (Krzywinski et al. 2009) and karyoploteR (Gel  
1407 and Serra 2017) to produce figures 1, 2 and S1.

1408  
1409 To enable convenient liftover of coordinates between assemblies, a 5-way Cactus whole-genome  
1410 alignment (WGA) (Armstrong et al. 2020) was produced including the v4, v5, CC-503 v6, CC-  
1411 4532 v6 and CC-1690 assemblies. Each assembly was soft-masked for repeats by providing  
1412 coordinates of TEs and tandem repeats (see above) to BEDtools v2.26.0 maskfasta (-soft)  
1413 (Quinlan and Hall 2010). An arbitrary guide tree for Cactus was provided as “(CC-  
1414 4532\_v6:0.001,(CC-1690:0.001,(CC-503\_v4:0.001,(CC-503\_v5:0.001,CC-  
1415 503\_v6:0.001):0.001):0.001):0.001)”, and all assemblies were set to reference quality. Liftover  
1416 of genomic coordinates in BED (Browser Extensible Data) format could then be performed  
1417 between any two assemblies in the HAL (Hierarchical ALignment) format WGA using the HAL  
1418 tools command halLiftover (Hickey et al. 2013). This approach was used to convert v5  
1419 coordinates of hypermethylated regions (Lopez et al. 2015) to CC-4532 v6 (Figure 1) and CC-  
1420 1690 (Supplemental Figure S2) coordinates. Coordinates of v5 assembly gaps were also  
1421 converted to CC-4532 v6 coordinates to investigate the sequence properties of filled gaps in the  
1422 updated assembly (see Figure 3).

1423  
1424 The genotyping data from Kathir et al. (2003) were kindly provided by Paul Lefebvre. The  
1425 genomic coordinates (v5 assembly, as chromosome and position, in bp) were determined for all  
1426 markers by BLAST search in Phytozome using the sequence deposited for each marker  
1427 ([https://www.chlamycollection.org/BAC/MARKER\\_index.htm](https://www.chlamycollection.org/BAC/MARKER_index.htm)), or by keyword search using the  
1428 gene name in Phytozome. The markers were then ordered based on their assigned v5  
1429 chromosome and position. All genotyping data were assembled into a tab-delimited file and used  
1430 as input for R/QTL (Broman et al. 2003) with the functions *read.cross*, *est.rf*, *plotMap*, *plotRF*,  
1431 and *summaryMap*. The genotyping data for the CC-2935 × CC-2936 progeny (12 full tetrads)  
1432 were obtained from Liu et al. (2018). Since the genotypes were encoded as either 1 or 2, a matrix  
1433 (of the same size as the genotype matrix) was calculated whereby each n+1 position received the  
1434 difference between the genotype at the n+1 position and the genotype at position n. Any SNP  
1435 with a value not equal to zero was retained to estimate the genetic map, as described above. The  
1436 genomic coordinates of mismapped markers or SNPs were manually corrected based on the CC-  
1437 503 v6 or CC-1690 assemblies before re-running the genetic map construction, as above. The  
1438 quality of the assemblies was assessed by plotting the recombination frequencies across the  
1439 entire genome (*plotRF*) and by calculating the total length of the genetic map (*summaryMap*).

1440

## 1441 **Structural annotations**

1442 Protein-coding genes for the CC-4532 v6 and CC-503 v6 assemblies were annotated using  
1443 several sources of evidence. Input data were ~1.6 billion 150-bp paired-end RNA-seq reads from  
1444 the JGI Gene Atlas (strain CC-1690), ~6.4 million 454-sequenced ESTs generated by previous  
1445 versions of the genome project (CC-1690), and ~1.6 million PacBio Iso-Seq reads (pooled  
1446 samples from CC-4532, CC-5390, CC-4348, CC-4349, CC-4565, CC-4566 and CC-4567, see  
1447 Gallaher et al. (2021)). The Gene Atlas samples are described by Sreedasyam et al. (2022) and  
1448 can be browsed at <https://phytozome-next.jgi.doe.gov/geneatlas/>. Specifically for the CC-4532  
1449 v6 annotation, ~520 million unpaired 50 bp RNA-seq reads were included that were generated  
1450 from CC-4532 grown under a range of conditions including heterotrophic and photoautotrophic  
1451 growth, and in iron (Fe)-replete and Fe-limited media (NCBI SRA accessions PRJNA842032  
1452 and PRJNA717804). The RNA-seq and 454 reads were first assembled using PERTRAN (Shu et  
1453 al. 2013), which conducts genome-guided transcriptome short-read assembly via GSNAP (Wu  
1454 and Nacu 2010) and builds splice alignment graphs after alignment validation, realignment and  
1455 correction. Iso-Seq circular consensus sequencing (CCS) reads were corrected and collapsed  
1456 using a pipeline that aligns CCS reads to the genome with GMAP (Wu and Watanabe 2005),  
1457 performs intron correction for small InDels in splice junctions (if any), and clusters alignments  
1458 where all introns are shared for multi-exonic transcripts, or have 95% overlap for single-exon  
1459 transcripts. A combined assembly of all transcriptomic data was then produced using PASA  
1460 (Haas et al. 2003), yielding 287,891 assembled transcripts for CC-4532 v6 and 293,991 of CC-  
1461 503 v6.

1462  
1463 Preliminary loci were then identified using a combination of several tools and the relevant  
1464 transcriptome assembly or splice alignments. This complex pipeline involved extensive post-  
1465 processing, including the transfer of “missing” genes from previous assemblies, the identification  
1466 of low coding potential and TE genes, and the manual curation of several gene models. These  
1467 steps are described in detail in Supplemental Note S2.

### 1468 1469 **ChIP-seq and proteomics**

1470 Intergenic H3K4me3 ChIP-seq peaks called against the v5 assembly were retrieved from  
1471 Strenkert et al. (2022). Peak coordinates from the three time points in their experiment were  
1472 merged and subsequently converted to CC-4532 v6 coordinates using `halLiftover` (see above, a  
1473 peak was defined as successfully lifted over if  $\geq 90\%$  of sites were converted). Following  
1474 Strenkert et al. (2022), distance from the midpoint of each peak to the nearest TSS was  
1475 calculated, and a peak was assigned to a TSS if it was within 750 bp. Peaks that were still  
1476 classified as intergenic after this analysis were compared to the TE annotation and conservatively  
1477 called as TE-associated if  $\geq 80\%$  of sites within the peak overlapped a single TE copy.

1478  
1479 The proteomics analysis was performed as in Gallaher et al. (2018), using datasets generated in  
1480 that study. Briefly, peptides were identified by mass spectrometry and compared to the v5.6 and  
1481 CC-4532 v6.1 predicted proteins. The total number of gene models encoding proteins with at

1482 least one assigned peptide was estimated, as was the total number of unique peptides assigned to  
1483 each annotation, and the total number of peptides assigned overall.

1484

### 1485 **Identification of structural mutations and transposable element insertions**

1486 Structural variants (i.e. >50 bp) were called between the CC-503 v6 and CC-4532 v6 assemblies  
1487 using MUM&Co (O'Donnell and Fischer 2020), which identifies putative variants from  
1488 MUMmer alignments (Kurtz et al. 2004). MUM&Co was run on each chromosome individually,  
1489 and for chromosomes 2 and 9 the CC-503 v6 chromosomes were split at the translocation  
1490 breakpoints and the relevant parts of each chromosome were included. All variant calls were  
1491 then visualized and curated in IGV by comparing the CC-503 v6, CC-4532 v6 and CC-1690  
1492 assemblies (using alignments produced by minimap2, as performed above) and raw PacBio  
1493 reads. Variants called within tandem repeats or within regions where CC-4532 carried haplotype  
1494 2 were not considered. Confirmed variants were polarized as mutations by comparison of the  
1495 three assemblies i.e. the allele present in two assemblies (one of the v6 assemblies and CC-1690)  
1496 was assumed to be ancestral. Structural mutations unique to CC-1690 were not called.

1497

1498 Structural mutations identified in CC-503 v6 were subsequently compared to past assembly  
1499 versions and were called as consistent (present) or inconsistent (absent). Genes putatively  
1500 affected by structural mutations were identified from the assembly and annotation featuring the  
1501 ancestral state i.e. genes from the CC-4532 v6.1 annotation were identified at the regions  
1502 overlapping CC-503 v6 structural mutations (see Supplemental Datasets S7, S8, S10 and S11).

1503

1504 TE insertions were called as specific cases of insertion variants called by MUM&Co. All  
1505 insertions were compared against the annotations derived from the Chlamydomonas repeat  
1506 library (see above) and called as TE insertions where genomic coordinates of a TE perfectly  
1507 intersected those of the insertion. Similarly, a small number of “deletions” were called as  
1508 excision events of cut-and-paste DNA transposons (e.g. *Gulliver*).

1509

1510 To identify insertions of *Gypsy-7a\_cRei* in laboratory strains, whole-genome resequencing data  
1511 from 14 strains (Gallaher et al. 2015) were aligned using bwa mem (Li 2013) to a version of CC-  
1512 4532 v6 that had been hard-masked for TEs and had the Chlamydomonas repeat library  
1513 appended (causing all reads derived from *Gypsy-7a\_cRei* copies to map to the single consensus  
1514 sequence of this TE in the repeat library). Read pairs with at least one read mapped to the *Gypsy-  
1515 7a\_cRei* sequence and a mapping quality score >10 were extracted with samtools view (v1.15)  
1516 (“-b -h -P -q 10”) (Danecek et al. 2021). The resulting BAM files were used to generate  
1517 bedgraph files of read coverage using bedtools genomecov v2.30 (“-bg -split”) (Quinlan and Hall  
1518 2010). Peaks with <5 reads were filtered out. The resulting tracks were visualized in IGV v2.9.4  
1519 (Robinson et al. 2011). Peaks of coverage were manually identified for each strain.

1520

### 1521 **Phylogenetic analysis of RecQ3 helicases**

1522 Peptide sequences were collected by searching for similar proteins to Cre16.g801898,  
 1523 Cre16.g673393, and At4g35740 using the Phycocosm (Grigoriev et al. 2021), Phytozome  
 1524 (Goodstein et al. 2012) and NCBI databases. Sequences were aligned with MAFFT (v7.305)  
 1525 (Kato and Standley 2013) through the CIPRES web portal (Miller et al. 2010) and phylogenetic  
 1526 reconstruction was performed using W-IQ-TREE with default parameters (Trifinopoulos et al.  
 1527 2016). The consensus tree was visualized in iTOL (Letunic and Bork 2019), and the sequences  
 1528 from the subtree representing the RecQ3 subfamily were extracted, realigned, and used to build a  
 1529 RecQ3 phylogeny.

1530  
 1531 **Table 1. Comparison of assembly metrics between v6 assemblies, previous reference genome**  
 1532 **versions and the CC-1690 assembly.**  
 1533

Assembly strain/version	CC-503 v4	CC-503 v5	CC-503 v6	CC-4532 v6	CC-1690
Year	2008	2012	2022	2022	2020
Technology	Sanger	Sanger + 454	PacBio + Illumina	PacBio + Illumina	Nanopore + Illumina
Total length (Mb)	112.3	111.1	111.5	114.0	111.1
Unplaced scaffolds/contigs	71	37	42	40	1
Unplaced length (Mb)	9.68	2.20	1.45	1.72	1.65
Total contigs	2,739	1,495	145	120	21
Contig N50 (Mb)	0.09	0.22	2.92	2.65	3.58
GC (%)	64.1	64.1	64.1	64.1	64.1
Gaps/Ns (%)	7.54	3.65	1.66	0.81	<0.01
Transposable elements (%)	9.84	10.61	10.80	12.42	11.24
Microsatellites (%)	1.32	1.43	1.72	1.76	1.65
Satellite DNA (%)	3.33	3.68	4.79	5.25	5.09

1534  
 1535 Unplaced sequence was assembled as scaffolds in v4 and v5, and contigs in all other assemblies. The  
 1536 single unplaced contig in the released version of the CC-1690 assembly was later assembled to the right  
 1537 arm of chromosome 15 (Chaux-Jukic et al. 2021).

1538  
 1539 **Table 2. Comparison of structural annotations between reference genome versions.**  
 1540

Annotation	CC-503 v4.3	CC-503 v5.6	CC-503 v6.1	CC-4532 v6.1
Nuclear genes	17,114	17,741	16,795	16,801*
Alternative transcripts	/	1,789	14,874	14,979
Transposable element genes	/	/	647	810
Low coding potential genes	/	/	1,435	1,417
Plastome genes	/	/	74**	74**

Mitogenome genes	/	/	8	8
<b>BUSCO</b> ( <i>chlorophyta_odb10</i> , <i>N=1,519</i> )	C:96.7% [S:96.0%,D:0.7%] F:1.3%,M:2.0%	C:98.9% [S:98.2%,D:0.7%] F:0.3%,M:0.8%	C:100.0% [S:99.3%,D:0.7%] F:0.1%,M:0.0%	C:99.8% [S:98.8%,D:1.0%] F:0.1%,M:0.1%

- 1541 C, complete; S, single-copy; D, duplicated; F, fragmented; M, missing.  
1542 \*CC-4532 v6.1 contains 16 *MT+* specific genes (see below).  
1543 \*\*the three trans-spliced exons of *psaA* are here counted as individual models.  
1544  
1545  
1546  
1547 **SUPPLEMENTAL FILES**  
1548  
1549 **Supplemental Note S1.** Gene symbol naming rules.  
1550 **Supplemental Note S2.** Detailed gene annotation methods.  
1551  
1552 **Supplemental Figure S1.** Misassemblies in version 5 and their resolution in version 6.  
1553 **Supplemental Figure S2.** CG methylation and repeat landscape of the CC-1690 assembly.  
1554 **Supplemental Figure S3.** Full recombination frequency plots for the estimation of the genetic  
1555 maps.  
1556 **Supplemental Figure S4.** Summary of InDels present at CC-503 reciprocal  
1557 translocation/inversion double-strand breaks and repair points.  
1558 **Supplemental Figure S5.** Browser views of genes at double-strand breaks associated with the  
1559 CC-503 reciprocal translocation/inversion mutation.  
1560 **Supplemental Figure S6.** Browser views of whole-genome resequencing data at double-strand  
1561 breaks associated with the CC-503 reciprocal translocation/inversion mutation.  
1562 **Supplemental Figure S7.** Browser view of the CC-503 specific deletion of a prolyl 4-  
1563 hydroxylase gene.  
1564 **Supplemental Figure S8.** CC-4532 v6 haplotype 2 regions and unique structural mutations.  
1565 **Supplemental Figure S9.** Browser view of a v5.6 split gene model merged in CC-4532 v6.1.  
1566 **Supplemental Figure S10.** Analyses of coding potential for CC-4532 v6.1.  
1567 **Supplemental Figure S11.** Analyses of coding potential for CC-503 v6.1.  
1568 **Supplemental Figure S12.** Intersect between coding sequence of CC-503 v6.1 gene models  
1569 and transposable elements.  
1570 **Supplemental Figure S13.** Genomic distribution of haplotype 1 and 2 among laboratory strains.  
1571  
1572 **Supplemental Dataset S1.** Summary statistics, gene density and repeat content of the CC-  
1573 4532 v6 chromosomes.  
1574 **Supplemental Dataset S2.** Coordinate map between CC-4532 v6 chromosome 15 and the v5  
1575 assembly.  
1576 **Supplemental Dataset S3.** Summary statistics of the CC-4532 v6 genome split by site class  
1577 with respect to the CC-4532 v6.1 annotation.  
1578 **Supplemental Dataset S4.** Metrics and sequence context of all CC-4532 v6 assembly gaps.  
1579 **Supplemental Dataset S5.** Putative centromere metrics of the CC-1690 and CC-4532 v6  
1580 assemblies.  
1581 **Supplemental Dataset S6.** Approximate genomic coordinates from the markers of Kathir et al.  
1582 (2003).

1583 **Supplemental Dataset S7.** Curated structural mutations in the CC-503 v6 assembly.  
1584 **Supplemental Dataset S8.** Curated structural mutations in the CC-4532 v6 assembly.  
1585 **Supplemental Dataset S9.** Proteins, alignment and phylogeny for RECQ3 analysis.  
1586 **Supplemental Dataset S10.** Curated TE insertions/excisions in the CC-503 v6 assembly.  
1587 **Supplemental Dataset S11.** Curated TE insertions/excisions in the CC-4532 v6 assembly.  
1588 **Supplemental Dataset S12.** Approximate coordinates of *Gypsy-7a\_cRei* copies among  
1589 laboratory strains.  
1590 **Supplemental Dataset S13.** CC-4532 low coding potential genes.  
1591 **Supplemental Dataset S14.** CC-503 low coding potential genes.  
1592 **Supplemental Dataset S15.** Latest Chlamydomonas repeat library (v3.4).  
1593 **Supplemental Dataset S16.** Mating type locus R domain genes in CC-4532 v6.1 and CC-503  
1594 v6.1.  
1595 **Supplemental Dataset S17.** Haplotype 2 regions in CC-4532 v6.  
1596 **Supplemental Dataset S18.** Haplotype 2 coordinates in v5 and CC-4532 v6, and changes  
1597 between the assembly versions.  
1598 **Supplemental Dataset S19.** Comparison of proteomic validation of v5.6 and CC-4532 v6.1  
1599 proteins.  
1600 **Supplemental Dataset S20.** Master annotation table of CC-4532 v6.1.  
1601 **Supplemental Dataset S21.** Automated and expert annotations of v5.6 and CC-4532 v6.1  
1602 structural annotations.  
1603 **Supplemental Dataset S22.** List of genes with gene symbols or previous identifiers in v5.6 and  
1604 v6.1.  
1605

## 1606 **ACKNOWLEDGMENTS**

1607 The work (proposals: 10.46936/10.25585/60007932, 10.46936/10.25585/60001051, and  
1608 10.46936/10.25585/60000843) conducted by the U.S. Department of Energy Joint Genome  
1609 Institute (<https://ror.org/04xm1d337>), a DOE Office of Science User Facility, is supported by the  
1610 Office of Science of The U.S. Department of Energy operated under Contract No. DE-AC02-  
1611 05CH11231. Proteomics analyses were performed under the Facilities Integrating Collaborations  
1612 for User Science Program Proposals 49262, 49840, 49960, and 50797 and used resources at the  
1613 US DOE Joint Genome Institute and the Environmental Molecular Sciences Laboratory (EMSL;  
1614 grid.436923.9), which are DOE Office of Science User Facilities.  
1615

1616 We thank four reviewers for their comments that substantially improved an earlier version. We  
1617 would like to thank the following for their expert advice in assigning descriptions and gene  
1618 symbols to the v6.1 annotations: Jean Alric, Marius Arend, Ariane Atteia, Olga Baidukova,  
1619 Steven G. Ball, Matteo Ballotari, Gabriella Benko, Christoph Benning, Robert Bloodgood,  
1620 Alexandre-Viola Bohne, Pierre Cardol, Yen Peng Chew, Yves Choquet, José L. Crespo, David  
1621 Dauvillée, Dion Dunford, Susan K. Dutcher, Emilio Fernández-Reyes, Aurora Galván, Michel  
1622 Goldschmidt-Clermont, Arthur R. Grossman, Patrice P. Hamel, Thomas Happe, Peter  
1623 Hegemann, Michael Hippler, Martin Jonikas, Steve King, J. Clark Lagarias, Stéphane D.  
1624 Lemaire, Younghua Li-Beisson, Takuya Matsuo, David Mitchell, Aurora Nedelcu, Jörg  
1625 Nickelsen, Adrian Nievergeld, Krishna K. Niyogi, Junmin Pan, Dhruv Patel, Matthew C.  
1626 Posewitz, Claire Remacle, Nicolas Rouhier, Emanuel Sanz-Luque, Michael Schroda, James  
1627 Umen, Setsuko Wakao, Florent Waltz, Robert Willows, Felix Willmund, George B. Witman,

1628 Francis-André Wollman, Katia Wostrikoff, and William Zerges. We would like to thank Julianne  
1629 Oshiro and Jordan L. Chastain for assistance tracking down PMID accessions for incorporation  
1630 into Phytozome.

1631

1632

1633

## 1634 **AUTHOR CONTRIBUTIONS**

1635 JWJ, RJC and OV contributed to genome assembly. SS, RJC, SDG, OV and DMG performed  
1636 gene annotation and post-processing. SDG, JK, JG, KB, CD and YY performed and managed  
1637 nucleic acids preparation and sequencing. RJC, SDG, OV, PAS, CEB, SP, SO and DS performed  
1638 bioinformatics analyses. SDG, SSM and OV curated gene symbols and contributed annotation.  
1639 JS and SSM conceived, coordinated and supervised the study. RJC wrote the manuscript with  
1640 major contributions from SDG, PAS, OV and SSM. All authors read and commented on the  
1641 manuscript.

1642

## 1643 **DATA AVAILABILITY**

1644 CC-4532 v6 is available at Phytozome (<https://phytozome-next.jgi.doe.gov>). CC-4532 PacBio  
1645 reads and the CC-4532 v6 assembly and annotation are deposited at NCBI under the BioProject  
1646 PRJNA887768. CC-503 PacBio reads and the CC-503 v6 assembly and annotation are deposited  
1647 at NCBI under the BioProject PRJNA887764.

1648

## 1649 **REFERENCES**

- 1650 Arabidopsis Genome Initiative. 2000. Analysis of the genome sequence of the flowering plant  
1651 *Arabidopsis thaliana*. *Nature* **408**: 796-815.
- 1652 Armstrong J, Hickey G, Diekhans M, Fiddes IT, Novak AM, Deran A, Fang Q, Xie D, Feng S,  
1653 Stiller J et al. 2020. Progressive Cactus is a multiple-genome aligner for the thousand-  
1654 genome era. *Nature* **587**: 246-251.
- 1655 Bao W, Kojima KK, Kohany O. 2015. Repbase Update, a database of repetitive elements in  
1656 eukaryotic genomes. *Mobile DNA* **6**: 11.
- 1657 Bayer PE, Golicz AA, Scheben A, Batley J, Edwards D. 2020. Plant pan-genomes are the new  
1658 reference. *Nat Plants* **6**: 914-920.
- 1659 Benson G. 1999. Tandem repeats finder: a program to analyze DNA sequences. *Nucleic Acids*  
1660 *Res* **27**: 573-580.
- 1661 Blaby IK, Blaby-Haas CE. 2017. Genomics and functional genomics in *Chlamydomonas*  
1662 *reinhardtii*. In *Chlamydomonas: Molecular genetics and physiology*, (ed. M Hippler).  
1663 Springer.
- 1664 Blaby IK, Blaby-Haas CE, Tourasse N, Hom EF, Lopez D, Aksoy M, Grossman A, Umen J,  
1665 Dutcher S, Porter M et al. 2014. The *Chlamydomonas* genome project: a decade on.  
1666 *Trends in Plant Science* **19**: 672-680.



1667 Blaby-Haas CE, Castruita M, Fitz-Gibbon ST, Kropat J, Merchant SS. 2016. Ni induces the  
1668 CRR1-dependent regulon revealing overlap and distinction between hypoxia and Cu  
1669 deficiency responses in *Chlamydomonas reinhardtii*. *Metallomics* **8**: 679-691.

1670 Blaby-Haas CE, Merchant SS. 2019. Comparative and functional algal genomics. *Annual Review*  
1671 *of Plant Biology* **70**: 605-638.

1672 Blanc G, Agarkova I, Grimwood J, Kuo A, Brueggeman A, Dunigan DD, Gurnon J, Ladunga I,  
1673 Lindquist E, Lucas S et al. 2012. The genome of the polar eukaryotic microalga  
1674 *Coccomyxa subellipsoidea* reveals traits of cold adaptation. *Genome Biol* **13**.

1675 Boulouis A, Drapier D, Razafimanantsoa H, Wostrikoff K, Tourasse NJ, Pascal K, Girard-  
1676 Bascou J, Vallon O, Wollman FA, Choquet Y. 2015. Spontaneous dominant mutations in  
1677 *Chlamydomonas* highlight ongoing evolution by gene diversification. *Plant Cell* **27**: 984-  
1678 1001.

1679 Brand H, Collins RL, Hanscom C, Rosenfeld JA, Pillalamarri V, Stone MR, Kelley F, Mason T,  
1680 Margolin L, Eggert S et al. 2015. Paired-duplication signatures mark cryptic inversions  
1681 and other complex structural variation. *Am J Hum Genet* **97**: 170-176.

1682 Broman KW, Wu H, Sen S, Churchill GA. 2003. R/qtl: QTL mapping in experimental crosses.  
1683 *Bioinformatics* **19**: 889-890.

1684 Cavaiuolo M, Kuras R, Wollman FA, Choquet Y, Vallon O. 2017. Small RNA profiling in  
1685 *Chlamydomonas*: insights into chloroplast RNA metabolism. *Nucleic Acids Res* **45**:  
1686 10783-10799.

1687 Chaux-Jukic F, O'Donnell S, Craig RJ, Eberhard S, Vallon O, Xu Z. 2021. Architecture and  
1688 evolution of subtelomeres in the unicellular green alga *Chlamydomonas reinhardtii*.  
1689 *Nucleic Acids Res* **49**: 7571-7587.

1690 Craig RJ. 2021. The evolutionary genomics of *Chlamydomonas*. PhD thesis. University of  
1691 Edinburgh. <http://dx.doi.org/10.7488/era/1603>

1692 Craig RJ, Böndel KB, Arakawa K, Nakada T, Ito T, Bell G, Colegrave N, Keightley PD, Ness  
1693 RW. 2019. Patterns of population structure and complex haplotype sharing among field  
1694 isolates of the green alga *Chlamydomonas reinhardtii*. *Mol Ecol* **28**: 3977-3993.

1695 Craig RJ, Hasan AR, Ness RW, Keightley PD. 2021a. Comparative genomics of  
1696 *Chlamydomonas*. *Plant Cell* **33**: 1016-1041.

1697 Craig RJ, Yushenova IA, Rodriguez F, Arkhipova IR. 2021b. An ancient clade of *Penelope*-like  
1698 retroelements with permuted domains is present in the green lineage and protists, and  
1699 dominates many invertebrate genomes. *Mol Biol Evol* **38**: 5005-5020.

1700 Cross FR. 2015. Tying down loose ends in the *Chlamydomonas* genome: functional significance  
1701 of abundant upstream open reading frames. *G3 (Bethesda)* **6**: 435-446.

1702 Cross FR, Umen JG. 2015. The *Chlamydomonas* cell cycle. *The Plant Journal* **82**: 370-392.

1703 Croteau DL, Popuri V, Opresko PL, Bohr VA. 2014. Human RecQ helicases in DNA repair,  
1704 recombination, and replication. *Annu Rev Biochem* **83**: 519-552.

1705 Crozet P, Navarro FJ, Willmund F, Mehrshahi P, Bakowski K, Lauersen KJ, Perez-Perez ME,  
1706 Auroy P, Gorchs Rovira A, Sauret-Gueto S et al. 2018. Birth of a photosynthetic chassis:  
1707 a MoClo toolkit enabling synthetic biology in the microalga *Chlamydomonas reinhardtii*.  
1708 *ACS Synth Biol* **7**: 2074-2086.

1709 Cui J, Zhang Z, Shao Y, Zhang K, Leng P, Liang Z. 2015. Genome-wide identification,  
1710 evolutionary, and expression analyses of histone H3 variants in plants. *Biomed Res Int*  
1711 **2015**: 341598.

1712 Danecek P, Bonfield JK, Liddle J, Marshall J, Ohan V, Pollard MO, Whitwham A, Keane T,  
1713 McCarthy SA, Davies RM et al. 2021. Twelve years of SAMtools and BCFtools.  
1714 *Gigascience* **10**: giab008.

1715 Davies DR. 1972. Cell wall organisation in *Chlamydomonas reinhardi*. The role of extra-nuclear  
1716 systems. *Mol Gen Genet* **115**: 334-348.

1717 Day A, Schirmerrahire M, Kuchka MR, Mayfield SP, Rochaix JD. 1988. A transposon with an  
1718 unusual arrangement of long terminal repeats in the green alga *Chlamydomonas*  
1719 *reinhardtii*. *EMBO Journal* **7**: 1917-1927.

1720 De Hoff PL, Ferris P, Olson BJSC, Miyagi A, Geng S, Umen JG. 2013. Species and population  
1721 level molecular profiling reveals cryptic recombination and emergent asymmetry in the  
1722 dimorphic mating locus of *C. reinhardtii*. *PLoS Genet* **9**.

1723 Deisseroth K, Hegemann P. 2017. The form and function of channelrhodopsin. *Science* **357**.

1724 Dorn A, Puchta H. 2019. DNA helicases as safekeepers of genome stability in plants. *Genes*  
1725 (*Basel*) **10**: 1028.

1726 Dutcher SK. 2014. The awesome power of dikaryons for studying flagella and basal bodies in  
1727 *Chlamydomonas reinhardtii*. *Cytoskeleton* **71**: 79-94.

1728 Dutcher SK, Power J, Galloway RE, Porter ME. 1991. Reappraisal of the genetic map of  
1729 *Chlamydomonas reinhardtii*. *J Hered* **82**: 295-301.

1730 Engel BD, Schaffer M, Kuhn Cuellar L, Villa E, Plitzko JM, Baumeister W. 2015. Native  
1731 architecture of the *Chlamydomonas* chloroplast revealed by in situ cryo-electron  
1732 tomography. *eLife* **4**: e04889.

1733 Fauser F, Vilarrasa-Blasi J, Onishi M, Ramundo S, Patena W, Millican M, Osaki J, Philp C,  
1734 Nemeth M, Salome PA et al. 2022. Systematic characterization of gene function in the  
1735 photosynthetic alga *Chlamydomonas reinhardtii*. *Nat Genet* **54**: 705-714.

1736 Fédry J, Liu Y, Pehau-Arnaudet G, Pei J, Li W, Tortorici MA, Traincard F, Meola A, Bricogne  
1737 G, Grishin NV et al. 2017. The ancient gamete fusogen HAP2 is a eukaryotic class II  
1738 fusion protein. *Cell* **168**: 904-915.e910.

1739 Ferris P, Olson BJ, De Hoff PL, Douglass S, Casero D, Prochnik S, Geng S, Rai R, Grimwood J,  
1740 Schmutz J et al. 2010. Evolution of an expanded sex-determining locus in *Volvox*.  
1741 *Science* **328**: 351-354.

1742 Ferris PJ. 1989. Characterization of a *Chlamydomonas* transposon, *Gulliver*, resembling those in  
1743 higher-plants. *Genetics* **122**: 363-377.

1744 Ferris PJ, Armbrust EV, Goodenough UW. 2002. Genetic structure of the mating-type locus of  
1745 *Chlamydomonas reinhardtii*. *Genetics* **160**: 181-200.

1746 Ferris PJ, Goodenough UW. 1994. The mating-type locus of *Chlamydomonas reinhardtii*  
1747 contains highly rearranged DNA sequences. *Cell* **76**: 1135-1145.

1748 Flowers JM, Hazzouri KM, Pham GM, Rosas U, Bahmani T, Khraiwesh B, Nelson DR, Jijakli  
1749 K, Abdrabu R, Harris EH et al. 2015. Whole-genome resequencing reveals extensive  
1750 natural variation in the model green alga *Chlamydomonas reinhardtii*. *Plant Cell* **27**:  
1751 2353-2369.

1752 Freeman Rosenzweig ES, Xu B, Kuhn Cuellar L, Martinez-Sanchez A, Schaffer M, Strauss M,  
1753 Cartwright HN, Ronceray P, Plitzko JM, Forster F et al. 2017. The eukaryotic CO<sub>2</sub>-  
1754 concentrating organelle is liquid-like and exhibits dynamic reorganization. *Cell* **171**: 148-  
1755 162.e119.

1756 Gallaher SD, Craig RJ, Ganesan I, Purvine SO, McCorkle S, Grimwood J, Strenkert D, Davidi L,  
1757 Roth MS, Jeffers TL et al. 2021. Widespread polycistronic gene expression in green  
1758 algae. *Proc Natl Acad Sci U S A* **118**: e2017714118.

1759 Gallaher SD, Fitz-Gibbon ST, Glaesener AG, Pellegrini M, Merchant SS. 2015. *Chlamydomonas*  
1760 genome resource for laboratory strains reveals a mosaic of sequence variation, identifies  
1761 true strain histories, and enables strain-specific studies. *Plant Cell* **27**: 2335-2352.

1762 Gallaher SD, Fitz-Gibbon ST, Strenkert D, Purvine SO, Pellegrini M, Merchant SS. 2018. High-  
1763 throughput sequencing of the chloroplast and mitochondrion of *Chlamydomonas*  
1764 *reinhardtii* to generate improved *de novo* assemblies, analyze expression patterns and  
1765 transcript speciation, and evaluate diversity among laboratory strains and wild isolates.  
1766 *Plant J* **93**: 545-565.

1767 Gel B, Serra E. 2017. karyoploteR: an R/Bioconductor package to plot customizable genomes  
1768 displaying arbitrary data. *Bioinformatics* **33**: 3088-3090.

1769 Goff SA, Ricke D, Lan TH, Presting G, Wang R, Dunn M, Glazebrook J, Sessions A, Oeller P,  
1770 Varma H et al. 2002. A draft sequence of the rice genome (*Oryza sativa* L. ssp.  
1771 *japonica*). *Science* **296**: 92-100.

1772 Goodstein DM, Shu S, Howson R, Neupane R, Hayes RD, Fazo J, Mitros T, Dirks W, Hellsten  
1773 U, Putnam N et al. 2012. Phytozome: a comparative platform for green plant genomics.  
1774 *Nucleic Acids Res* **40**: D1178-1186.

1775 Goodwin TJ, Poulter RT. 2004. A new group of tyrosine recombinase-encoding  
1776 retrotransposons. *Mol Biol Evol* **21**: 746-759.

1777 Gorres KL, Raines RT. 2010. Prolyl 4-hydroxylase. *Crit Rev Biochem Mol Biol* **45**: 106-124.

1778 Grigoriev IV, Hayes RD, Calhoun S, Kamel B, Wang A, Ahrendt S, Dusheyko S, Nikitin R,  
1779 Mondo SJ, Salamov A et al. 2021. PhycoCosm, a comparative algal genomics resource.  
1780 *Nucleic Acids Res* **49**: D1004-D1011.

1781 Grossman AR, Harris EE, Hauser C, Lefebvre PA, Martinez D, Rokhsar D, Shrager J, Silflow  
1782 CD, Stern D, Vallon O et al. 2003. *Chlamydomonas reinhardtii* at the crossroads of  
1783 genomics. *Eukaryot Cell* **2**: 1137-1150.

1784 Haas BJ, Delcher AL, Mount SM, Wortman JR, Smith RK, Jr., Hannick LI, Maiti R, Ronning  
1785 CM, Rusch DB, Town CD et al. 2003. Improving the *Arabidopsis* genome annotation  
1786 using maximal transcript alignment assemblies. *Nucleic Acids Res* **31**: 5654-5666.

1787 Hamaji T, Kawai-Toyooka H, Uchimura H, Suzuki M, Noguchi H, Minakuchi Y, Toyoda A,  
1788 Fujiyama A, Miyagishima S, Umen JG et al. 2018. Anisogamy evolved with a reduced  
1789 sex-determining region in volvocine green algae. *Communications Biology* **1**: 17.

1790 Helliwell KE, Collins S, Kazamia E, Purton S, Wheeler GL, Smith AG. 2015. Fundamental shift  
1791 in vitamin B12 eco-physiology of a model alga demonstrated by experimental evolution.  
1792 *ISME J* **9**: 1446-1455.

1793 Hickey G, Paten B, Earl D, Zerbino D, Haussler D. 2013. HAL: a hierarchical format for storing  
1794 and analyzing multiple genome alignments. *Bioinformatics* **29**: 1341-1342.

1795 Hyams J, Davies DR. 1972. Induction and characterization of cell-wall mutants of  
1796 *Chlamydomonas reinhardi*. *Mutat Res* **14**: 381-&.

1797 Ito H, Gaubert H, Bucher E, Mirouze M, Vaillant I, Paszkowski J. 2011. An siRNA pathway  
1798 prevents transgenerational retrotransposition in plants subjected to stress. *Nature* **472**:  
1799 115-119.

1800 Jiao Y, Peluso P, Shi J, Liang T, Stitzer MC, Wang B, Campbell MS, Stein JC, Wei X, Chin CS  
1801 et al. 2017. Improved maize reference genome with single-molecule technologies. *Nature*  
1802 **546**: 524-527.

1803 Joo S, Kariyawasam T, Kim M, Jin E, Goodenough U, Lee JH. 2022. Sex-linked deubiquitinase  
1804 establishes uniparental transmission of chloroplast DNA. *Nat Commun* **13**: 1133.

1805 Kaina B. 2004. Mechanisms and consequences of methylating agent-induced SCEs and  
1806 chromosomal aberrations: a long road traveled and still a far way to go. *Cytogenet*  
1807 *Genome Res* **104**: 77-86.

1808 Kapitonov VV, Jurka J. 2003. The esterase and PHD domains in CR1-like non-LTR  
1809 retrotransposons. *Mol Biol Evol* **20**: 38-46.

1810 Kathir P, LaVoie M, Brazelton WJ, Haas NA, Lefebvre PA, Silflow CD. 2003. Molecular map  
1811 of the *Chlamydomonas reinhardtii* nuclear genome. *Eukaryot Cell* **2**: 362-379.

1812 Katoh K, Standley DM. 2013. MAFFT multiple sequence alignment software version 7:  
1813 improvements in performance and usability. *Mol Biol Evol* **30**: 772-780.

1814 Keskiäho K, Hieta R, Sormunen R, Myllyharju J. 2007. *Chlamydomonas reinhardtii* has multiple  
1815 prolyl 4-hydroxylases, one of which is essential for proper cell wall assembly. *Plant Cell*  
1816 **19**: 256-269.

1817 Kim KS, Kustu S, Inwood W. 2006. Natural history of transposition in the green alga  
1818 *Chlamydomonas reinhardtii*: Use of the AMT4 locus as an experimental system.  
1819 *Genetics* **173**: 2005-2019.

1820 Koren S, Walenz BP, Berlin K, Miller JR, Bergman NH, Phillippy AM. 2017. Canu: scalable  
1821 and accurate long-read assembly via adaptive k-mer weighting and repeat separation.  
1822 *Genome Res* **27**: 722-736.

1823 Krzywinski M, Schein J, Birol I, Connors J, Gascoyne R, Horsman D, Jones SJ, Marra MA.  
1824 2009. Circos: an information aesthetic for comparative genomics. *Genome Res* **19**: 1639-  
1825 1645.

1826 Kück U, Choquet Y, Schneider M, Dron M, Bennoun P. 1987. Structural and transcription  
1827 analysis of two homologous genes for the P700 chlorophyll a-apoproteins in  
1828 *Chlamydomonas reinhardtii*: evidence for in vivo trans-splicing. *EMBO J* **6**: 2185-2195.

1829 Kurtz S, Phillippy A, Delcher AL, Smoot M, Shumway M, Antonescu C, Salzberg SL. 2004.  
1830 Versatile and open software for comparing large genomes. *Genome Biol* **5**: R12.

1831 Labadorf A, Link A, Rogers MF, Thomas J, Reddy AS, Ben-Hur A. 2010. Genome-wide  
1832 analysis of alternative splicing in *Chlamydomonas reinhardtii*. *Bmc Genomics* **11**: 114.

1833 Letunic I, Bork P. 2019. Interactive Tree Of Life (iTOL) v4: recent updates and new  
1834 developments. *Nucleic Acids Res* **47**: W256-W259.

1835 Lex A, Gehlenborg N, Strobelt H, Vuillemot R, Pfister H. 2014. UpSet: visualization of  
1836 intersecting sets. *IEEE Trans Vis Comput Graph* **20**: 1983-1992.

1837 Li H. 2013. Aligning sequence reads, clone sequences and assembly contigs with BWA-MEM.  
1838 *arXiv* doi:arXiv:1303.3997.

1839 Li H. 2018. Minimap2: pairwise alignment for nucleotide sequences. *Bioinformatics* **34**: 3094-  
1840 3100.

1841 Li X, Patena W, Fauser F, Jinkerson RE, Saroussi S, Meyer MT, Ivanova N, Robertson JM, Yue  
1842 R, Zhang R et al. 2019. A genome-wide algal mutant library and functional screen  
1843 identifies genes required for eukaryotic photosynthesis. *Nat Genet* **51**: 627-635.

- 1844 Lin H, Cliften PF, Dutcher SK. 2018. MAPINS, a highly efficient detection method that  
 1845 identifies insertional mutations and complex DNA rearrangements. *Plant Physiol* **178**:  
 1846 1436-1447.
- 1847 Lin H, Miller ML, Granas DM, Dutcher SK. 2013. Whole genome sequencing identifies a  
 1848 deletion in protein phosphatase 2A that affects its stability and localization in  
 1849 *Chlamydomonas reinhardtii*. *PLoS Genet* **9**: e1003841.
- 1850 Liu H, Huang J, Sun X, Li J, Hu Y, Yu L, Liti G, Tian D, Hurst LD, Yang S. 2018. Tetrad  
 1851 analysis in plants and fungi finds large differences in gene conversion rates but no GC  
 1852 bias. *Nat Ecol Evol* **2**: 164-173.
- 1853 Liu J, Seetharam AS, Chougule K, Ou S, Swentowsky KW, Gent JI, Llaca V, Woodhouse MR,  
 1854 Manchanda N, Presting GG et al. 2020. Gapless assembly of maize chromosomes using  
 1855 long-read technologies. *Genome Biol* **21**: 121.
- 1856 Liu Q, Fang L, Yu G, Wang D, Xiao CL, Wang K. 2019. Detection of DNA base modifications  
 1857 by deep recurrent neural network on Oxford Nanopore sequencing data. *Nat Commun* **10**:  
 1858 2449.
- 1859 Lopez D, Hamaji T, Kropat J, De Hoff P, Morselli M, Rubbi L, Fitz-Gibbon S, Gallaher SD,  
 1860 Merchant SS, Umen J et al. 2015. Dynamic changes in the transcriptome and methylome  
 1861 of *Chlamydomonas reinhardtii* throughout Its life cycle. *Plant Physiol* **169**: 2730-2743.
- 1862 López-Cortegano E, Craig RJ, Chebib J, Balogun EJ, Keightley PD. 2022. Rates and spectra of  
 1863 *de novo* structural mutation in *Chlamydomonas reinhardtii*. *Biorxiv*  
 1864 doi:<https://doi.org/10.1101/2022.05.23.493040>.
- 1865 Lu H, Davis AJ. 2021. Human RecQ helicases in DNA double-strand break repair. *Front Cell*  
 1866 *Dev Biol* **9**: 640755.
- 1867 Manni M, Berkeley MR, Seppey M, Simão FA, Zdobnov EM. 2021. BUSCO update: novel and  
 1868 streamlined workflows along with broader and deeper phylogenetic coverage for scoring  
 1869 of eukaryotic, prokaryotic, and viral genomes. *Mol Biol Evol* **38**: 4647-4654.
- 1870 Maul JE, Lilly JW, Cui L, dePamphilis CW, Miller W, Harris EH, Stern DB. 2002. The  
 1871 *Chlamydomonas reinhardtii* plastid chromosome: islands of genes in a sea of repeats.  
 1872 *Plant Cell* **14**: 2659-2679.
- 1873 McCarthy SS, Kobayashi MC, Niyogi KK. 2004. White mutants of *Chlamydomonas reinhardtii*  
 1874 are defective in phytoene synthase. *Genetics* **168**: 1249-1257.
- 1875 McKenna A, Hanna M, Banks E, Sivachenko A, Cibulskis K, Kernytsky A, Garimella K,  
 1876 Altshuler D, Gabriel S, Daly M et al. 2010. The Genome Analysis Toolkit: a MapReduce  
 1877 framework for analyzing next-generation DNA sequencing data. *Genome Res* **20**: 1297-  
 1878 1303.
- 1879 Merchant SS Prochnik SE Vallon O Harris EH Karpowicz SJ Witman GB Terry A Salamov A  
 1880 Fritz-Laylin LK Marechal-Drouard L et al. 2007. The *Chlamydomonas* genome reveals  
 1881 the evolution of key animal and plant functions. *Science* **318**: 245-250.
- 1882 Miller RJ, Pfeiffer W, Schwartz T. 2010. Creating the CIPRES Science Gateway for inference of  
 1883 large phylogenetic trees. In *2010 Gateway Computing Environments Workshop (GCE)*,  
 1884 doi:10.1109/GCE.2010.5676129, pp. 1-8. IEEE.
- 1885 Moseley JL, Page MD, Alder NP, Eriksson M, Quinn J, Soto F, Theg SM, Hippler M, Merchant  
 1886 S. 2002. Reciprocal expression of two candidate di-iron enzymes affecting photosystem I  
 1887 and light-harvesting complex accumulation. *Plant Cell* **14**: 673-688.
- 1888 Navrátilová A, Koblížková A, Macas J. 2008. Survey of extrachromosomal circular DNA  
 1889 derived from plant satellite repeats. *BMC Plant Biol* **8**: 90.

1890 Neupert J, Gallaher SD, Lu Y, Strenkert D, Segal N, Barahimipour R, Fitz-Gibbon ST, Schroda  
1891 M, Merchant SS, Bock R. 2020. An epigenetic gene silencing pathway selectively acting  
1892 on transgenic DNA in the green alga *Chlamydomonas*. *Nat Commun* **11**: 6269.

1893 Ngan CY, Wong CH, Choi C, Yoshinaga Y, Louie K, Jia J, Chen C, Bowen B, Cheng H,  
1894 Leonelli L et al. 2015. Lineage-specific chromatin signatures reveal a regulator of lipid  
1895 metabolism in microalgae. *Nat Plants* **1**: 15107.

1896 Ni P, Huang N, Zhang Z, Wang DP, Liang F, Miao Y, Xiao CL, Luo F, Wang J. 2019.  
1897 DeepSignal: detecting DNA methylation state from Nanopore sequencing reads using  
1898 deep-learning. *Bioinformatics* **35**: 4586-4595.

1899 Ning J, Otto TD, Pfander C, Schwach F, Brochet M, Bushell E, Goulding D, Sanders M,  
1900 Lefebvre PA, Pei J et al. 2013. Comparative genomics in *Chlamydomonas* and  
1901 *Plasmodium* identifies an ancient nuclear envelope protein family essential for sexual  
1902 reproduction in protists, fungi, plants, and vertebrates. *Genes Dev* **27**: 1198-1215.

1903 Novoselov SV, Rao M, Onoshko NV, Zhi H, Kryukov GV, Xiang Y, Weeks DP, Hatfield DL,  
1904 Gladyshev VN. 2002. Selenoproteins and selenocysteine insertion system in the model  
1905 plant cell system, *Chlamydomonas reinhardtii*. *EMBO J* **21**: 3681-3693.

1906 O'Donnell S, Chaux F, Fischer G. 2020. Highly contiguous Nanopore genome assembly of  
1907 *Chlamydomonas reinhardtii* CC-1690. *Microbiol Resour Announc* **9**: e00726-00720.

1908 O'Donnell S, Fischer G. 2020. MUM&Co: accurate detection of all SV types through whole-  
1909 genome alignment. *Bioinformatics* **36**: 3242-3243.

1910 Ozawa SI, Cavaiuolo M, Jarrige D, Kuras R, Rutgers M, Eberhard S, Drapier D, Wollman FA,  
1911 Choquet Y. 2020. The OPR protein MTHI1 controls the expression of two different  
1912 subunits of ATP synthase CFo in *Chlamydomonas reinhardtii*. *Plant Cell* **32**: 1179-1203.

1913 Perez-Alegre M, Dubus A, Fernandez E. 2005. REM1, a new type of long terminal repeat  
1914 retrotransposon in *Chlamydomonas reinhardtii*. *Mol Cell Biol* **25**: 10628-10638.

1915 Petracek ME, Lefebvre PA, Silflow CD, Berman J. 1990. *Chlamydomonas* telomere sequences  
1916 are A+T-rich but contain three consecutive G-C base pairs. *Proc Natl Acad Sci U S A* **87**:  
1917 8222-8226.

1918 Philippsen GS, Avaca-Crusca JS, Araujo APU, DeMarco R. 2016. Distribution patterns and  
1919 impact of transposable elements in genes of green algae. *Gene* **594**: 151-159.

1920 Porter ME, Knott JA, Myster SH, Farlow SJ. 1996. The dynein gene family in *Chlamydomonas*  
1921 *reinhartii*. *Genetics* **144**: 569-585.

1922 Preuss D, Mets L. 2002. Plant centromere functions defined by tetrad analysis and artificial  
1923 chromosomes. *Plant Physiol* **129**: 421-422.

1924 Prochnik SE, Umen J, Nedelcu AM, Hallmann A, Miller SM, Nishii I, Ferris P, Kuo A, Mitros  
1925 T, Fritz-Laylin LK et al. 2010. Genomic analysis of organismal complexity in the  
1926 multicellular green alga *Volvox carteri*. *Science* **329**: 223-226.

1927 Pröschold T, Harris EH, Coleman AW. 2005. Portrait of a species: *Chlamydomonas reinhardtii*.  
1928 *Genetics* **170**: 1601-1610.

1929 Quinlan AR, Hall IM. 2010. BEDTools: a flexible suite of utilities for comparing genomic  
1930 features. *Bioinformatics* **26**: 841-842.

1931 Raj-Kumar PK, Vallon O, Liang C. 2017. *In silico* analysis of the sequence features responsible  
1932 for alternatively spliced introns in the model green alga *Chlamydomonas reinhardtii*.  
1933 *Plant Mol Biol* **94**: 253-265.

1934 Riddle NC, Elgin SCR. 2018. The *Drosophila* dot chromosome: where genes flourish amidst  
1935 repeats. *Genetics* **210**: 757-772.

- 1936 Robinson JT, Thorvaldsdóttir H, Winckler W, Guttman M, Lander ES, Getz G, Mesirov JP.  
1937 2011. Integrative Genomics Viewer. *Nat Biotechnol* **29**: 24-26.
- 1938 Röhrig S, Dorn A, Enderle J, Schindele A, Herrmann NJ, Knoll A, Puchta H. 2018. The RecQ-  
1939 like helicase HRQ1 is involved in DNA crosslink repair in Arabidopsis in a common  
1940 pathway with the Fanconi anemia-associated nuclease FAN1 and the postreplicative  
1941 repair ATPase RAD5A. *New Phytol* **218**: 1478-1490.
- 1942 Roth MS, Cokus SJ, Gallaher SD, Walter A, Lopez D, Erickson E, Endelman B, Westcott D,  
1943 Larabell CA, Merchant SS et al. 2017. Chromosome-level genome assembly and  
1944 transcriptome of the green alga *Chromochloris zofingiensis* illuminates astaxanthin  
1945 production. *Proc Natl Acad Sci U S A* **114**: E4296-E4305.
- 1946 Ruiz-Ruano FJ, López-León MD, Cabrero J, Camacho JPM. 2016. High-throughput analysis of  
1947 the satellitome illuminates satellite DNA evolution. *Sci Rep* **6**: 28333.
- 1948 Rymarquis LA, Handley JM, Thomas M, Stern DB. 2005. Beyond complementation. Map-based  
1949 cloning in *Chlamydomonas reinhardtii*. *Plant Physiol* **137**: 557-566.
- 1950 Salinas-Giegé T, Cavaiuolo M, Cognat V, Ubrig E, Remacle C, Duchene AM, Vallon O,  
1951 Marechal-Drouard L. 2017. Polycytidylation of mitochondrial mRNAs in  
1952 *Chlamydomonas reinhardtii*. *Nucleic Acids Res* **45**: 12963-12973.
- 1953 Salomé PA, Merchant SS. 2019. A Series of fortunate events: Introducing *Chlamydomonas* as a  
1954 reference organism. *Plant Cell* **31**: 1682-1707.
- 1955 Schnell RA, Lefebvre PA. 1993. Isolation of the *Chlamydomonas* regulatory gene NIT2 by  
1956 transposon tagging. *Genetics* **134**: 737-747.
- 1957 Shu S, Goodstein D, Rokhsar D. 2013. PERTRAN: genome-guided RNA-seq read assembler. In  
1958 *OSTIgov: US Department of Energy - Office of Scientific and Technical Information*.
- 1959 Smit AFA, Hubley R, Green P. 2013-2015. RepeatMasker Open-4.0.  
1960 <http://www.repeatmasker.org>.
- 1961 Smith DR, Craig RJ. 2021. Does mitochondrial DNA replication in *Chlamydomonas* require a  
1962 reverse transcriptase? *New Phytol* **229**: 1192-1195.
- 1963 Smith DR, Lee RW. 2009. Nucleotide diversity of the *Chlamydomonas reinhardtii* plastid  
1964 genome: addressing the mutational-hazard hypothesis. *BMC Evol Biol* **9**: 120.
- 1965 Smith EF, Lefebvre PA. 1997. *PF20* gene product contains WD repeats and localizes to the  
1966 intermicrotubule bridges in *Chlamydomonas* flagella. *Mol Biol Cell* **8**: 455-467.
- 1967 Sreedasyam A, Plott C, Shadkhawat Hossain M, Lovell JT, Grimwood J, Jenkins JW, Daum C,  
1968 Barry K, Carlson J, Shu S et al. 2022. JGI Plant Gene Atlas: An updateable transcriptome  
1969 resource to improve structural annotations and functional gene descriptions across the  
1970 plant kingdom. *Biorxiv* doi:doi.org/10.1101/2022.09.30.510380.
- 1971 Sterken MG, Snoek LB, Kammenga JE, Andersen EC. 2015. The laboratory domestication of  
1972 *Caenorhabditis elegans*. *Trends Genet* **31**: 224-231.
- 1973 Strenkert D, Yildirim A, Yan J, Yoshinaga Y, Pellegrini M, O'Malley RC, Merchant SS, Umen  
1974 JG. 2022. The landscape of *Chlamydomonas* histone H3 lysine 4 methylation reveals  
1975 both constant features and dynamic changes during the diurnal cycle. *Plant J*  
1976 doi:10.1111/tpj.15948.
- 1977 Sumper M, Hallmann A. 1998. Biochemistry of the extracellular matrix of *Volvox*. *Int Rev Cytol*  
1978 **180**: 51-85.
- 1979 Trifinopoulos J, Nguyen LT, von Haeseler A, Minh BQ. 2016. W-IQ-TREE: a fast online  
1980 phylogenetic tool for maximum likelihood analysis. *Nucleic Acids Res* **44**: W232-235.

1981 Tulin F, Cross FR. 2014. A microbial avenue to cell cycle control in the plant superkingdom.  
1982 *Plant Cell* **26**: 4019-4038.

1983 Tulin F, Cross FR. 2016. Patching holes in the *Chlamydomonas* genome. *G3 (Bethesda)* **6**: 1899-  
1984 1910.

1985 Ueki N, Nishii I. 2008. Idaten is a new cold-inducible transposon of *Volvox carteri* that can be  
1986 used for tagging developmentally important genes. *Genetics* **180**: 1343-1353.

1987 Vahrenholz C, Riemen G, Pratje E, Dujon B, Michaelis G. 1993. Mitochondrial DNA of  
1988 *Chlamydomonas reinhardtii*: the structure of the ends of the linear 15.8-kb genome  
1989 suggests mechanisms for DNA replication. *Curr Genet* **24**: 241-247.

1990 Wang SC, Schnell RA, Lefebvre PA. 1998. Isolation and characterization of a new transposable  
1991 element in *Chlamydomonas reinhardtii*. *Plant Molecular Biology* **38**: 681-687.

1992 Wiedemann G, van Gessel N, Kochl F, Hunn L, Schulze K, Maloukh L, Nogue F, Decker EL,  
1993 Hartung F, Reski R. 2018. RecQ helicases function in development, DNA repair, and  
1994 gene targeting in *Physcomitrella patens*. *Plant Cell* **30**: 717-736.

1995 Williams BA, Slamovits CH, Patron NJ, Fast NM, Keeling PJ. 2005. A high frequency of  
1996 overlapping gene expression in compacted eukaryotic genomes. *Proc Natl Acad Sci U S*  
1997 *A* **102**: 10936-10941.

1998 Woessner JP, Goodenough UW. 1994. Volvocine cell walls and their constituent glycoproteins:  
1999 an evolutionary perspective. *Protoplasma* **181**: 245-258.

2000 Wright BW, Molloy MP, Jaschke PR. 2022. Overlapping genes in natural and engineered  
2001 genomes. *Nat Rev Genet* **23**: 154-168.

2002 Wu TD, Nacu S. 2010. Fast and SNP-tolerant detection of complex variants and splicing in short  
2003 reads. *Bioinformatics* **26**: 873-881.

2004 Wu TD, Watanabe CK. 2005. GMAP: a genomic mapping and alignment program for mRNA  
2005 and EST sequences. *Bioinformatics* **21**: 1859-1875.

2006 Wyatt MD, Pittman DL. 2006. Methylating agents and DNA repair responses: Methylated bases  
2007 and sources of strand breaks. *Chem Res Toxicol* **19**: 1580-1594.

2008 Xiao CL, Chen Y, Xie SQ, Chen KN, Wang Y, Han Y, Luo F, Xie Z. 2017. MECAT: fast  
2009 mapping, error correction, and de novo assembly for single-molecule sequencing reads.  
2010 *Nat Methods* **14**: 1072-1074.

2011 Yamamoto K, Hamaji T, Kawai-Toyooka H, Matsuzaki R, Takahashi F, Nishimura Y, Kawachi  
2012 M, Noguchi H, Minakuchi Y, Umen JG et al. 2021. Three genomes in the algal genus  
2013 *Volvox* reveal the fate of a haploid sex-determining region after a transition to  
2014 homothallism. *Proc Natl Acad Sci U S A* **118**.

2015 Yamamoto R, Obbineni JM, Alford LM, Ide T, Owa M, Hwang J, Kon T, Inaba K, James N,  
2016 King SM et al. 2017. *Chlamydomonas* DYX1C1/PF23 is essential for axonemal assembly  
2017 and proper morphology of inner dynein arms. *PLoS Genet* **13**: e1006996.

2018 Zhao Z, Guo C, Sutharzan S, Li P, Echt CS, Zhang J, Liang C. 2014. Genome-wide analysis of  
2019 tandem repeats in plants and green algae. *G3 (Bethesda)* **4**: 67-78.

2020



## Parsed Citations

- Arabidopsis Genome Initiative. 2000. Analysis of the genome sequence of the flowering plant *Arabidopsis thaliana*. *Nature* 408: 796-815.**  
Google Scholar: [Author Only](#) [Title Only](#) [Author and Title](#)
- Armstrong J, Hickey G, Diekhans M, Fiddes IT, Novak AM, Deran A, Fang Q, Xie D, Feng S, Stiller J et al. 2020. Progressive Cactus is a multiple-genome aligner for the thousand-genome era. *Nature* 587: 246-251.**  
Google Scholar: [Author Only](#) [Title Only](#) [Author and Title](#)
- Bao W, Kojima KK, Kohany O. 2015. Repbase Update, a database of repetitive elements in eukaryotic genomes. *Mobile DNA* 6: 11.**  
Google Scholar: [Author Only](#) [Title Only](#) [Author and Title](#)
- Bayer PE, Golicz AA, Scheben A, Batley J, Edwards D. 2020. Plant pan-genomes are the new reference. *Nat Plants* 6: 914-920.**  
Google Scholar: [Author Only](#) [Title Only](#) [Author and Title](#)
- Benson G. 1999. Tandem repeats finder: a program to analyze DNA sequences. *Nucleic Acids Res* 27: 573-580.**  
Google Scholar: [Author Only](#) [Title Only](#) [Author and Title](#)
- Blaby IK, Blaby-Haas CE. 2017. Genomics and functional genomics in *Chlamydomonas reinhardtii*. In *Chlamydomonas: Molecular genetics and physiology*, (ed. M Hippler). Springer.**  
Google Scholar: [Author Only](#) [Title Only](#) [Author and Title](#)
- Blaby IK, Blaby-Haas CE, Tourasse N, Hom EF, Lopez D, Aksoy M, Grossman A, Umen J, Dutcher S, Porter M et al. 2014. The *Chlamydomonas* genome project: a decade on. *Trends in Plant Science* 19: 672-680.**  
Google Scholar: [Author Only](#) [Title Only](#) [Author and Title](#)
- Blaby-Haas CE, Castruita M, Fitz-Gibbon ST, Kropat J, Merchant SS. 2016. Ni induces the CRR1-dependent regulon revealing overlap and distinction between hypoxia and Cu deficiency responses in *Chlamydomonas reinhardtii*. *Metallomics* 8: 679-691.**  
Google Scholar: [Author Only](#) [Title Only](#) [Author and Title](#)
- Blaby-Haas CE, Merchant SS. 2019. Comparative and functional algal genomics. *Annual Review of Plant Biology* 70: 605-638.**  
Google Scholar: [Author Only](#) [Title Only](#) [Author and Title](#)
- Blanc G, Agarkova I, Grimwood J, Kuo A, Brueggeman A, Dunigan DD, Gurnon J, Ladunga I, Lindquist E, Lucas S et al. 2012. The genome of the polar eukaryotic microalga *Coccomyxa subellipsoidea* reveals traits of cold adaptation. *Genome Biol* 13.**  
Google Scholar: [Author Only](#) [Title Only](#) [Author and Title](#)
- Boulouis A, Drapier D, Razafimanantsoa H, Wostrikoff K, Tourasse NJ, Pascal K, Girard-Bascou J, Vallon O, Wollman FA, Choquet Y. 2015. Spontaneous dominant mutations in *Chlamydomonas* highlight ongoing evolution by gene diversification. *Plant Cell* 27: 984-1001.**  
Google Scholar: [Author Only](#) [Title Only](#) [Author and Title](#)
- Brand H, Collins RL, Hanscom C, Rosenfeld JA, Pillalamarri V, Stone MR, Kelley F, Mason T, Margolin L, Eggert S et al. 2015. Paired-duplication signatures mark cryptic inversions and other complex structural variation. *Am J Hum Genet* 97: 170-176.**  
Google Scholar: [Author Only](#) [Title Only](#) [Author and Title](#)
- Broman KW, Wu H, Sen S, Churchill GA. 2003. R/qtl: QTL mapping in experimental crosses. *Bioinformatics* 19: 889-890.**  
Google Scholar: [Author Only](#) [Title Only](#) [Author and Title](#)
- Cavaiuolo M, Kuras R, Wollman FA, Choquet Y, Vallon O. 2017. Small RNA profiling in *Chlamydomonas*: insights into chloroplast RNA metabolism. *Nucleic Acids Res* 45: 10783-10799.**  
Google Scholar: [Author Only](#) [Title Only](#) [Author and Title](#)
- Chaux-Jukic F, O'Donnell S, Craig RJ, Eberhard S, Vallon O, Xu Z. 2021. Architecture and evolution of subtelomeres in the unicellular green alga *Chlamydomonas reinhardtii*. *Nucleic Acids Res* 49: 7571-7587.**  
Google Scholar: [Author Only](#) [Title Only](#) [Author and Title](#)
- Craig RJ. 2021. The evolutionary genomics of *Chlamydomonas*. PhD thesis in Institute of Evolutionary Biology, Vol PhD. University of Edinburgh. <http://dx.doi.org/10.7488/era/1603>**  
Google Scholar: [Author Only](#) [Title Only](#) [Author and Title](#)
- Craig RJ, Böndel KB, Arakawa K, Nakada T, Ito T, Bell G, Colegrave N, Keightley PD, Ness RW. 2019. Patterns of population structure and complex haplotype sharing among field isolates of the green alga *Chlamydomonas reinhardtii*. *Mol Ecol* 28: 3977-3993.**  
Google Scholar: [Author Only](#) [Title Only](#) [Author and Title](#)
- Craig RJ, Hasan AR, Ness RW, Keightley PD. 2021a. Comparative genomics of *Chlamydomonas*. *Plant Cell* 33: 1016-1041.**  
Google Scholar: [Author Only](#) [Title Only](#) [Author and Title](#)

- Craig RJ, Yushenova IA, Rodriguez F, Arkhipova IR. 2021b. An ancient clade of Penelope-like retroelements with permuted domains is present in the green lineage and protists, and dominates many invertebrate genomes. *Mol Biol Evol* 38: 5005-5020.  
Google Scholar: [Author Only](#) [Title Only](#) [Author and Title](#)
- Cross FR. 2015. Tying down loose ends in the *Chlamydomonas* genome: functional significance of abundant upstream open reading frames. *G3 (Bethesda)* 6: 435-446.  
Google Scholar: [Author Only](#) [Title Only](#) [Author and Title](#)
- Cross FR, Umen JG. 2015. The *Chlamydomonas* cell cycle. *The Plant Journal* 82: 370-392.  
Google Scholar: [Author Only](#) [Title Only](#) [Author and Title](#)
- Croteau DL, Popuri V, Opresko PL, Bohr VA. 2014. Human RecQ helicases in DNA repair, recombination, and replication. *Annu Rev Biochem* 83: 519-552.  
Google Scholar: [Author Only](#) [Title Only](#) [Author and Title](#)
- Crozet P, Navarro FJ, Willmund F, Mehrshahi P, Bakowski K, Lauersen KJ, Perez-Perez ME, Auroy P, Gorchs Rovira A, Sauret-Gueto S et al. 2018. Birth of a photosynthetic chassis: a MoClo toolkit enabling synthetic biology in the microalga *Chlamydomonas reinhardtii*. *ACS Synth Biol* 7: 2074-2086.  
Google Scholar: [Author Only](#) [Title Only](#) [Author and Title](#)
- Cui J, Zhang Z, Shao Y, Zhang K, Leng P, Liang Z. 2015. Genome-wide identification, evolutionary, and expression analyses of histone H3 variants in plants. *Biomed Res Int* 2015: 341598.  
Google Scholar: [Author Only](#) [Title Only](#) [Author and Title](#)
- Danecek P, Bonfield JK, Liddle J, Marshall J, Ohan V, Pollard MO, Whitwham A, Keane T, McCarthy SA, Davies RM et al. 2021. Twelve years of SAMtools and BCFtools. *Gigascience* 10: giab008.  
Google Scholar: [Author Only](#) [Title Only](#) [Author and Title](#)
- Davies DR. 1972. Cell wall organisation in *Chlamydomonas reinhardtii*. The role of extra-nuclear systems. *Mol Gen Genet* 115: 334-348.  
Google Scholar: [Author Only](#) [Title Only](#) [Author and Title](#)
- Day A, Schirmerrahire M, Kuchka MR, Mayfield SP, Rochaix JD. 1988. A transposon with an unusual arrangement of long terminal repeats in the green alga *Chlamydomonas reinhardtii*. *EMBO Journal* 7: 1917-1927.  
Google Scholar: [Author Only](#) [Title Only](#) [Author and Title](#)
- De Hoff PL, Ferris P, Olson BJSC, Miyagi A, Geng S, Umen JG. 2013. Species and population level molecular profiling reveals cryptic recombination and emergent asymmetry in the dimorphic mating locus of *C. reinhardtii*. *PLoS Genet* 9.  
Google Scholar: [Author Only](#) [Title Only](#) [Author and Title](#)
- Deisseroth K, Hegemann P. 2017. The form and function of channelrhodopsin. *Science* 357.  
Google Scholar: [Author Only](#) [Title Only](#) [Author and Title](#)
- Dorn A, Puchta H. 2019. DNA helicases as safekeepers of genome stability in plants. *Genes (Basel)* 10: 1028.  
Google Scholar: [Author Only](#) [Title Only](#) [Author and Title](#)
- Dutcher SK. 2014. The awesome power of dikaryons for studying flagella and basal bodies in *Chlamydomonas reinhardtii*. *Cytoskeleton* 71: 79-94.  
Google Scholar: [Author Only](#) [Title Only](#) [Author and Title](#)
- Dutcher SK, Power J, Galloway RE, Porter ME. 1991. Reappraisal of the genetic map of *Chlamydomonas reinhardtii*. *J Hered* 82: 295-301.  
Google Scholar: [Author Only](#) [Title Only](#) [Author and Title](#)
- Engel BD, Schaffer M, Kuhn Cuellar L, Villa E, Plitzko JM, Baumeister W. 2015. Native architecture of the *Chlamydomonas* chloroplast revealed by in situ cryo-electron tomography. *eLife* 4: e04889.  
Google Scholar: [Author Only](#) [Title Only](#) [Author and Title](#)
- Fausser F, Vilarrasa-Blasi J, Onishi M, Ramundo S, Patena W, Millican M, Osaki J, Philp C, Nemeth M, Salome PA et al. 2022. Systematic characterization of gene function in the photosynthetic alga *Chlamydomonas reinhardtii*. *Nat Genet* 54: 705-714.  
Google Scholar: [Author Only](#) [Title Only](#) [Author and Title](#)
- Fédry J, Liu Y, Pehau-Arnaudet G, Pei J, Li W, Tortorici MA, Traincard F, Meola A, Bricogne G, Grishin NV et al. 2017. The ancient gamete fusogen HAP2 is a eukaryotic class II fusion protein. *Cell* 168: 904-915.e910.  
Google Scholar: [Author Only](#) [Title Only](#) [Author and Title](#)
- Ferris P, Olson BJ, De Hoff PL, Douglass S, Casero D, Prochnik S, Geng S, Rai R, Grimwood J, Schmutz J et al. 2010. Evolution of an expanded sex-determining locus in *Volvox*. *Science* 328: 351-354.  
Google Scholar: [Author Only](#) [Title Only](#) [Author and Title](#)
- Ferris PJ. 1989. Characterization of a *Chlamydomonas* transposon, Gulliver, resembling those in higher-plants. *Genetics* 122:

363-377.

Google Scholar: [Author Only](#) [Title Only](#) [Author and Title](#)

Ferris PJ, Armbrust EV, Goodenough UW. 2002. Genetic structure of the mating-type locus of *Chlamydomonas reinhardtii*. *Genetics* 160: 181-200.

Google Scholar: [Author Only](#) [Title Only](#) [Author and Title](#)

Ferris PJ, Goodenough UW. 1994. The mating-type locus of *Chlamydomonas reinhardtii* contains highly rearranged DNA sequences. *Cell* 76: 1135-1145.

Google Scholar: [Author Only](#) [Title Only](#) [Author and Title](#)

Flowers JM, Hazzouri KM, Pham GM, Rosas U, Bahmani T, Khraiweh B, Nelson DR, Jijakli K, Abdrabu R, Harris EH et al. 2015. Whole-genome resequencing reveals extensive natural variation in the model green alga *Chlamydomonas reinhardtii*. *Plant Cell* 27: 2353-2369.

Google Scholar: [Author Only](#) [Title Only](#) [Author and Title](#)

Freeman Rosenzweig ES, Xu B, Kuhn Cuellar L, Martinez-Sanchez A, Schaffer M, Strauss M, Cartwright HN, Ronceray P, Plitzko JM, Forster F et al. 2017. The eukaryotic CO<sub>2</sub>-concentrating organelle is liquid-like and exhibits dynamic reorganization. *Cell* 171: 148-162.e119.

Google Scholar: [Author Only](#) [Title Only](#) [Author and Title](#)

Gallaher SD, Craig RJ, Ganesan I, Purvine SO, McCorkle S, Grimwood J, Strenkert D, Davidi L, Roth MS, Jeffers TL et al. 2021. Widespread polycistronic gene expression in green algae. *Proc Natl Acad Sci U S A* 118: e2017714118.

Google Scholar: [Author Only](#) [Title Only](#) [Author and Title](#)

Gallaher SD, Fitz-Gibbon ST, Glaesener AG, Pellegrini M, Merchant SS. 2015. *Chlamydomonas* genome resource for laboratory strains reveals a mosaic of sequence variation, identifies true strain histories, and enables strain-specific studies. *Plant Cell* 27: 2335-2352.

Google Scholar: [Author Only](#) [Title Only](#) [Author and Title](#)

Gallaher SD, Fitz-Gibbon ST, Strenkert D, Purvine SO, Pellegrini M, Merchant SS. 2018. High-throughput sequencing of the chloroplast and mitochondrion of *Chlamydomonas reinhardtii* to generate improved de novo assemblies, analyze expression patterns and transcript speciation, and evaluate diversity among laboratory strains and wild isolates. *Plant J* 93: 545-565.

Google Scholar: [Author Only](#) [Title Only](#) [Author and Title](#)

Gel B, Serra E. 2017. karyoploteR: an R/Bioconductor package to plot customizable genomes displaying arbitrary data. *Bioinformatics* 33: 3088-3090.

Google Scholar: [Author Only](#) [Title Only](#) [Author and Title](#)

Goff SA, Ricke D, Lan TH, Presting G, Wang R, Dunn M, Glazebrook J, Sessions A, Oeller P, Varma H et al. 2002. A draft sequence of the rice genome (*Oryza sativa* L. ssp. japonica). *Science* 296: 92-100.

Google Scholar: [Author Only](#) [Title Only](#) [Author and Title](#)

Goodstein DM, Shu S, Howson R, Neupane R, Hayes RD, Fazo J, Mitros T, Dirks W, Hellsten U, Putnam N et al. 2012. Phytozome: a comparative platform for green plant genomics. *Nucleic Acids Res* 40: D1178-1186.

Google Scholar: [Author Only](#) [Title Only](#) [Author and Title](#)

Goodwin TJ, Poulter RT. 2004. A new group of tyrosine recombinase-encoding retrotransposons. *Mol Biol Evol* 21: 746-759.

Google Scholar: [Author Only](#) [Title Only](#) [Author and Title](#)

Gorres KL, Raines RT. 2010. Prolyl 4-hydroxylase. *Crit Rev Biochem Mol Biol* 45: 106-124.

Google Scholar: [Author Only](#) [Title Only](#) [Author and Title](#)

Grigoriev IV, Hayes RD, Calhoun S, Kamel B, Wang A, Ahrendt S, Dusheyko S, Nikitin R, Mondo SJ, Salamov A et al. 2021. PhycoCosm, a comparative algal genomics resource. *Nucleic Acids Res* 49: D1004-D1011.

Google Scholar: [Author Only](#) [Title Only](#) [Author and Title](#)

Grossman AR, Harris EE, Hauser C, Lefebvre PA, Martinez D, Rokhsar D, Shrager J, Silflow CD, Stern D, Vallon O et al. 2003. *Chlamydomonas reinhardtii* at the crossroads of genomics. *Eukaryot Cell* 2: 1137-1150.

Google Scholar: [Author Only](#) [Title Only](#) [Author and Title](#)

Haas BJ, Delcher AL, Mount SM, Wortman JR, Smith RK, Jr., Hannick LI, Maiti R, Ronning CM, Rusch DB, Town CD et al. 2003. Improving the *Arabidopsis* genome annotation using maximal transcript alignment assemblies. *Nucleic Acids Res* 31: 5654-5666.

Google Scholar: [Author Only](#) [Title Only](#) [Author and Title](#)

Hamaji T, Kawai-Toyooka H, Uchimura H, Suzuki M, Noguchi H, Minakuchi Y, Toyoda A, Fujiyama A, Miyagishima S, Umen JG et al. 2018. Anisogamy evolved with a reduced sex-determining region in volvocine green algae. *Communications Biology* 1: 17.

Google Scholar: [Author Only](#) [Title Only](#) [Author and Title](#)

Helliwell KE, Collins S, Kazamia E, Purton S, Wheeler GL, Smith AG. 2015. Fundamental shift in vitamin B12 eco-physiology of a

model alga demonstrated by experimental evolution. *ISME J* 9: 1446-1455.

Google Scholar: [Author Only](#) [Title Only](#) [Author and Title](#)

Hickey G, Paten B, Earl D, Zerbino D, Haussler D. 2013. HAL: a hierarchical format for storing and analyzing multiple genome alignments. *Bioinformatics* 29: 1341-1342.

Google Scholar: [Author Only](#) [Title Only](#) [Author and Title](#)

Hyams J, Davies DR. 1972. Induction and characterization of cell-wall mutants of *Chlamydomonas reinhardi*. *Mutat Res* 14: 381-&.

Google Scholar: [Author Only](#) [Title Only](#) [Author and Title](#)

Ito H, Gaubert H, Bucher E, Mirouze M, Vaillant I, Paszkowski J. 2011. An siRNA pathway prevents transgenerational retrotransposition in plants subjected to stress. *Nature* 472: 115-119.

Google Scholar: [Author Only](#) [Title Only](#) [Author and Title](#)

Jiao Y, Peluso P, Shi J, Liang T, Stitzer MC, Wang B, Campbell MS, Stein JC, Wei X, Chin CS et al. 2017. Improved maize reference genome with single-molecule technologies. *Nature* 546: 524-527.

Google Scholar: [Author Only](#) [Title Only](#) [Author and Title](#)

Joo S, Kariyawasam T, Kim M, Jin E, Goodenough U, Lee JH. 2022. Sex-linked deubiquitinase establishes uniparental transmission of chloroplast DNA. *Nat Commun* 13: 1133.

Google Scholar: [Author Only](#) [Title Only](#) [Author and Title](#)

Kaina B. 2004. Mechanisms and consequences of methylating agent-induced SCEs and chromosomal aberrations: a long road traveled and still a far way to go. *Cytogenet Genome Res* 104: 77-86.

Google Scholar: [Author Only](#) [Title Only](#) [Author and Title](#)

Kapitonov W, Jurka J. 2003. The esterase and PHD domains in CR1-like non-LTR retrotransposons. *Mol Biol Evol* 20: 38-46.

Google Scholar: [Author Only](#) [Title Only](#) [Author and Title](#)

Kathir P, LaVoie M, Brazelton WJ, Haas NA, Lefebvre PA, Silflow CD. 2003. Molecular map of the *Chlamydomonas reinhardtii* nuclear genome. *Eukaryot Cell* 2: 362-379.

Google Scholar: [Author Only](#) [Title Only](#) [Author and Title](#)

Katoh K, Standley DM. 2013. MAFFT multiple sequence alignment software version 7: improvements in performance and usability. *Mol Biol Evol* 30: 772-780.

Google Scholar: [Author Only](#) [Title Only](#) [Author and Title](#)

Keskiaho K, Hieta R, Sormunen R, Myllyharju J. 2007. *Chlamydomonas reinhardtii* has multiple prolyl 4-hydroxylases, one of which is essential for proper cell wall assembly. *Plant Cell* 19: 256-269.

Google Scholar: [Author Only](#) [Title Only](#) [Author and Title](#)

Kim KS, Kustu S, Inwood W. 2006. Natural history of transposition in the green alga *Chlamydomonas reinhardtii*: Use of the AMT4 locus as an experimental system. *Genetics* 173: 2005-2019.

Google Scholar: [Author Only](#) [Title Only](#) [Author and Title](#)

Koren S, Walenz BP, Berlin K, Miller JR, Bergman NH, Phillippy AM. 2017. Canu: scalable and accurate long-read assembly via adaptive k-mer weighting and repeat separation. *Genome Res* 27: 722-736.

Google Scholar: [Author Only](#) [Title Only](#) [Author and Title](#)

Krzywinski M, Schein J, Birol I, Connors J, Gascoyne R, Horsman D, Jones SJ, Marra MA. 2009. Circos: an information aesthetic for comparative genomics. *Genome Res* 19: 1639-1645.

Google Scholar: [Author Only](#) [Title Only](#) [Author and Title](#)

Kück U, Choquet Y, Schneider M, Dron M, Bennoun P. 1987. Structural and transcription analysis of two homologous genes for the P700 chlorophyll a-apoproteins in *Chlamydomonas reinhardtii*: evidence for in vivo trans-splicing. *EMBO J* 6: 2185-2195.

Google Scholar: [Author Only](#) [Title Only](#) [Author and Title](#)

Kurtz S, Phillippy A, Delcher AL, Smoot M, Shumway M, Antonescu C, Salzberg SL. 2004. Versatile and open software for comparing large genomes. *Genome Biol* 5: R12.

Google Scholar: [Author Only](#) [Title Only](#) [Author and Title](#)

Labadorf A, Link A, Rogers MF, Thomas J, Reddy AS, Ben-Hur A. 2010. Genome-wide analysis of alternative splicing in *Chlamydomonas reinhardtii*. *Bmc Genomics* 11: 114.

Google Scholar: [Author Only](#) [Title Only](#) [Author and Title](#)

Letunic I, Bork P. 2019. Interactive Tree Of Life (iTOL) v4: recent updates and new developments. *Nucleic Acids Res* 47: W256-W259.

Google Scholar: [Author Only](#) [Title Only](#) [Author and Title](#)

Lex A, Gehlenborg N, Strobel H, Vuillemot R, Pfister H. 2014. UpSet: visualization of intersecting sets. *IEEE Trans Vis Comput Graph* 20: 1983-1992.

Google Scholar: [Author Only](#) [Title Only](#) [Author and Title](#)

**Li H. 2013. Aligning sequence reads, clone sequences and assembly contigs with BWA-MEM. arXiv doi:arXiv:1303.3997.**

Google Scholar: [Author Only](#) [Title Only](#) [Author and Title](#)

**Li H. 2018. Minimap2: pairwise alignment for nucleotide sequences. Bioinformatics 34: 3094-3100.**

Google Scholar: [Author Only](#) [Title Only](#) [Author and Title](#)

**Li X, Patena W, Fauser F, Jinkerson RE, Saroussi S, Meyer MT, Ivanova N, Robertson JM, Yue R, Zhang R et al. 2019. A genome-wide algal mutant library and functional screen identifies genes required for eukaryotic photosynthesis. Nat Genet 51: 627-635.**

Google Scholar: [Author Only](#) [Title Only](#) [Author and Title](#)

**Lin H, Cliften PF, Dutcher SK. 2018. MAPINS, a highly efficient detection method that identifies insertional mutations and complex DNA rearrangements. Plant Physiol 178: 1436-1447.**

Google Scholar: [Author Only](#) [Title Only](#) [Author and Title](#)

**Lin H, Miller ML, Granas DM, Dutcher SK. 2013. Whole genome sequencing identifies a deletion in protein phosphatase 2A that affects its stability and localization in *Chlamydomonas reinhardtii*. PLoS Genet 9: e1003841.**

Google Scholar: [Author Only](#) [Title Only](#) [Author and Title](#)

**Liu H, Huang J, Sun X, Li J, Hu Y, Yu L, Liti G, Tian D, Hurst LD, Yang S. 2018. Tetrad analysis in plants and fungi finds large differences in gene conversion rates but no GC bias. Nat Ecol Evol 2: 164-173.**

Google Scholar: [Author Only](#) [Title Only](#) [Author and Title](#)

**Liu J, Seetharam AS, Chougule K, Ou S, Swentowsky KW, Gent JI, Llaca V, Woodhouse MR, Manchanda N, Presting GG et al. 2020. Gapless assembly of maize chromosomes using long-read technologies. Genome Biol 21: 121.**

Google Scholar: [Author Only](#) [Title Only](#) [Author and Title](#)

**Liu Q, Fang L, Yu G, Wang D, Xiao CL, Wang K. 2019. Detection of DNA base modifications by deep recurrent neural network on Oxford Nanopore sequencing data. Nat Commun 10: 2449.**

Google Scholar: [Author Only](#) [Title Only](#) [Author and Title](#)

**Lopez D, Hamaji T, Kropat J, De Hoff P, Morselli M, Rubbi L, Fitz-Gibbon S, Gallaher SD, Merchant SS, Umen J et al. 2015. Dynamic changes in the transcriptome and methylome of *Chlamydomonas reinhardtii* throughout its life cycle. Plant Physiol 169: 2730-2743.**

Google Scholar: [Author Only](#) [Title Only](#) [Author and Title](#)

**López-Cortegano E, Craig RJ, Chebib J, Balogun EJ, Keightley PD. 2022. Rates and spectra of de novo structural mutation in *Chlamydomonas reinhardtii*. Biorxiv doi:https://doi.org/10.1101/2022.05.23.493040.**

Google Scholar: [Author Only](#) [Title Only](#) [Author and Title](#)

**Lu H, Davis AJ. 2021. Human RecQ helicases in DNA double-strand break repair. Front Cell Dev Biol 9: 640755.**

Google Scholar: [Author Only](#) [Title Only](#) [Author and Title](#)

**Manni M, Berkeley MR, Seppely M, Simão FA, Zdobnov EM. 2021. BUSCO update: novel and streamlined workflows along with broader and deeper phylogenetic coverage for scoring of eukaryotic, prokaryotic, and viral genomes. Mol Biol Evol 38: 4647-4654.**

Google Scholar: [Author Only](#) [Title Only](#) [Author and Title](#)

**Maul JE, Lilly JW, Cui L, dePamphilis CW, Miller W, Harris EH, Stern DB. 2002. The *Chlamydomonas reinhardtii* plastid chromosome: islands of genes in a sea of repeats. Plant Cell 14: 2659-2679.**

Google Scholar: [Author Only](#) [Title Only](#) [Author and Title](#)

**McCarthy SS, Kobayashi MC, Niyogi KK. 2004. White mutants of *Chlamydomonas reinhardtii* are defective in phytoene synthase. Genetics 168: 1249-1257.**

Google Scholar: [Author Only](#) [Title Only](#) [Author and Title](#)

**McKenna A, Hanna M, Banks E, Sivachenko A, Cibulskis K, Kernysky A, Garimella K, Altshuler D, Gabriel S, Daly M et al. 2010. The Genome Analysis Toolkit: a MapReduce framework for analyzing next-generation DNA sequencing data. Genome Res 20: 1297-1303.**

Google Scholar: [Author Only](#) [Title Only](#) [Author and Title](#)

**Merchant SS, Prochnik SE, Vallon O, Harris EH, Karpowicz SJ, Witman GB, Terry A, Salamov A, Fritz-Laylin LK, Marechal-Drouard L et al. 2007. The *Chlamydomonas* genome reveals the evolution of key animal and plant functions. Science 318: 245-250.**

Google Scholar: [Author Only](#) [Title Only](#) [Author and Title](#)

**Miller RJ, Pfeiffer W, Schwartz T. 2010. Creating the CIPRES Science Gateway for inference of large phylogenetic trees. In 2010 Gateway Computing Environments Workshop (GCE), doi:10.1109/GCE.2010.5676129, pp. 1-8. IEEE.**

Google Scholar: [Author Only](#) [Title Only](#) [Author and Title](#)

**Moseley JL, Page MD, Alder NP, Eriksson M, Quinn J, Soto F, Theg SM, Hippler M, Merchant S. 2002. Reciprocal expression of**

two candidate di-iron enzymes affecting photosystem I and light-harvesting complex accumulation. *Plant Cell* 14: 673-688.

Google Scholar: [Author Only](#) [Title Only](#) [Author and Title](#)

Navrátilová A, Koblížková A, Macas J. 2008. Survey of extrachromosomal circular DNA derived from plant satellite repeats. *BMC Plant Biol* 8: 90.

Google Scholar: [Author Only](#) [Title Only](#) [Author and Title](#)

Neupert J, Gallaher SD, Lu Y, Strenkert D, Segal N, Barahimipour R, Fitz-Gibbon ST, Schroda M, Merchant SS, Bock R. 2020. An epigenetic gene silencing pathway selectively acting on transgenic DNA in the green alga *Chlamydomonas*. *Nat Commun* 11: 6269.

Google Scholar: [Author Only](#) [Title Only](#) [Author and Title](#)

Ngan CY, Wong CH, Choi C, Yoshinaga Y, Louie K, Jia J, Chen C, Bowen B, Cheng H, Leonelli L et al. 2015. Lineage-specific chromatin signatures reveal a regulator of lipid metabolism in microalgae. *Nat Plants* 1: 15107.

Google Scholar: [Author Only](#) [Title Only](#) [Author and Title](#)

Ni P, Huang N, Zhang Z, Wang DP, Liang F, Miao Y, Xiao CL, Luo F, Wang J. 2019. DeepSignal: detecting DNA methylation state from Nanopore sequencing reads using deep-learning. *Bioinformatics* 35: 4586-4595.

Google Scholar: [Author Only](#) [Title Only](#) [Author and Title](#)

Ning J, Otto TD, Pfander C, Schwach F, Brochet M, Bushell E, Goulding D, Sanders M, Lefebvre PA, Pei J et al. 2013. Comparative genomics in *Chlamydomonas* and *Plasmodium* identifies an ancient nuclear envelope protein family essential for sexual reproduction in protists, fungi, plants, and vertebrates. *Genes Dev* 27: 1198-1215.

Google Scholar: [Author Only](#) [Title Only](#) [Author and Title](#)

Novoselov SV, Rao M, Onoshko NV, Zhi H, Kryukov GV, Xiang Y, Weeks DP, Hatfield DL, Gladyshev VN. 2002. Selenoproteins and selenocysteine insertion system in the model plant cell system, *Chlamydomonas reinhardtii*. *EMBO J* 21: 3681-3693.

Google Scholar: [Author Only](#) [Title Only](#) [Author and Title](#)

O'Donnell S, Chaux F, Fischer G. 2020. Highly contiguous Nanopore genome assembly of *Chlamydomonas reinhardtii* CC-1690. *Microbiol Resour Announc* 9: e00726-00720.

Google Scholar: [Author Only](#) [Title Only](#) [Author and Title](#)

O'Donnell S, Fischer G. 2020. MUM&Co: accurate detection of all SV types through whole-genome alignment. *Bioinformatics* 36: 3242-3243.

Google Scholar: [Author Only](#) [Title Only](#) [Author and Title](#)

Ozawa SI, Cavaiuolo M, Jarrige D, Kuras R, Rutgers M, Eberhard S, Drapier D, Wollman FA, Choquet Y. 2020. The OPR protein MTH1 controls the expression of two different subunits of ATP synthase CFo in *Chlamydomonas reinhardtii*. *Plant Cell* 32: 1179-1203.

Google Scholar: [Author Only](#) [Title Only](#) [Author and Title](#)

Perez-Alegre M, Dubus A, Fernandez E. 2005. REM1, a new type of long terminal repeat retrotransposon in *Chlamydomonas reinhardtii*. *Mol Cell Biol* 25: 10628-10638.

Google Scholar: [Author Only](#) [Title Only](#) [Author and Title](#)

Petracek ME, Lefebvre PA, Silflow CD, Berman J. 1990. *Chlamydomonas* telomere sequences are A+T-rich but contain three consecutive G-C base pairs. *Proc Natl Acad Sci U S A* 87: 8222-8226.

Google Scholar: [Author Only](#) [Title Only](#) [Author and Title](#)

Philippesen GS, Avaca-Crusca JS, Araujo APU, DeMarco R. 2016. Distribution patterns and impact of transposable elements in genes of green algae. *Gene* 594: 151-159.

Google Scholar: [Author Only](#) [Title Only](#) [Author and Title](#)

Porter ME, Knott JA, Myster SH, Farlow SJ. 1996. The dynein gene family in *Chlamydomonas reinhardtii*. *Genetics* 144: 569-585.

Google Scholar: [Author Only](#) [Title Only](#) [Author and Title](#)

Preuss D, Mets L. 2002. Plant centromere functions defined by tetrad analysis and artificial chromosomes. *Plant Physiol* 129: 421-422.

Google Scholar: [Author Only](#) [Title Only](#) [Author and Title](#)

Prochnik SE, Umen J, Nedelcu AM, Hallmann A, Miller SM, Nishii I, Ferris P, Kuo A, Mitros T, Fritz-Laylin LK et al. 2010. Genomic analysis of organismal complexity in the multicellular green alga *Volvox carteri*. *Science* 329: 223-226.

Google Scholar: [Author Only](#) [Title Only](#) [Author and Title](#)

Pröschold T, Harris EH, Coleman AW. 2005. Portrait of a species: *Chlamydomonas reinhardtii*. *Genetics* 170: 1601-1610.

Google Scholar: [Author Only](#) [Title Only](#) [Author and Title](#)

Quinlan AR, Hall IM. 2010. BEDTools: a flexible suite of utilities for comparing genomic features. *Bioinformatics* 26: 841-842.

Google Scholar: [Author Only](#) [Title Only](#) [Author and Title](#)

- Raj-Kumar PK, Vallon O, Liang C. 2017. In silico analysis of the sequence features responsible for alternatively spliced introns in the model green alga *Chlamydomonas reinhardtii*. *Plant Mol Biol* 94: 253-265.  
Google Scholar: [Author Only](#) [Title Only](#) [Author and Title](#)
- Riddle NC, Elgin SCR. 2018. The *Drosophila* dot chromosome: where genes flourish amidst repeats. *Genetics* 210: 757-772.  
Google Scholar: [Author Only](#) [Title Only](#) [Author and Title](#)
- Robinson JT, Thorvaldsdóttir H, Winckler W, Guttman M, Lander ES, Getz G, Mesirov JP. 2011. Integrative Genomics Viewer. *Nat Biotechnol* 29: 24-26.  
Google Scholar: [Author Only](#) [Title Only](#) [Author and Title](#)
- Röhrig S, Dorn A, Enderle J, Schindele A, Herrmann NJ, Knoll A, Puchta H. 2018. The RecQ-like helicase HRQ1 is involved in DNA crosslink repair in *Arabidopsis* in a common pathway with the Fanconi anemia-associated nuclease FAN1 and the postreplicative repair ATPase RAD5A. *New Phytol* 218: 1478-1490.  
Google Scholar: [Author Only](#) [Title Only](#) [Author and Title](#)
- Roth MS, Cokus SJ, Gallaher SD, Walter A, Lopez D, Erickson E, Endelman B, Westcott D, Larabell CA, Merchant SS et al. 2017. Chromosome-level genome assembly and transcriptome of the green alga *Chromochloris zofingiensis* illuminates astaxanthin production. *Proc Natl Acad Sci U S A* 114: E4296-E4305.  
Google Scholar: [Author Only](#) [Title Only](#) [Author and Title](#)
- Ruiz-Ruano FJ, López-León MD, Cabrero J, Camacho JPM. 2016. High-throughput analysis of the satellitome illuminates satellite DNA evolution. *Sci Rep* 6: 28333.  
Google Scholar: [Author Only](#) [Title Only](#) [Author and Title](#)
- Rymarquis LA, Handley JM, Thomas M, Stern DB. 2005. Beyond complementation. Map-based cloning in *Chlamydomonas reinhardtii*. *Plant Physiol* 137: 557-566.  
Google Scholar: [Author Only](#) [Title Only](#) [Author and Title](#)
- Salinas-Giegé T, Cavaiuolo M, Cognat V, Ubrig E, Remacle C, Duchene AM, Vallon O, Marechal-Drouard L. 2017. Polycytidylation of mitochondrial mRNAs in *Chlamydomonas reinhardtii*. *Nucleic Acids Res* 45: 12963-12973.  
Google Scholar: [Author Only](#) [Title Only](#) [Author and Title](#)
- Salomé PA, Merchant SS. 2019. A Series of fortunate events: Introducing *Chlamydomonas* as a reference organism. *Plant Cell* 31: 1682-1707.  
Google Scholar: [Author Only](#) [Title Only](#) [Author and Title](#)
- Schnell RA, Lefebvre PA. 1993. Isolation of the *Chlamydomonas* regulatory gene NIT2 by transposon tagging. *Genetics* 134: 737-747.  
Google Scholar: [Author Only](#) [Title Only](#) [Author and Title](#)
- Shu S, Goodstein D, Rokhsar D. 2013. PERTRAN: genome-guided RNA-seq read assembler. In OSTIgov: US Department of Energy - Office of Scientific and Technical Information.  
Google Scholar: [Author Only](#) [Title Only](#) [Author and Title](#)
- Smit AFA, Hubley R, Green P. 2013-2015. RepeatMasker Open-4.0. <http://www.repeatmasker.org>.  
Google Scholar: [Author Only](#) [Title Only](#) [Author and Title](#)
- Smith DR, Craig RJ. 2021. Does mitochondrial DNA replication in *Chlamydomonas* require a reverse transcriptase? *New Phytol* 229: 1192-1195.  
Google Scholar: [Author Only](#) [Title Only](#) [Author and Title](#)
- Smith DR, Lee RW. 2009. Nucleotide diversity of the *Chlamydomonas reinhardtii* plastid genome: addressing the mutational-hazard hypothesis. *BMC Evol Biol* 9: 120.  
Google Scholar: [Author Only](#) [Title Only](#) [Author and Title](#)
- Smith EF, Lefebvre PA. 1997. PF20 gene product contains WD repeats and localizes to the intermicrotubule bridges in *Chlamydomonas* flagella. *Mol Biol Cell* 8: 455-467.  
Google Scholar: [Author Only](#) [Title Only](#) [Author and Title](#)
- Sreedasyam A, Plott C, Shadkhawat Hossain M, Lovell JT, Grimwood J, Jenkins JW, Daum C, Barry K, Carlson J, Shu S et al. 2022. JGI Plant Gene Atlas: An updateable transcriptome resource to improve structural annotations and functional gene descriptions across the plant kingdom. *Biorxiv* doi:doi.org/10.1101/2022.09.30.510380.  
Google Scholar: [Author Only](#) [Title Only](#) [Author and Title](#)
- Sterken MG, Snoek LB, Kammenga JE, Andersen EC. 2015. The laboratory domestication of *Caenorhabditis elegans*. *Trends Genet* 31: 224-231.  
Google Scholar: [Author Only](#) [Title Only](#) [Author and Title](#)
- Strenkert D, Yildirim A, Yan J, Yoshinaga Y, Pellegrini M, O'Malley RC, Merchant SS, Umen JG. 2022. The landscape of

**Chlamydomonas histone H3 lysine 4 methylation reveals both constant features and dynamic changes during the diurnal cycle. Plant J doi:10.1111/tpj.15948.**

Google Scholar: [Author Only](#) [Title Only](#) [Author and Title](#)

**Sumper M, Hallmann A. 1998. Biochemistry of the extracellular matrix of Volvox. Int Rev Cytol 180: 51-85.**

Google Scholar: [Author Only](#) [Title Only](#) [Author and Title](#)

**Trifinopoulos J, Nguyen LT, von Haeseler A, Minh BQ. 2016. W-IQ-TREE: a fast online phylogenetic tool for maximum likelihood analysis. Nucleic Acids Res 44: W232-235.**

Google Scholar: [Author Only](#) [Title Only](#) [Author and Title](#)

**Tulin F, Cross FR. 2014. A microbial avenue to cell cycle control in the plant superkingdom. Plant Cell 26: 4019-4038.**

Google Scholar: [Author Only](#) [Title Only](#) [Author and Title](#)

**Tulin F, Cross FR. 2016. Patching holes in the Chlamydomonas genome. G3 (Bethesda) 6: 1899-1910.**

Google Scholar: [Author Only](#) [Title Only](#) [Author and Title](#)

**Ueki N, Nishii I. 2008. Idaten is a new cold-inducible transposon of Volvox carteri that can be used for tagging developmentally important genes. Genetics 180: 1343-1353.**

Google Scholar: [Author Only](#) [Title Only](#) [Author and Title](#)

**Vahrenholz C, Riemen G, Pratz E, Dujon B, Michaelis G. 1993. Mitochondrial DNA of Chlamydomonas reinhardtii: the structure of the ends of the linear 15.8-kb genome suggests mechanisms for DNA replication. Curr Genet 24: 241-247.**

Google Scholar: [Author Only](#) [Title Only](#) [Author and Title](#)

**Wang SC, Schnell RA, Lefebvre PA. 1998. Isolation and characterization of a new transposable element in Chlamydomonas reinhardtii. Plant Molecular Biology 38: 681-687.**

Google Scholar: [Author Only](#) [Title Only](#) [Author and Title](#)

**Wiedemann G, van Gessel N, Kochl F, Hunn L, Schulze K, Maloukh L, Nogue F, Decker EL, Hartung F, Reski R. 2018. RecQ helicases function in development, DNA repair, and gene targeting in Physcomitrella patens. Plant Cell 30: 717-736.**

Google Scholar: [Author Only](#) [Title Only](#) [Author and Title](#)

**Williams BA, Slamovits CH, Patron NJ, Fast NM, Keeling PJ. 2005. A high frequency of overlapping gene expression in compacted eukaryotic genomes. Proc Natl Acad Sci U S A 102: 10936-10941.**

Google Scholar: [Author Only](#) [Title Only](#) [Author and Title](#)

**Woessner JP, Goodenough UW. 1994. Volvocine cell walls and their constituent glycoproteins: an evolutionary perspective. Protoplasma 181: 245-258.**

Google Scholar: [Author Only](#) [Title Only](#) [Author and Title](#)

**Wright BW, Molloy MP, Jaschke PR. 2022. Overlapping genes in natural and engineered genomes. Nat Rev Genet 23: 154-168.**

Google Scholar: [Author Only](#) [Title Only](#) [Author and Title](#)

**Wu TD, Nacu S. 2010. Fast and SNP-tolerant detection of complex variants and splicing in short reads. Bioinformatics 26: 873-881.**

Google Scholar: [Author Only](#) [Title Only](#) [Author and Title](#)

**Wu TD, Watanabe CK. 2005. GMAP: a genomic mapping and alignment program for mRNA and EST sequences. Bioinformatics 21: 1859-1875.**

Google Scholar: [Author Only](#) [Title Only](#) [Author and Title](#)

**Wyatt MD, Pittman DL. 2006. Methylating agents and DNA repair responses: Methylated bases and sources of strand breaks. Chem Res Toxicol 19: 1580-1594.**

Google Scholar: [Author Only](#) [Title Only](#) [Author and Title](#)

**Xiao CL, Chen Y, Xie SQ, Chen KN, Wang Y, Han Y, Luo F, Xie Z. 2017. MECAT: fast mapping, error correction, and de novo assembly for single-molecule sequencing reads. Nat Methods 14: 1072-1074.**

Google Scholar: [Author Only](#) [Title Only](#) [Author and Title](#)

**Yamamoto K, Hamaji T, Kawai-Toyooka H, Matsuzaki R, Takahashi F, Nishimura Y, Kawachi M, Noguchi H, Minakuchi Y, Umen JG et al. 2021. Three genomes in the algal genus Volvox reveal the fate of a haploid sex-determining region after a transition to homothallism. Proc Natl Acad Sci U S A 118.**

Google Scholar: [Author Only](#) [Title Only](#) [Author and Title](#)

**Yamamoto R, Obbineni JM, Alford LM, Ide T, Owa M, Hwang J, Kon T, Inaba K, James N, King SM et al. 2017. Chlamydomonas DYX1C1/PF23 is essential for axonemal assembly and proper morphology of inner dynein arms. PLoS Genet 13: e1006996.**

Google Scholar: [Author Only](#) [Title Only](#) [Author and Title](#)

**Zhao Z, Guo C, Sutharzan S, Li P, Echt CS, Zhang J, Liang C. 2014. Genome-wide analysis of tandem repeats in plants and green algae. G3 (Bethesda) 4: 67-78.**

Google Scholar: [Author Only](#) [Title Only](#) [Author and Title](#)



